Implementation of Coupled Thermo-Mechanical Topology Optimization Methods for Effective Additive Manufacturing of a Gas Turbine Component

by

Pouyan Rahnama

A thesis

presented to the University of Waterloo

in fulfillment of the

thesis requirement for the degree of

Master of Applied Science

in

Mechanical and Mechatronics Engineering

Waterloo, Ontario, Canada, 2020

AUTHOR'S DECLARATION

I hereby declare that I am the sole author of this thesis. This is a true copy of the thesis, including any required final revisions, as accepted by my examiners.

I understand that my thesis may be made electronically available to the public.

Abstract

Additive manufacturing (AM) is a relatively new technology that is making its way into different industries at a fast pace. In order to take full advantage of flexibility and freedom that this technology provides, a proper and comprehensive approach towards Design for Additive Manufacturing (DfAM) is necessary. Topology optimization is one of the tools that is commonly used to design or redesign a component to be printed by AM technologies. Utilizing topology optimization, the best design for a component subjected to various loading conditions can be obtained. The implementation of topology optimization becomes more challenging when the part is subjected to different loading cases, especially at high thermal loads.

In this thesis, a new method is proposed to perform coupled thermo-mechanical topology optimization, and then a workflow is presented to implement this method in DfAM. In the suggested guideline, the effect of different filters, as well as initial setup conditions, are considered for topology optimization. In addition, some common software tools for topology optimization are also discussed. Among the existing software systems, HyperWorks is selected to be utilized in this study due to its distinguished capabilities which offer favorable controllability over the process. Then, the proposed method and workflow for DfAM are applied in HyperWorks to redesign a gas turbine rotor seal, which is subjected to high temperature, high pressure, and centrifugal loads. Also, In order to validate the workflow and the methodology, an experimental setup is designed to test the performance of a topology optimized cantilever under thermo-mechanical loadings. The experimental results validated simulations and proved that the part

designed based on thermo-mechanical optimization has a better performance overall for thermal and mechanical loads.

Acknowledgment

First and foremost, I would like to express my sincere appreciation to my supervisor, Professor Ehsan Toyserkani for the opportunity he granted me to be a part of his wonderful team in the MSAM lab. His valuable guidance and leading was a great help to me during my study. Likewise, I would like to thank Professor Mihaela Vlasea for her support and encouragement in these years.

Moreover, I want to thank Dr. Ehsan Marzbanrad and Dr. Yahya Mahmoudkhani, and Dr. Usman Ali. I got benefited from their comments and supports all the way over the length of my research especially in the experimental part of my work. Also, I want to thank Jerry Ratthapakdee, Grace Kurosad, and Karl Rautenberg, the MSAM lab technicians, who made it possible to provide proper testing samples for my study. They have helped me with their comments on my designs as well as preparing the required samples for the thesis.

I could not be more thankful to Dr. Zhidong Zhang and Osezua Ibhadode for the great supports they provided by sharing their broad knowledge over the topic. They walked me through the process of obtaining my master's degree and were involved in each step of my research. I would like to extend my sincere appreciation to thank Milad Azvar, Shahriar Imani Shahabad, Elham Davoodi, and Sepehr Taeb for their great support and encouragement over these years. They have been assisting me a lot in every aspect of my life and study ever since the beginning of my study at the University of Waterloo. I also would like to thank all of my other colleagues at the MSAM lab. Alex Martinez, Dr. Farzad Liravi, Henry Ma, Dr. Bahareh Marzbanrad, Dr. Hanieh Fayazfar, and Dr. Mehrnaz Salarian for their help in different stages of my study. Last but not the least, I would like to thank all of my other colleagues in the Siemens project who supported me from the

beginning of this project and my study. Dr. Ali Bonakdar, Francis Dibia, Reza Esmaeilizadeh, Ali Keshavarz Kermani, Ken Nsiempba, Dr. Hamed Asgari, Dr. Yuze Sam Huang, and Dr. Farid Ahmed.

Dedication

To my beloved family

My parents, Hossein and Batoul, and my brothers, Ramin and Kamran

Table of Contents

List of Figures

List of Tables

Chapter 1
Introduction

1.1 Motivation

Additive manufacturing (AM), as opposed to subtractive manufacturing, firstly was limited to producing primitive structures and prototypes [1]. Nevertheless, due to the unprecedented advancements in material science, machine tools, and computer science, AM processes have been significantly developed over the past decade. It might be slightly early to efficiently manufacture an entire system employing AM which seems to be the ultimate goal of this realm. Intuitively, in order to move towards this end, researchers are developing different processes suitable for various materials [2]. While AM was initially developed for polymeric materials, waxes, and paper laminates, gradually more materials such as composites, metals, and ceramics were introduced to this technology when new AM processes were introduced [1]. Development of the liquid-based, solid-based, and powder-based AM techniques, make it possible to use a vast number of materials for AM purposes [3]. Amongst all the materials available for AM, metal additive manufacturing is one of the major categories. Similar to all of AM categories, metal AM technologies can be classified based on the material feedstock type, energy source, etc. Generally, it can be divided into three broad types of powder-bed, powder-fed, and wire-fed systems [4].

One of the main advantages of AM over conventional manufacturing processes is its feature that provides designers with flexibility and freedom. Design for Additive Manufacturing (DfAM) becomes challenging since designers need to have overall information about the AM process and

its restrictions [5]. This information is essential to be considered based on each specific AM technique to ensure the printability of the part and reducing the post-processing time.

Topology optimization is one of the challenging yet useful tools in the process of DfAM. This tool became more popular with the introduction and development of AM technologies, which enabled manufacturers to fabricate geometries with a high level of complexity [6]. Topology optimization helps to obtain the best geometry for a component to withstand a specific loading condition in order to achieve a favorable performance at the end. During the topology optimization, many mathematical methods are employed to maintain the most important features in the design space, not only to maximize the performance of the part but also to generate a valid geometry. Solid Isotropic Material with Penalization (SIMP) is one of these methods that is widely used by researchers and industries. In this method, which is the first density-based method, FEM analysis should be performed to ensure if the element should be filled with material or left as a void [7].

The importance of topology optimization is realized when the objective is to enhance the performance of a structure under various loading conditions. Such structures are frequently used in different industries, especially aerospace and automobile. For instance, a turbine blade used in a jet engine is under severe pressure as well as thermal and centrifugal loadings. Hence, it is necessary to adopt AM in the fabrication of these structures as well as obtaining a methodology to enhance their performance while reducing the weight.

Although topology optimization for mechanical loads is becoming easier to use due to available commercial software tools, implementing thermal load in topology optimization is still challenging. Since the nature of the thermal load is different than mechanical loads such as

concentrated force, pressure load, or gravity, it is difficult to extract feasible geometry from topology optimization based on thermal loads. This issue becomes even more challenging when combining thermal and mechanical loads.

1.2 Objectives

To employ topology optimization in designing a component that is working under different loading conditions, it is essential to contemplate specific considerations. The importance of this issue is more significant when the part is subjected to thermal load as well. Implementation of thermo-mechanical topology optimization with respect to the combination of different factors and filters affects the final result which is the goal of this thesis. Motivated with these ideas, the objectives of this work are presented as follows:

1. Propose a workflow for thermo-mechanical topology optimization in order to address one-way coupled or fully-coupled thermo-mechanical load into the optimization process;
2. Introduce a design or redesign methodology for additive manufacturing based on thermo-mechanical topology optimization;
3. Design a gas turbine rotor seal that is subjected to extreme loading conditions of high pressure and temperature and centrifugal load;
4. Validate the result of thermo-mechanical topology optimization by design of an experiment and measurement of the component performance under thermo-mechanical loads.

1.3 Outline

The presented thesis is structured in 6 chapters. Herein, an overview of the thesis is presented while the thesis motivations and objectives were presented at the beginning of the current chapter.

In Chapter 2, the background and a brief overview of additive manufacturing technologies are presented. Design for additive manufacturing as well as a few workflows in this context is discussed. In addition, structural optimization and related sub-categories are presented. Lastly, available commercial software tools for topology optimization were investigated and three of them were discussed in detail.

Chapter 3 provides the methodologies used for thermo-mechanical topology optimization. In this chapter, firstly, the density-based methods are compared. Considering available software tools, HyperWorks is chosen in order to perform the optimization. Additionally, some of the available control modulus and functions in the selected software are presented. Next, a workflow is introduced to perform thermo-mechanical topology optimization. In the end, a workflow is proposed for DfAM based on the proposed thermo-mechanical topology optimization.

In Chapter 4, the thermo-mechanical topology optimization is employed in the proposed workflow to redesign a gas turbine rotor seal. Firstly, load conditions and the factors affecting topology optimization are introduced. A set of variables and decision processes are proposed and 256 optimization simulations are performed. Then, a set of acceptable designs are selected using generated Matlab code, and a decision matrix is provided. Finally, one design is selected and generated using CAD software.

In Chapter 5, the validation of thermo-mechanical topology optimization and the proposed workflow for DfAM is investigated by designing an experiment. First, a cantilever is subjected to thermo-mechanical topology optimization. Three other parts with various designs are generated to be compared to this one. All four are printed with Laser Powder Bed Fusion (LPBF) technology with Ti6Al6V powder. An experimental setup is assembled to apply thermo-mechanical loads. In the end, the experimental data are compared to the results of heat transfer and applied force obtained from FEM.

Chapter 6. In the end, future work, based on the findings of the current thesis, is presented.

Chapter 2
Literature Review

2.1 Additive manufacturing

Additive manufacturing (AM), which is referred to as 3D printing is the formal phrase of a more general expression called rapid prototyping (RP) that is used in a variety of industrial applications [8]. An exact definition of AM is given by ASTM F2792-12A [9]: "*a process of joining materials to make objects from 3D model data, usually layer upon layer, as opposed to subtractive manufacturing methodologies*". There are also other terms used for AM including freeform fabrication, additive fabrication, additive techniques, additive processes, additive layer manufacturing, and layer manufacturing.

Additive manufacturing (AM) technologies have significantly advanced over the past thirty years. Stereolithography (SLA or SL) was the first 3D printing process that commercialized in 1987. SLA/SL is a laser/light-based process that works based on solidifying/crosslinking thin layers of chemical monomers layer by layer to form a 3D polymeric part [10]. Thereafter, many AM technologies were commercialized over the years. Interestingly, the commercialized AM technologies were not bounded to plastic or polymers, but also included metal and ceramic materials. The selective laser melting (SLM) system was developed for printing steel-based powder in 1991 [10]. A history of AM milestone and its impact on the aerospace industry is shown in Figure 2.1. AM processes can be categorized differently based on material feedstock, energy source or build volume [4]. Generally, AM technologies can be classified into 3 different categories: Gas-based, liquid-based, and solid-based printers [3], [11].

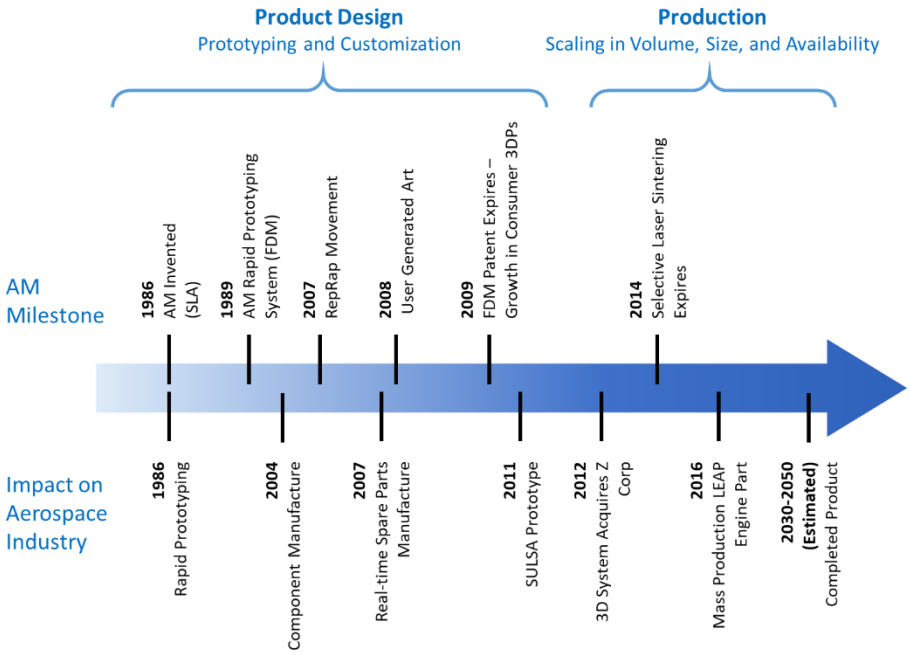

Figure 2.1 Additive manufacturing history [12]

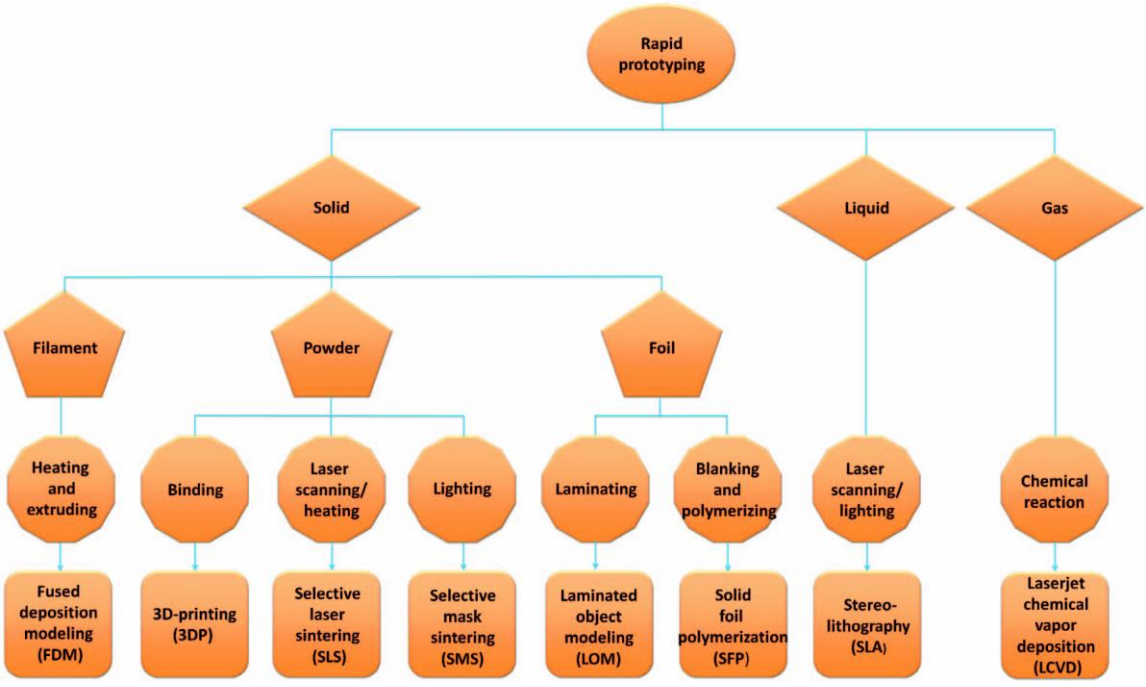

Figure 2.2 Additive manufacturing general categorization [11]

Different AM processes are displayed in Figure 2.2. The other classification of AM technologies and some of the popular printers used for each type of 3D printing are presented in Figure 2.3.

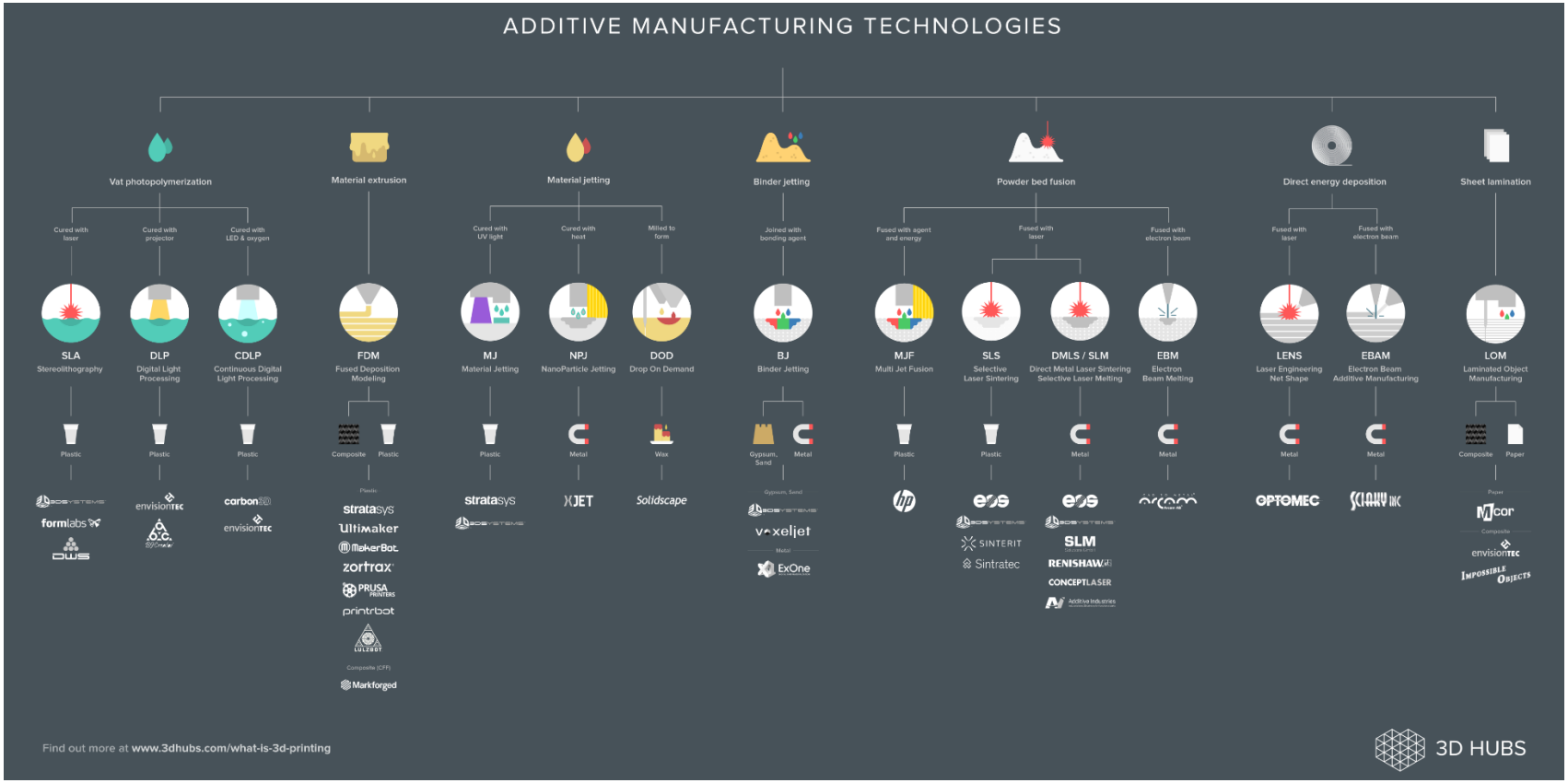

Figure 2.3 Additive manufacturing processes and some printers designed for each process [13]

2.1.1 Metal additive manufacturing

The AM technologies developed for 3D printing of metallic parts can be classified into three main categories including powder-bed, powder-fed and wire-fed systems [4].

2.1.1.1 Wire-fed Systems

Wire-fed systems are classified into 3 groups based on their heat and melting sources: laser-based, arc welding-based, and electron beam-based.

Compared to powder-bed and powder-fed systems, wire-fed systems can print relatively larger components at a faster pace. However, the components manufactured using wire-fed systems require more post-processing processes to reduce surface roughness and geometric tolerances.

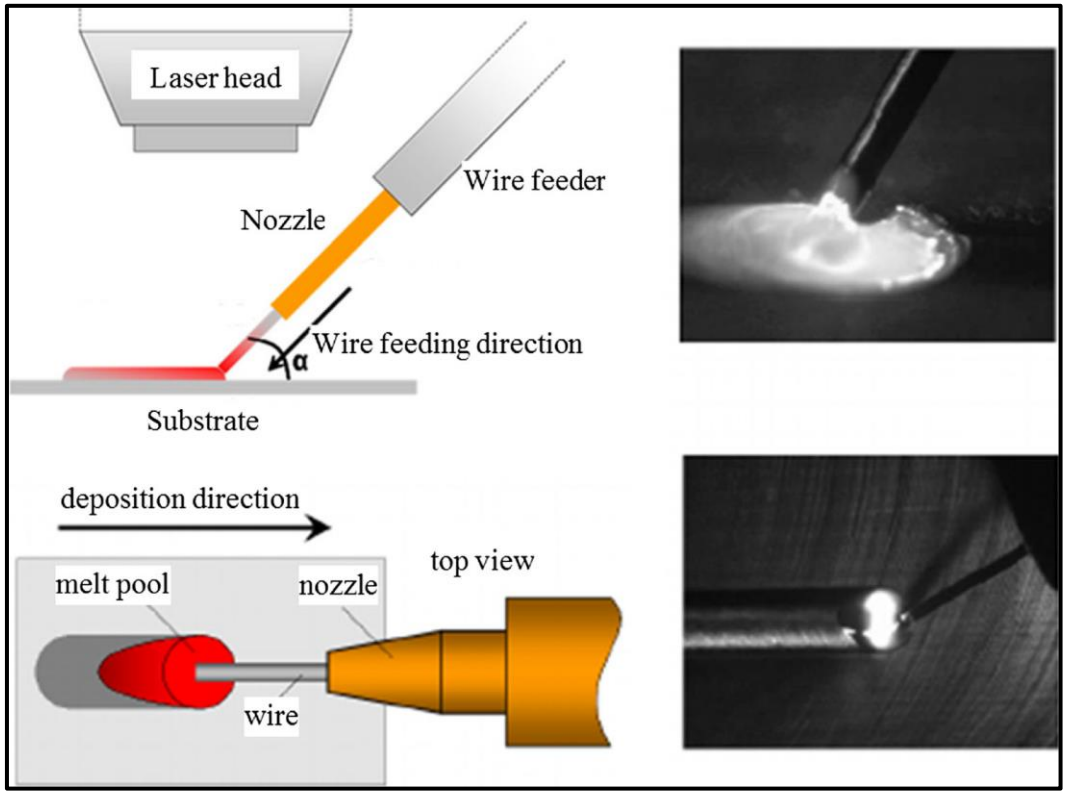

Figure 2.4 wire-fed system working process schematic [14]

2.1.1.2 Powder-fed systems

On the other hand, powder-fed systems are faster and can produce more complex and larger geometries. In these systems, the wire is replaced by powder and it is delivered to the substrate by a nozzle to form the desired shape [15], [16]. Direct Metal Deposition (DMD) and Laser Metal Deposition (LMD) are some other names commonly used for this process. These kinds of systems can be used to repair damaged components [4]. A schematic view of the powder-fed system is shown in Figure 2.5.

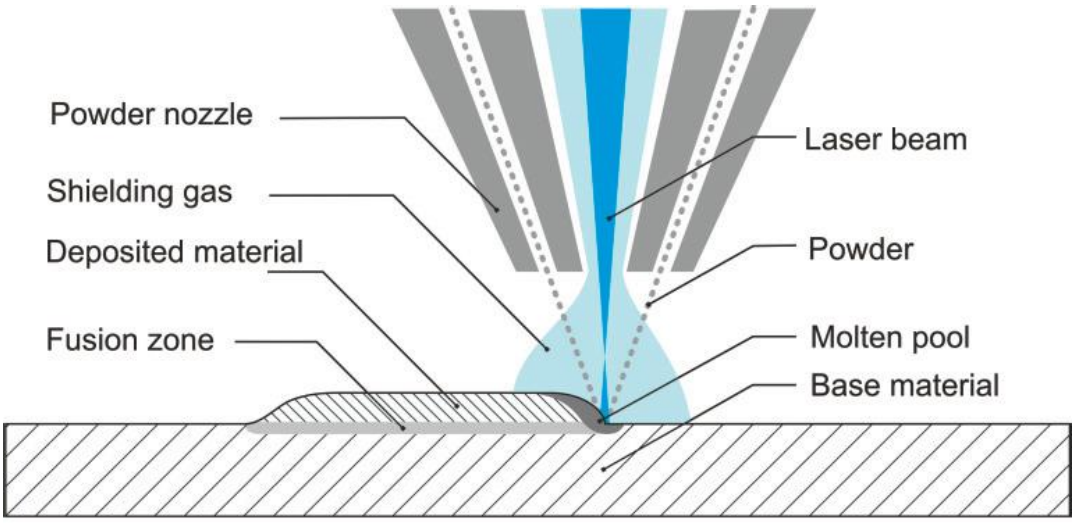

Figure 2.5 Schematic of laser metal deposition [17]

2.1.1.3 Powder-bed systems

Powder-bed systems, also known as Powder Bed Fusion (PBF), enable 3D printing of finer features in higher resolutions as the powder size or/and layer thickness decrease.

In PBF based technologies, a heat source liquefies selected regions of the powder-bed based on the imported CAD model. The main processes in PBF are known as Selective Laser Melting/Sintering (SLM/SLS), Electron Beam Melting (EBM), and Direct Metal Laser Sintering

(DMLS). SLM and DMLS are similar processes since both of them work based on a laser source. The main differences are the material used in the process and temperature of the powder-bed in which melting or sintering occurs [18]. On the other hand, the Electron Beam Melting (EBM) method uses an electron source to melt the powder under vacuum conditions [19].

2.1.1.4 Selective Laser Melting

Selective Laser Melting/Sintering (SLM/SLS), also known as Laser Powder Bed Fusion (LPBF), is one of the AM techniques. In this method, a high-power density laser is being used for selectively sintering and welding the powdered metallic materials together with the goal of forming a geometry. Unlike the SLS technique, SLM is capable of fully melting the metal powders and fusing them together. The printing process starts with preparing and slicing a CAD model followed by defining the printing parameters, tool paths, and etc. Then the file with all information in a specific format readable by the machine is loaded into the printer[20].

The printing process is conducted in a chamber with the controlled circulation of inert gases either argon or nitrogen. At first, the fine water or gas atomized metal powder is fed into the system through a hopper or container. The powder is transported to the sieving unit through the pipes and then to the distribution unit to be portioned based on the amount of powder used for one layer and fed to the system. Then a thin layer of the metal powder is uniformly spread on the build plate using a recoater or roller (see Figure 2.6). Each layer of the powder is about 15 to 500 μm depending on the machine. A high energy fiber laser selectively melts a thin layer of the powder to form a cross-section of the final part. Mirror reflecting units are used for redirecting the laser to manipulate the laser path for making the desired contours of the 2D slice. When the printing of each slice is finished, the recoater spreads a thin layer of the fresh powder on the build platform. The layer by layer process of selective melting of metal powder continues until the whole 3D

structure is built. Then the printed part is removed from the platform and after cleaning the excess powder on the surface and conducting the required post-processing procedures, the 3D part is ready to be used for the application [21], [22].

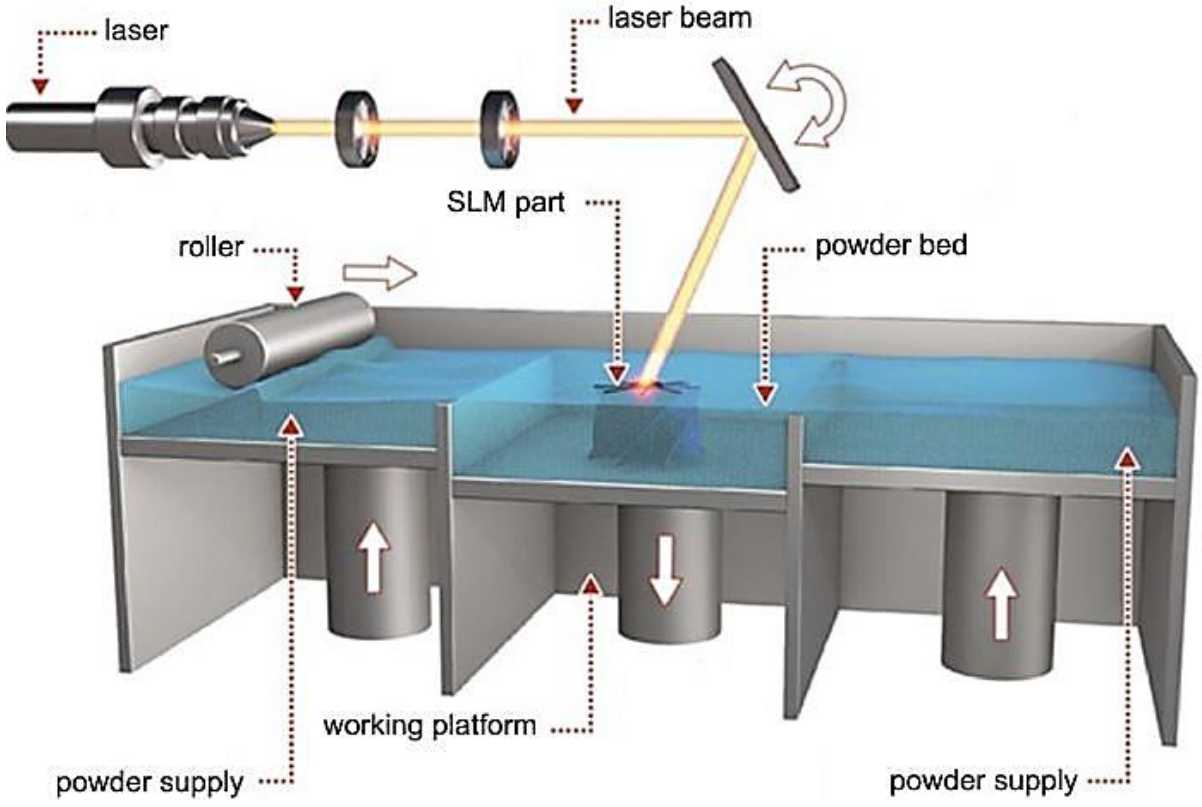

Figure 2.6. Schematic of SLM technology [23]

Reputable SLM Machine Manufacturers: EOS

EOS is a German company specialized in designing additive manufacturing machines founded in 1989. They currently have six metal printers on the market including EOS M100, EOS M290, EOS M300-4, EOS M400, EOS M400-4, and Precious M080 models [24], [25]. The technology used in these systems is mostly based on direct metal laser sintering (DMLS/SLM). EOS company also have plastic 3D printers working based on SLS technology [26]. The EOS M290 printer that contains a Ytterbium continuous fiber laser is utilized in the MSAM lab [24], [27].

Reputable SLM Machine Manufacturers: Renishaw

Renishaw is a British company that is an expert in the design and manufacturing of industrial 3D printers. They have developed four versions of metal 3D printers named RenAM 500M, RenAM 500Q, AM 250, and AM 400. These printers enable 3D printing of Titanium (Ti6Al4V), Aluminum (AlSi10Mg alloy), Cobalt chromium (CoCr), Stainless steel (316L) and Nickel alloys [25]. In this thesis, Renishaw AM400 is used to print the required samples for the experimental validation (Figure 2.7).

Figure 2.7 Renishaw AM 400 employed to print experimental samples

2.2 Design for Additive Manufacturing (DfAM)

After decades of evolutions and developments, AM is turning into one of the main manufacturing processes. AM gives more freedom to designers and allows them to produce more

complicated geometries [5], [28]. However, using AM to manufacture parts that are originally designed for conventional processes such as subtractive and casting techniques may not be beneficial. Therefore, to fully benefit from additive manufacturing advantages, parts are required to be designed and redesigned (if necessary)specifically for AM [5].

Hauge et al [29] presented some implications on designs for additive manufacturing and publicized some necessities and fundamentals for the design for additive manufacturing. After that, several methods and strategies were proposed as a guideline for DfAM. It is also called DAM, DLM (design for layer manufacturing), and DFX in some literature [1], [30]. In DFX, X stands for extra consideration which is required when designing for AM such as assembly, reliability, cost, accessibility, and etc. [5].

Some guidelines and methods for DfAM are proposed in the literature [1], [5], [28], [30]–[38]. Two of them are presented and discussed below to get familiar with the process and explore the workflow of the DfAM.

M.K. Thompson et al. [1] had drawn a complete workflow from a basic idea for designing a part to the fabrication of the component (Figure 2.8). This process includes two sections: digital and physical workflow. In the first section, 2D or 3D models are developed. These models can be generated using 3D scanners, CT scanners, or a simple draft of a part. Also, they can be directly imported to the system or reconstructed using CAD modeling software systems.

The next step is to add support structures to the part based on the direction of build. There are some software tools that can do this job automatically. The physical workflow starts with one of the seven available AM technologies that were mentioned before. These processes and the

potential materials that can be used in each process are presented in Figure 2.9. These groups of AM can be used to produce the end parts or tooling and fixtures for indirect production. [1].

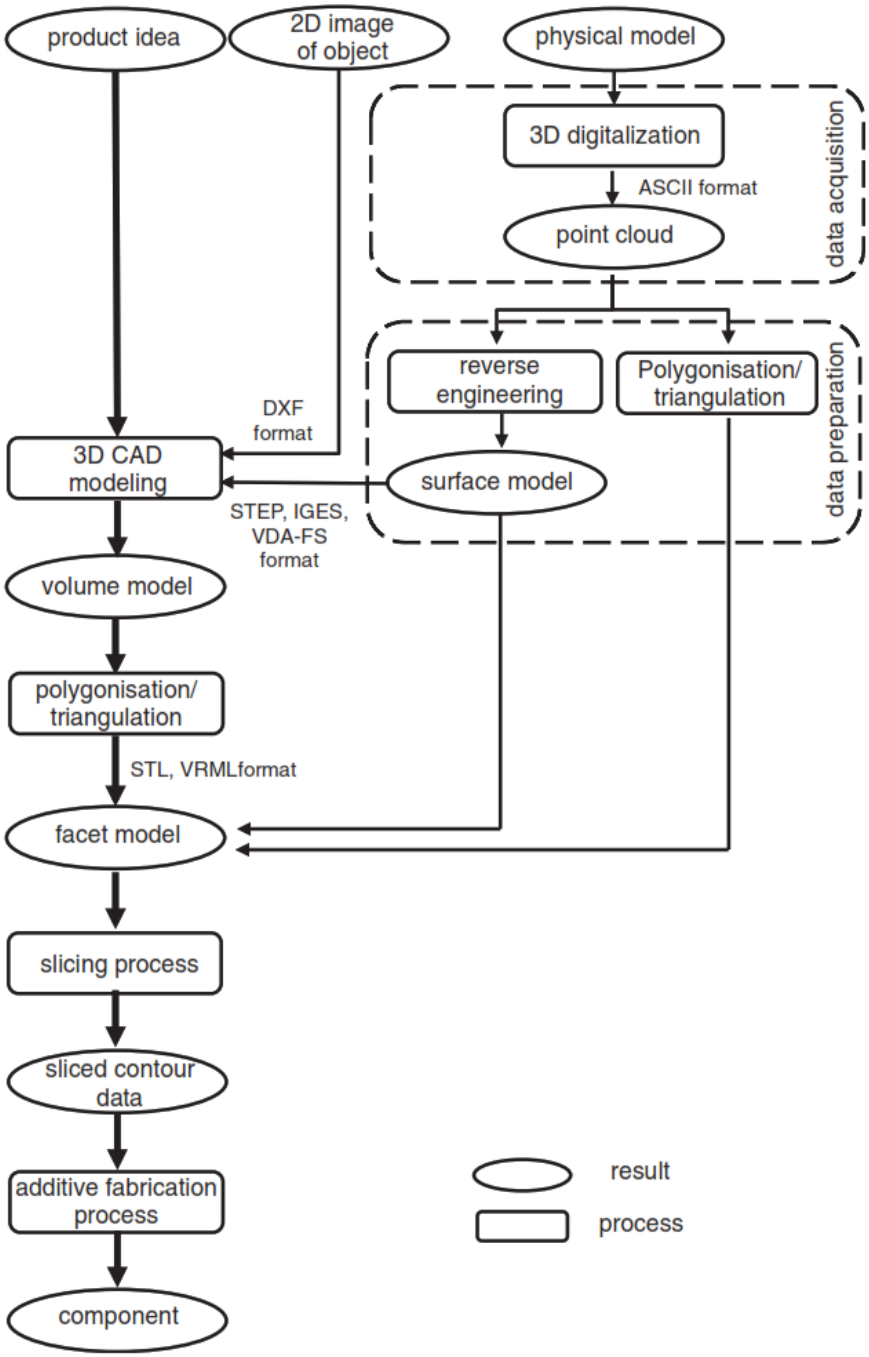

Figure 2.8 Proposed workflow for DFAM by M.K. Thompson et al. [1]

Materials	Example materials	Process categories						
		Vat photo-polymer-ization	Material jetting	Binder jetting	Powder bed fusion	Material extrusion	Directed energy deposition	Sheet lamination
Thermoset Polymers	Epoxies and acrylates	X	X					
Thermo-plastic polymers	Polyamide, ABS, PPSF		X	X	X	X		X
Wood	paper							X
Metals	Steel, Titanium alloys, Cobalt chromium			X	X		X	X
Industrial ceramic materials	Alumina, Zirconia, Silicone nitride	X		X	X			X
Structural ceramic materials	Cement, Foundry sand			X	X	X		
Note: Combinations of the above material classes, e.g. a composite, are possible								

Figure 2.9 Additive manufacturing processes and materials [1]

In addition to M.K. Thompson, Salonitis et al. [33] presented a methodology for redesigning components. Figure 2.10 illustrates a 5-step method for redesigning the components that were originally designed for conventional manufacturing.

The first step is to analyze and collect a set of functional specifications. Information such as loading conditions, material usage, and the manufacturing process need to be collected in this step. These kinds of information which are usually defined by design objectives should be taken into account during the early steps of the design to ensure that all the necessary factors are considered.

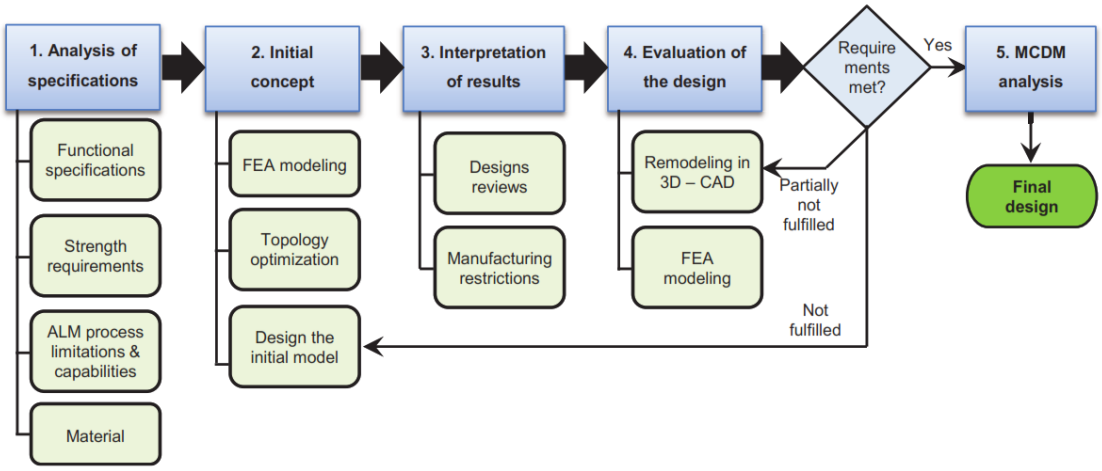

Figure 2.10 Proposed methodology for redesigning components by K. Salonitis et al. [33]

The second step starts with Finite Element Analysis (FEA) modeling to display the critical areas of the design such as high-stress regions or deformed areas. Usually, the FEA modeling is followed by a structural or topological optimization to ensure obtaining the optimal shape for a set of loads. Consequently, a conceptual design, which may contain complex features, can be achieved based on the FEA modeling and topology optimization.

The third step in the proposed process of redesigning a component is interpretation. On this level, the design should be reviewed to check the manufacturability of the part. A list of manufacturing restrictions should also be defined, and guidelines for the printing process such as minimum slicing thickness, speed of the laser, and need for support structure ought to be considered to make sure the part can be printed properly.

The fourth step is to evaluate the design by FEA modeling. This step can contain different simulations under different loading conditions to obtain improved mechanical strength and fatigue life. In this section, all the restrictions and guidelines should be taken into account. These processes should be repeated until the validation of the final result.

The goal of the final step which is called Multi-Criteria Decision Making (MCDM) is to choose the best design among all the acceptable concepts. Different methods can be used to choose the optimal design: The graph theory and matrix approach (GTMA), analytic hierarchy process (AHP), and technique for order of preference by similarity to ideal solution (TOPSIS) are amongst the methods that can be used.

2.3 Structural Optimization

Structural Optimization is the process of finding the optimal state of a component or a system under a certain loading. This process can be divided into different categories. Size optimization, shape optimization, and topology optimization are among the most important aspects types of structural optimization which are explained further in the next sections [39]. Moreover, topography and composite optimization are among the other aspects of structural optimization which can be mentioned herein.

2.3.1 Size Optimization

Size or truss optimization is one of the main aspects of structural optimization. The size of a continuum member or a truss has a significant effect on the performance and weight of a design [40], [41]. Size optimization provides the optimum cross-section of each feature of the design while minimizing the weight of the whole structure. Size optimization should also satisfy constraints that restrict the design variables. The main restriction in the size optimization is that an initial design with discrete number of features is required to start the process of optimizing.

Many methods have been developed to solve the problems associated with size optimization; however, ongoing attempts still exist to make the process more efficient [42]. Some of these methods were named as Simulated Annealing (SA) by Kirkpatrick[43], Cuckoo Search [44],

Genetic Algorithm (GA) [45], Ant Colony Optimization (ACO) [46], and Particle Swarm Optimization (PSO) [47].

2.3.2 Shape Optimization

Once computers got more powerful and FEA modeling become further developed, the importance of shape optimization received more attention by the time [48]. In this context, the goal is to find the optimum topology within a predesigned object [49]. Since in shape optimization, the variable is the general shape of the design, it is mathematically more complicated than size optimization where the variables are just the size of features. A simple example of shape optimization is a hole within a panel under certain loading conditions. In this example, the size optimization is just changing the size of the hole, while shape optimization tries to improve the performance of the component by changing the shape of the hole [50].

2.3.3 Topology Optimization

Topology optimization is defined as a mathematical method to distribute material within a design space with the aim of maximizing the performance of the system [51]. The first paper on topology optimization gets back to 1904 when the Australian researcher, Michell, discussed the optimal layout of trusses. Later in 1976 and 1977, Parger and Rozvany presented a general theory for topology optimization. About 10 years after that, by progress on finite element analysis, Bendsøe and Kikuchi offered a numerical method to solve topological optimization problems in 1988 [52].

A comparison between size, shape, and topology optimization is presented in Figure 2.11.

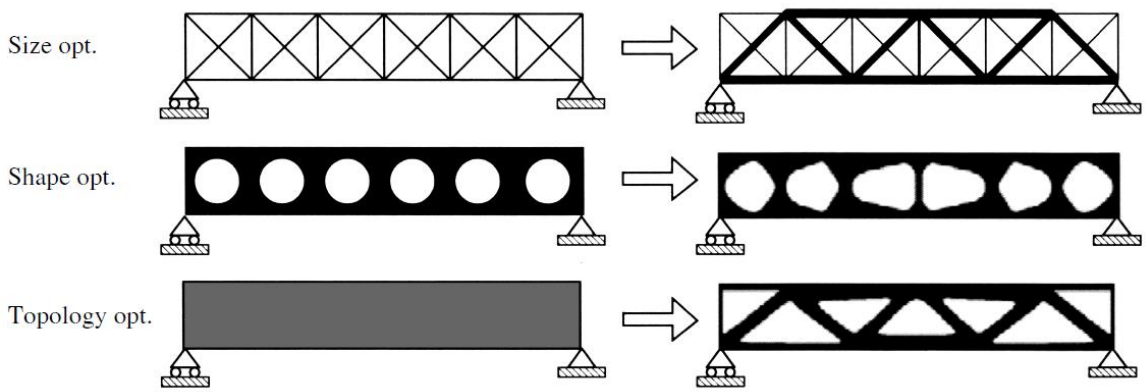

Figure 2.11 Structural optimization of a bridge using size, shape and topology optimization [53]

Three decades after Bendsøe's paper, several methods are investigated for topology optimization. These approaches are mainly characterized under 4 main categories of homogenization, hard kill, level set, and density-based methods [7], [51], [52]. Figure 2.12 shows these categories which are discussed below.

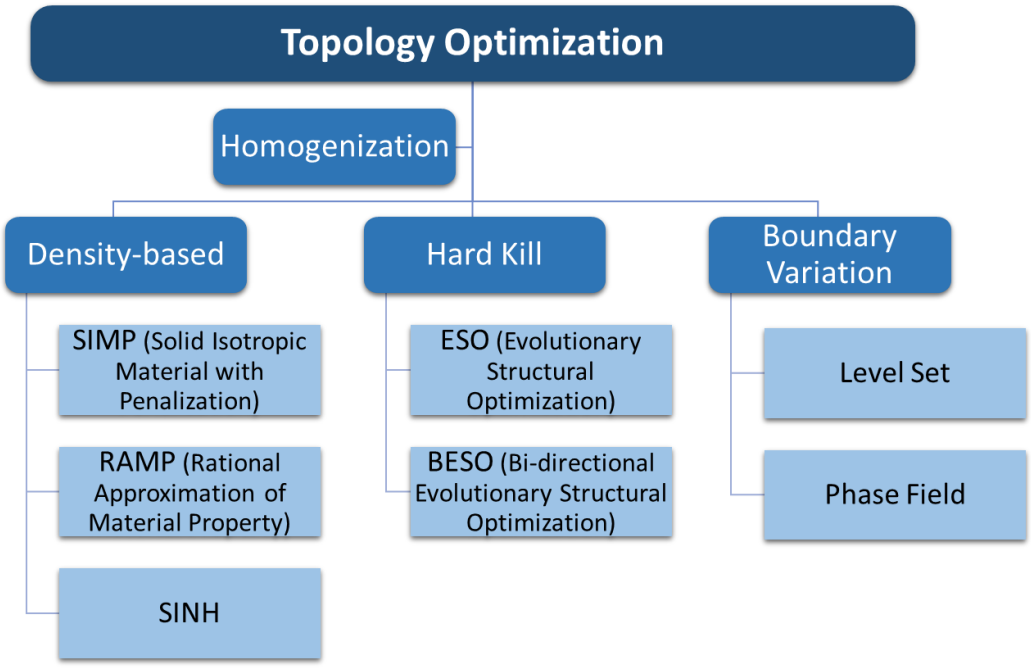

Figure 2.12 Topology optimization categories

2.3.3.1 Homogenization Method

The original homogenization method was introduced by Bendsøe and Kikuchi in 1988 [54], [55]. They realized that finding a solution is not likely unless they partition the problem set into smaller sections or areas with composite material. These smaller areas are basically micro size porous elements and the goal of the optimization is to find the proper porosity for each element[56]. Then the homogenization theory can be used to find out a relation between the material properties and the material density. In this way, the optimization turns into a density distribution problem [55]. This method was expanded into other methods and created the foundation of recent approaches [7].

2.3.3.2 Hard Kill Method

One of the important approaches for topology optimization is called “Hard Kill Method”. This method was developed by introducing Evolutionary Structural Optimization (ESO) which is the most-known method in this category [7]. ESO was first developed by Xie and Steven between 1993 to 1997 [57], [58]. It was initially suggested to reach an optimal criterion by gradually removing elements with the lowest stresses within the design domain. Later on, Chu et al. replaced stress by elements with the lowest strain energy in 1996 [57].

The problem associated with the ESO approach is that it is not able to add material as well as removing it. Thus, in 1998, Yang et al. proposed Bidirectional ESO (or BESO) which allows the material to be added on areas with the highest stress or sensitivity [57], [58]. Implementation of the BESO method in Matlab can be done by a few changes in the Matlab code published by Sigmond in 2001 which is originally developed for the density-based method [59].

2.3.3.3 Level Set Method

The Level Set Methods (LSMs) are complicated numerical techniques that are employed to find the optimal answer to a problem. Over the years, many researchers tackled structural optimization problems using these methods [60]. In these approaches, a Level Set Function (LSF) is employed to keep track of structural boundary motion under a controlled speed [60], [61]. LSMs were first introduced by Osher and Sethian [62]. These methods utilize the iso-surfaces of LSFs to implicitly target the outlines of the structure [60], [63].

2.3.3.4 Density-based Method

In 1988, only one year after introducing the homogenization method, Bendsøe presented a new approach to reduce the complexity of the homogenization method [7], [52]. This new method which is called Solid Isotropic Material with Penalization (SIMP), is the first density-based method presented in the literature. Thus, far, density-based methods are the most widely used approaches to an optimized structure within commercialized software tools [64]. Density-based methods, similar to the homogenization method, operate on a fixed design domain consisting of a finite number of elements. The goal is to obtain the optimal result by determining whether each element should be filled with material or represent a void [7], [64].

2.4 Software tools for topology optimization

As a result of advancements in different manufacturing processes, especially additive manufacturing, topology optimization gained more interest over the past years. Because of the significant body of research attracted to this field, lots of software developers and companies investigated the topology optimization modules. Many software tools have been introduced and each of them has its own pros and cons [65]. Some of these systems are educational tools and some

others are considered commercial systems. Table 2.1 shows some of these software tools and some of their capabilities are compared.

Exploring all of these software tools is challenging and time-consuming. Thus, in order to proceed with the project, three software tools that are commercially available have been focused on and discussed in the next sections.

Table 2.1 Comparison of some available software tools [65]

Software	Company	FEA platform(s)	Shape Optimization	Eigenvalue analysis/ optimization	Integrated result post-processing/ smoothing
Commercial tools					
Optistruct	Altair Engineering	Hyperworks, NASTRAN	Yes	Yes	Yes
Genesis	Vanderplaats R&D	Genesis, Ansys	Yes	Yes	Yes
SIMULA TOSCA STRUCTURE	FE_Design (Dassault Systems)	Ansys, Abaqus, NASTRAN	Yes	Yes	Yes
ATOM (Abaqus Unified FEA)	Dassault Systems	Abaqus	Yes	Yes	Yes
MSC.Nastran	MSC Software	NASTRAN	Yes	Yes	Yes
Inspire	SolidThinking (Altair Engineering)	Hyperworks (uses OptiStruct Solver)	No	Yes	Yes
Enhance	Within	integrated	Yes	Yes	Yes
PERMAS-TOPO	Intes	Permas	Yes	Yes	Yes
FEMtools optimization	Dynamic Design Soluthion	NASTRAN, Abaqus, Ansys	Yes	Yes	No
OPTISHAPE-TS	Quint	Ansys	Yes	Yes	Yes
NX	Siemens	NASTRAN	No	Yes	Yes
Educational tools:					
BESO3D	RMIT University	Abaqus	No	No	No
ParetoWorks	SciArt, LLC.	Integrated (Solidworks)	No	No	No
CATOPTO*	Creative Engineering Services	ABAQUS, ANSYS, NASTRAN, OPTISTRUCT, PERMAS, and TOSCA	No	Yes	No
topostruct	Sawpan Design	n/a	No	No	Yes
ProTOp	Center for Advanced Engineering Software and Simulations	standalone	No	No	No
SmartDO*	FEA-Opt Technology	Ansys (available workbench addin)	No	No	No
META4ABQ	n/a	Abaqus	No	No	No
TRINITAS	Linkoping University	standalone	No	No	No
TopOpt	TopOpt	standalone	No	No	No

*Outdated software

2.4.1 Siemens NX

Siemens NX is one of the most powerful software tools that can simulate an end-to-end process for topology optimization and design of a part for additive manufacturing. This software is CAD/CAM/CAE software that uses the Nastran platform to perform topology optimization. It is relatively easy to work with and the designer can use this software to do all of the necessary steps with no need for other software systems: from pre-processing and topology optimization, to validating and manufacturing simulation [66], [67]. Figure 2.13 shows an end-to-end workflow offered by Siemens for redesigning a part. Another advantage of this software is that the final results for topology optimization are much smoother than other software tools that the author worked with. However, other than a few options on the optimization modules, there are not enough areas for a researcher to investigate.

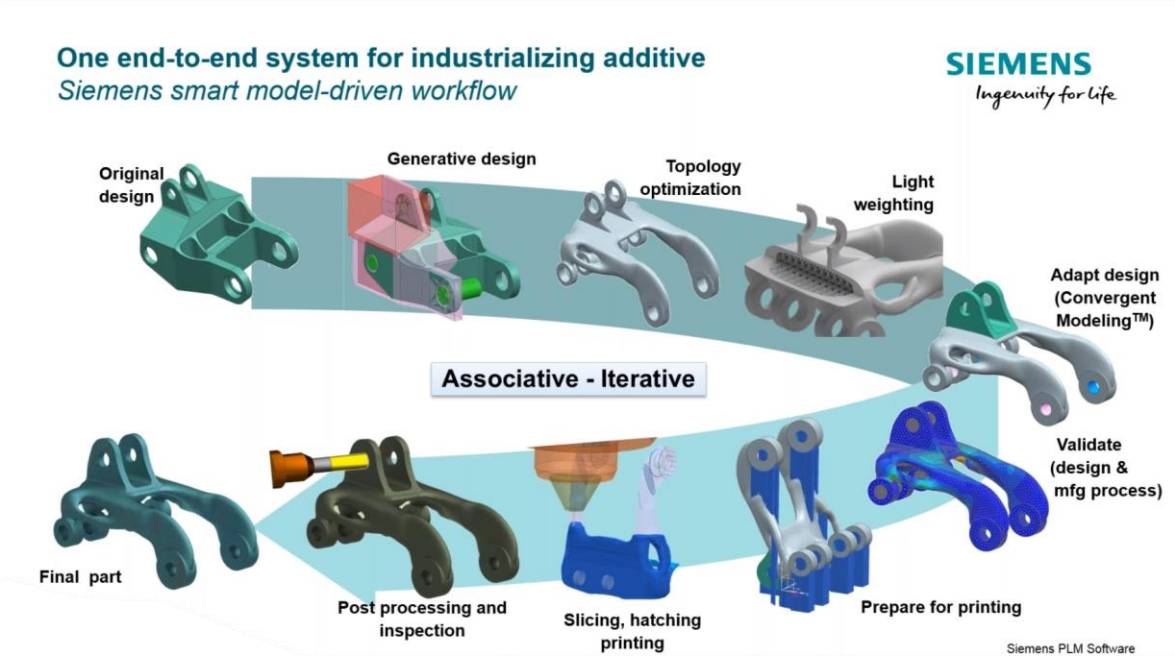

Figure 2.13 End-to-end process presented by Siemens NX [67]

2.4.2 SolidThinking Inspire

SolidThinking Inspire is one of the widely used topology optimization tools available on the market. This software that is presented by Altair Engineering Inc. is another user-friendly tool. One of the useful features that Inspire offers is PolyNURBS (which is also available on Siemens NX) [65]. This feature helps the user to build a CAD model based on the optimized part. Although this software provides the user with more features and modules than Siemens NX, the company still tries to keep everything as simple as possible.

Inspire is using OptiStruct solver to perform optimization [65]. An example of the Inspire interface is shown in Figure 2.14.

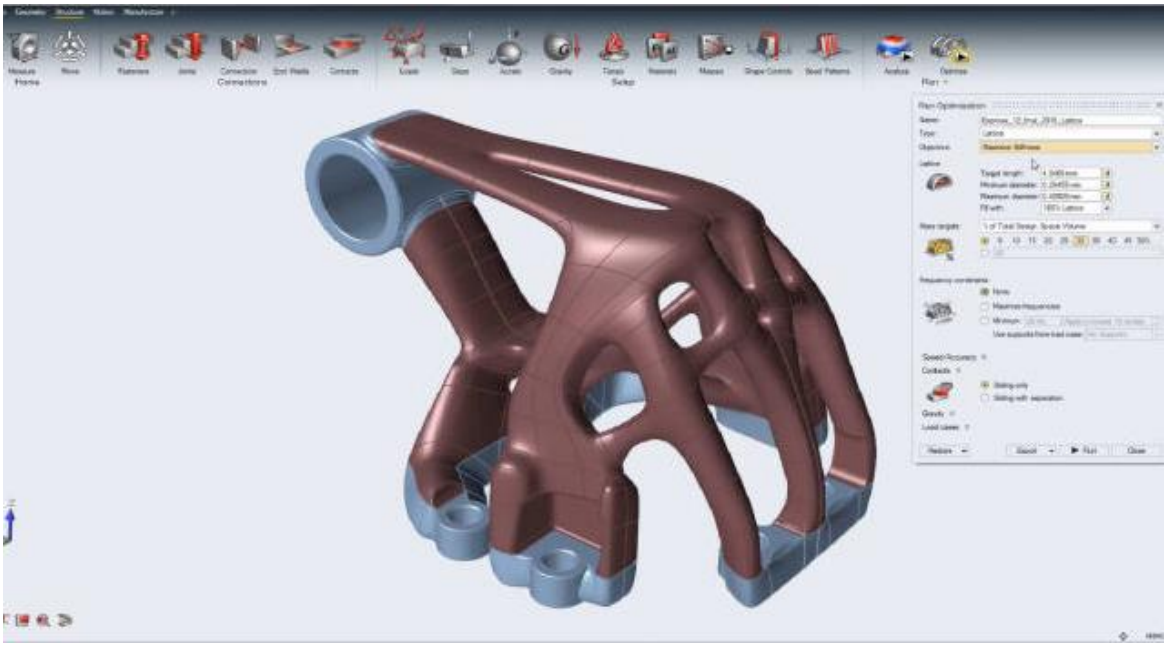

Figure 2.14 solidThinkig Inspire interface [68]

2.4.3 HyperMesh from HyperWorks

HyperWorks is another software by Altair Engineering. This platform has different modules for different applications. One of the well-known sub-software of the HyperWorks is HyperMesh.

This software, which is specially created to produce sophisticated mesh for FEM analysis, includes a topology optimization module that is well-known among its own kind.

The topology optimization module in HyperMesh, the same as Inspire, is using OptiStruct as a solver. Unlike Siemens NX and Inspire, it is relatively difficult to work with and has more features and control options. However, if a new user starts to work with HyperMesh with the aim of performing topology optimization, the software will produce reasonable results based on automatic assumptions for the specific case. It is also a proper tool if an expert wants to investigate more into topology optimization. A sample of workflow for topology optimization in HyperMesh is presented in Figure 2.15.

Because of the controllability of this software over the process as well as its advantages in performing multi-physics FEM analysis, it is chosen to be used in this thesis to implement thermo-mechanical topology optimization.

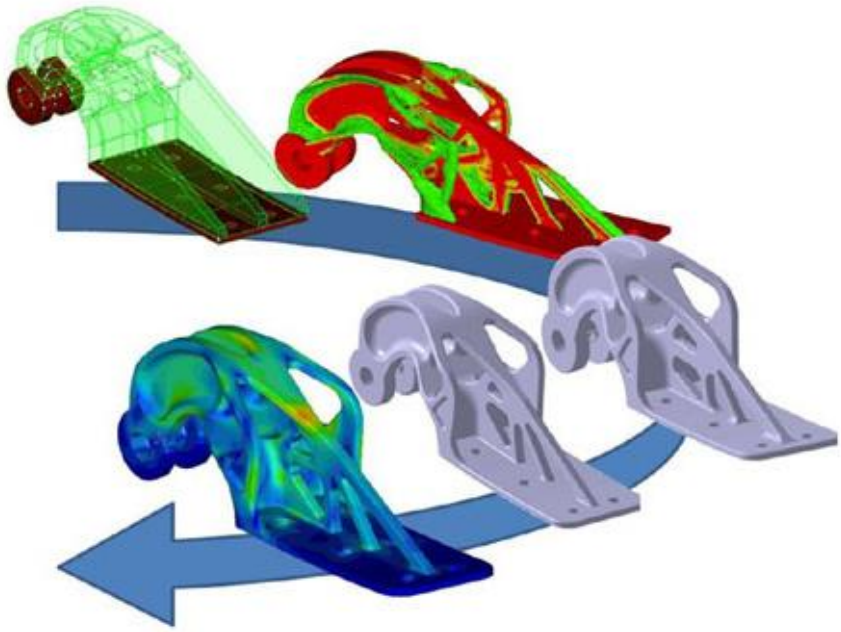

Figure 2.15 Component redesign flow by HyperMesh [69]

2.5 Summary

In this chapter, the history of additive manufacturing (AM) was presented, and its different categories were discussed. Then, the metal additive manufacturing as one of the significant categories of AM for commercialization was discussed in more details. A review of design methodologies for AM was also presented. Thereafter, different categories of structural optimization were presented. In the last section, different software tools for topology optimization were presented, and Siemens NX, SolidThinking Inspire, and Altair HyperWorks were discussed in detail and HyperWorks is selected to implement thermo-mechanical topology optimization. In the reviewed literature, the thermo-mechanical topology optimization was less investigated. This subject as well as combining different loads is investigated in the next chapter. Also, a workflow for DfAM based on thermo-mechanical topology optimization is discussed.

Chapter 3
Modeling and Topology Optimization

In Chapter 2, a brief description of density-based methods was presented. Herein, a more detailed approach to the mathematical presentation of the problem is taken.

3.1 Topology optimization based on SIMP method

A general optimization problem in Solid Isotropic Material with Penalization (SIMP) approach can be defined as:

$$\begin{aligned} &Minimize && l(u) \\ &subject\ to && a(u,v) = l(v), \quad \forall v \in V \\ &and && design\ constraints \end{aligned} \tag{3.1}$$

Above, $l(\mathbf{u})$ and $a(\boldsymbol{u},\boldsymbol{v})$ are respectively the external and internal work done on the structure. In density-based method structural optimization, the external work represents the compliance energy of the structure. As a result, equation 3.1 becomes [64]:

$$\begin{aligned} &min && f(x) = F^T U(x) \\ &subject\ to && K(x)U(x) = F \\ & && g_i(\rho, U) \leq 0 \\ & && 0 < \rho \leq 1 \end{aligned} \tag{3.2}$$

Above, f is the objective function (compliance energy), K and U are the stiffness and displacement matrixes, x is the design variable, ρ is the vector of density design variables, F is the force vector, and g is the design constraint.

The objective function of the structural optimization designed for density-based methods is usually defined to minimize the compliance or maximize the stiffness of the material.

$$f = c = U^T K U \tag{3.3}$$

Where *c* demonstrates compliance. Also, the constraint would be defined as:

$$g = \frac{V}{V_0} - v_f \leq 0 \tag{3.4}$$

Where V and V_0 are material and design domain volumes, and v_f is defined as allowable material volume.

The density of each element can be defined as:

$$0 < \rho_{min} \leq \rho_e \leq 1 \tag{3.5}$$

ρ_{min} is defined in a way to prevent the value of the density from reaching zero which causes some problems in specific cases. These problems are mainly caused by a singularity forms in finite element matric. This issue leads to difficulties in reappearing the elements with zero density into the calculations in the defined problem.

3.1.1 Sensitivity

It is important to recognize the most valuable elements within the design domain to preserve. As a result, calculating the sensitivity of each element regarding the applied force is required to decide which elements worth preserving. In all of the gradient-based methods, the process of

optimization depends on how changes in each design variable affect the objective function (here known as compliance). Thus, sensitivity can be calculated as:

$$\frac{\partial c}{\partial \rho_e} = \frac{\partial (f_e^T u_e)}{\partial \rho_e} \tag{3.6}$$

Based on equations 3.3 and 3.6, after rearrangement of terms, the sensitivity can be rewritten as [70]:

$$\frac{\partial c}{\partial \rho_e} = -u_e^T \frac{\partial (K)}{\partial \rho_e} u_e \tag{3.7}$$

Considering *K* as a function of the density of each element, equation 3.7 becomes:

$$\frac{\partial c}{\partial \rho_e} = \frac{\partial \Phi}{\partial \rho_e} E_0 u_e^T k_0 u_e \tag{3.8}$$

Where Φ is the interpolation function and E_0 is Young's modulus of the material.

3.1.2 Interpolation function

The equations discussed in the previous section are common for all density-based methods. Nevertheless, the difference is amongst the interpolation function that defines different approaches within this category. A critical aspect of density-based optimization is finding the proper interpolation function. The density and consequently Young's modulus of each element varies in this method[7], [64]. Different interpolation represents different approaches in this category. Some of the well-known interpolation schemes are recognized by Solid Isotropic Material with Penalization (SIMP), Rational Approximation of Material Properties (RAMP), and SINH (named because of usage of hyperbolic sine in the equation) presented below[70], [71].

$$SIMP: \quad E(\rho_e) = \rho_e^p E_0 \tag{3.9}$$

$$RAMP: \quad E(\rho_e) = \frac{\rho_e}{1 + p(1 - \rho_e)} E_0 \tag{3.10}$$

$$SINH: \quad E(\rho_e) = \eta E_0$$

$$where \quad \eta = \begin{cases} 1 & if\ p = 1 \\ 1 - \dfrac{sinh\big(p(1-\rho_e)\big)}{sinh(p)} & if\ \ p > 1 \end{cases} \tag{3.11}$$

The sensitivity of each element can be calculated based on the interpolation function. A comparison between different interpolation functions is shown in Figure 3.1. In this figure, ρ represents density and p is the penalization/penalty factor for the SIMP and SINH, and q is the penalization parameter for RAMP.

The SIMP method which is also referred to as the power-law or fractional material model has a zero sensitivity at densities close to zero. On the contrary, non-zero sensitivity of RAMP and SINH at densities close to zero would make it easier for the elements with lower density to reappear on the design domain. This is one of the advantages of these methods over SIMP. In addition, Figure 3.1 (c) demonstrates that the SINH interpolation function is almost a mirror of SIMP.

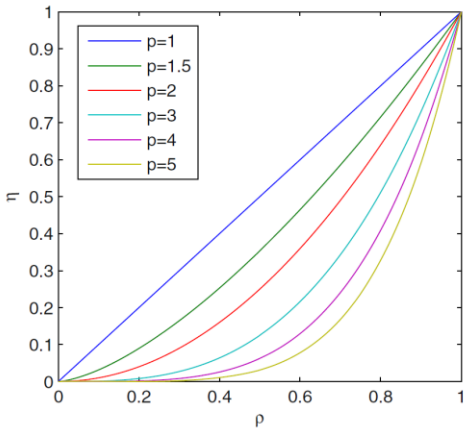

(a)

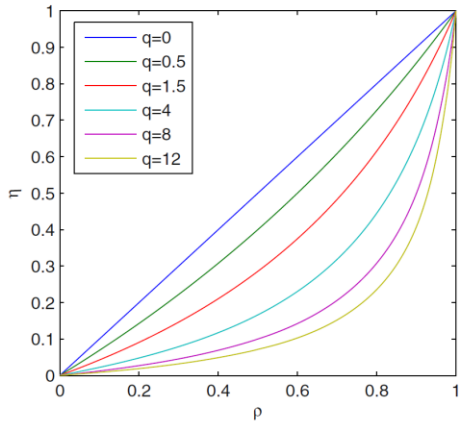

(b)

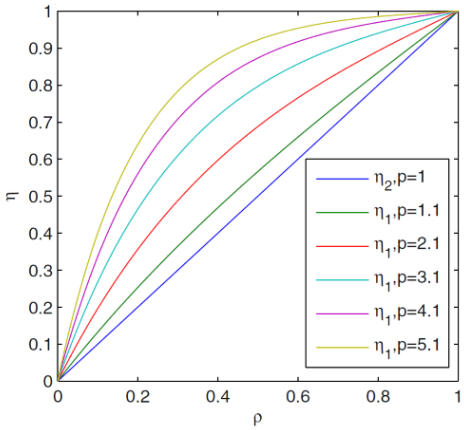

(c)

Figure 3.1 A comparison between interpolation functions of a) SIMP, b) RAMP, c) SINH [64]

Using the SIMP interpolation function, the topology optimization problem is defined as:

$$\begin{aligned} \min \quad & c(x) = F^T U = \sum (\rho_e)^P u_e^T k u_e \\ \text{subject to} \quad & KU = F = \sum F_m^e \\ & \frac{V}{V_0} - V_f \leq 0 \\ & 0 < \rho_{min} \leq \rho_e \leq 1 \end{aligned} \qquad 3.12$$

A general flowchart for topology optimization is presented in Figure 3.2. First of all, the essential information such as design space, loading, and meshing need to be imported. Then FEM analysis should be performed. Sensitivity analysis can be conducted based on the FEM results. Filtering is an optional step that improves the final result [72]. Mesh independence and checkerboard are among the more common filters that are discussed in the next chapter. Afterward, density distribution should be updated based on sensitivities. The abovementioned steps should be iteratively repeated until all the requirements are met and the process converges.

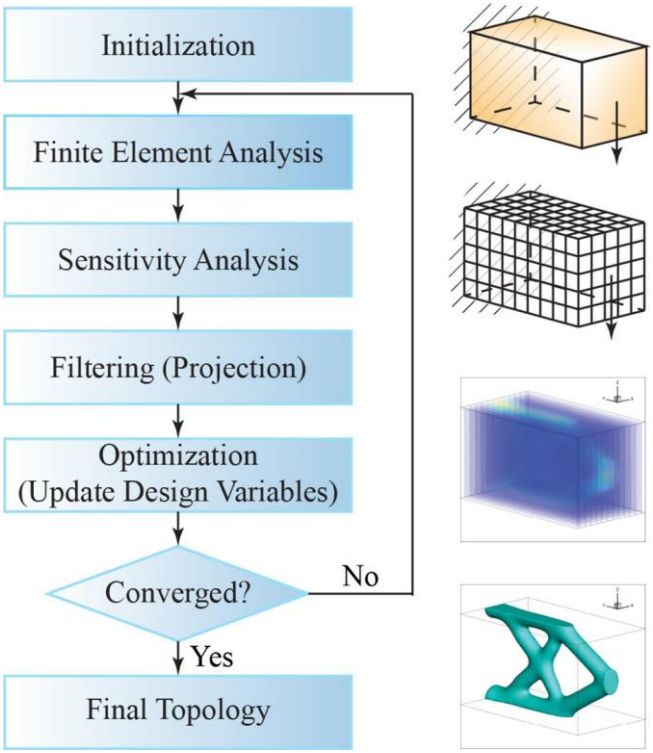

Figure 3.2 A general topology optimization scheme using SIMP method [72]

3.2 Software tool for topology optimization: HyperMesh

As mentioned in Chapter 1, in HyperMesh, the user has much more control over the process. One of the advantages of this software is to perform multiphysics FEM analysis that makes it possible to do thermo-mechanical topology optimization. Although post-processing on

HyperMesh is not as powerful as Siemens NX and Inspire, because of its advantages over the other software tools, it has been chosen to investigate more.

3.2.1 Control modules and functions in HyperMesh

Besides the sensitivity filtering which is quite necessary for topology optimization, lots of other filters can be used to reach the desired final part. Furthermore, many parameters can be changed to study their effect on the optimization result.

Some of these filters and parameters that can be controlled in HyperMesh are discussed below. Since there are different equations and methods to control each filter and parameter, it is not clear which one is implemented in OptiStruct. Thus, no equation is presented to avoid any confusion.

3.2.2 Checkerboard

In the process of topology optimization, sometimes the final result contains checkerboard-like patterns which are not desired in a design. The checkerboard filter can help to avoid this effect. However, the side effect of using this controller is that sometimes partial-dense elements will appear in the part of the transient section from full-dens elements to non-dens ones.

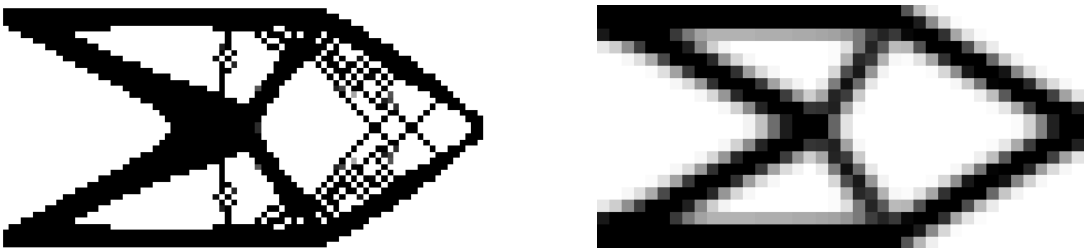

(a) (b)

Figure 3.3 a) checkerboard effect, b) optimization with checkerboard filtering [73]

3.2.3 Minimum and maximum member size

Restricting member or feature size is useful to get the preferred member minimum or maximum feature sizes within the part. Figure 3.4 shows how changes in minimum member size can change the final geometry. The figure presented in left (a) has a lower minimum filter than the right one (b).

(a) (b)

Figure 3.4 effect of minimum member size on topology optimization [74]

3.2.4 Overhang angle

An overhang angle filter is especially useful for AM fabrication. This filter is applied to assure a support-free part to reduce fabrication and post-processing costs. According to the literature, roughly 40%-70% of the fabrication costs can be reduced by manufacturing support-free components. [75].

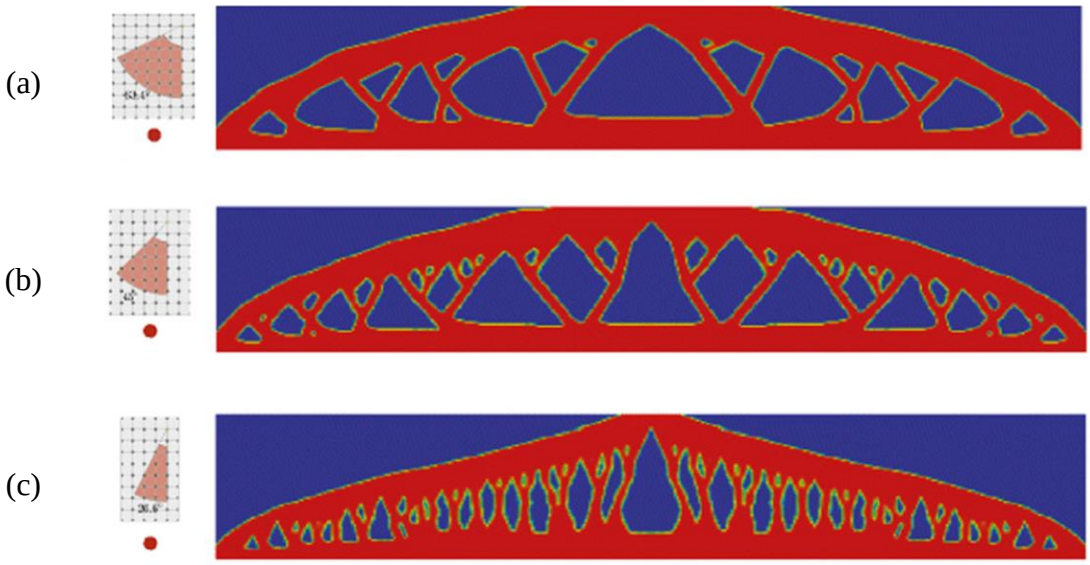

Figure 3.5 Optimization with overhang angle filter of a) 26, b) 45, c)63 degrees [75]

3.2.5 Weight factor

When a component is subjected to multiple load cases with different boundary conditions, weight factors can be applied to obtain a better result. The weight of each load case means the importance of that load for the optimizer module. Figure 3.6 demonstrates how the weight factor can change the final layout of the optimized part. In addition, it is usually necessary to use weight factor in multi-loading topology optimization; otherwise, the optimization may end up with a meaningless outcome.

Figure 3.7 brings up the issue of combining all the applied forces into a single load case. From the physical point of view, the final result is not reasonable since the density plot is not connected to the base or constraints sections. Thus, using multiple load cases seems necessary.

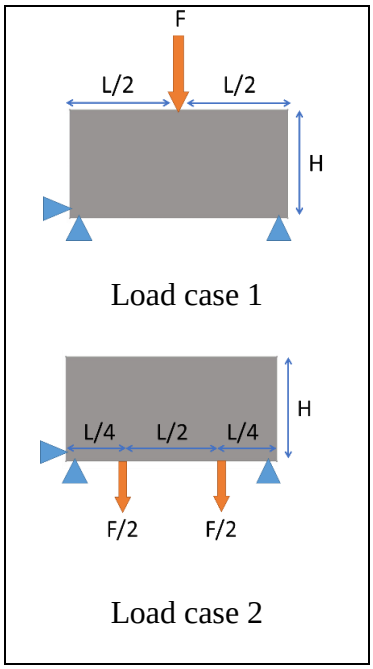

(a)

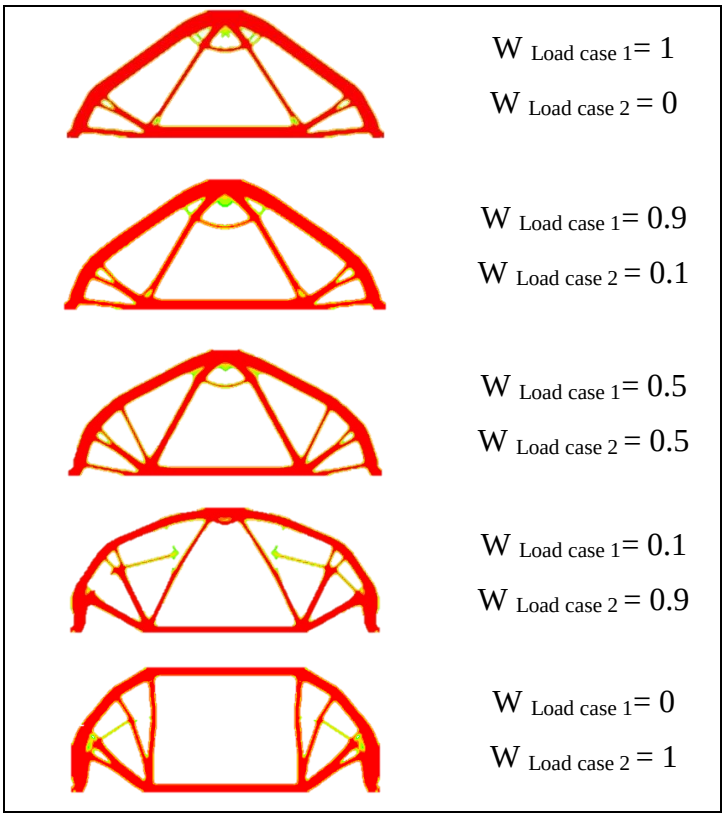

(b)

Figure 3.6 a) Two applied load cases,

b) Density plot determined subjected to weight factors (W)

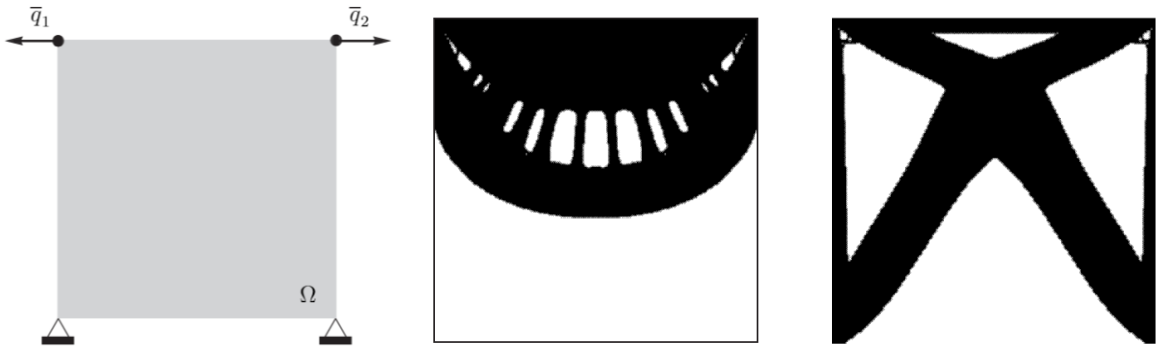

(a) (b) (c)

Figure 3.7 a) Initial boundary condition, b) Single load case, and c) Multiple load case [76]

3.2.6 Other control modules

There are numerous modules and controlling cards existing in the HyperMesh software tool that can be used in topology optimization. Mentioning all of these modules that bring incredible control over the process, may not be necessary, but some other control cards are named below:

- **Optimization algorithms:** in HyperMesh, different algorithms are provided that can be chosen for topology optimization.
- **Penalization factor:** choosing different values of penalization/penalty factor is another option provided by HyperMesh.
- **Extrusion:** this filter is applied when a uniform profile is needed through the part.
- **Draw:** this function is specially designed for traditional manufacturing and can be applied for specific processes such as milling that needs access through the part from one side.
- **Symmetry pattern:** in order to produce a symmetrical geometry over a plane, line, or a dot, this filter can be used.
- **Repetition pattern:** based on the designing requirement, a repetition pattern can be applied to the optimization process.
- **Fractional move limit:** the maximum move limit for updating densities on each iteration can be controlled by this function.
- **Lattice structure:** a relatively new feature added on HyperMesh is the lattice structure that can be used for optimization, however an output cad file cannot be provided for resultant lattice structures.
- **Convergence criterion:** if the relative change in the objective function between two iterations less than the convergence rate, the final result is achieved. Sometimes

optimization process stops at early stages because convergence has been met while the result does not make much sense. Decreasing convergence criterion can help to prevent the topology optimization to be caught in those stages.

3.3 Thermo-mechanical topology optimization

Coupled-field analysis is a finite element analysis that combines two or multiple physical fields. Generally, there are two methods to perform FEM on multi-physics problems: sequential and direct coupling [77]. Sequential coupling, which is used in this study, a physical field is analyzed before the second one starts. The results of the first analysis are considered as input for the second one as a boundary condition or load [77].

In this study, thermal and mechanical fields are coupled to obtain the final result. By performing a thermal FEM analysis, temperatures are obtained and form a boundary condition for the second stage of analysis and optimization. The global equation for thermal and mechanical force is explained as below:

$$KU = F = W_m F_m + W_{th} F_{th} \qquad 3.13$$

Where F_m is the global load and F_{th} represents the thermal load caused by temperature change. W_m and W_{th} are respectively the weight factors for mechanical and thermo-mechanical loads. This coupled analysis does not change the whole topology optimization process, while equation 3.2 turns into equation 3.14:

$$\begin{aligned} \min \quad & c(x) = F^T U = \sum (\rho_e)^P \, u_e^T k u_e \\ \text{subject to} \quad & KU = W_m F_m + W_{th} F_{th} \\ & = \sum W_m F_m^e + W_{th} F_{th}^e \\ & \frac{V}{V_0} - v_f \leq 0 \\ & 0 < \rho_{min} \leq \rho_e \leq 1 \end{aligned} \tag{3.14}$$

Also, the sensitivity can be defined as:

$$\frac{\partial c}{\partial \rho_e} = 2W_{th} U^T \frac{\partial (F_{th})}{\partial \rho_e} - W_m U^T \frac{\partial (K)}{\partial \rho_e} U \tag{3.15}$$

After a series of calculations, the sensitivity for thermo-mechanical topology optimization based on SIMP method can be obtained by [77]:

$$\begin{aligned} \frac{\partial c}{\partial \rho_e} = {} & 2W_{th} P \rho^{(2p-1)} U^T \frac{\alpha E \Delta T}{1-\mu} [-1 \; -1 \; 1 \; -1 \; 1 \; 1 \; -1 \; 1]^T \\ & - W_m P \rho^{P-1} U^T K U \end{aligned} \tag{3.16}$$

Based on HyperMesh and OptiStruct, and the number of features they provide, two different strategies can be developed for performing thermo-mechanical topology optimization. The modified versions of thermo-mechanical modeling based on the general topology optimization flowchart are provided in Figure 3.8.

The first method is demonstrated in the flowchart in Figure 3.8 (a). This process starts with defining design and non-design spaces with the goal of locating sections that need to be included in or excluded from topology optimization. Then, the loads and boundary conditions should be defined for starting the optimization. In this step, both mechanical and thermal boundary conditions should be considered. Then, a heat transfer analysis is performed based on the applied

boundary conditions following by extracting the nodal temperatures. In this stage, the extracted grid temperature acts as a boundary condition for static FEM analysis. The following steps are a typical optimization problem including sensitivity analysis, applying required filtering, and updating element densities (design variables). This flow should iteratively be repeated until the convergence occurs. Then, the final stages would be smoothing the optimal result and post-processing. As the diagram shows, the thermal analysis stage is performed on each iteration. Because of that, the total process time would be much higher than classic topology optimization. Although step-by-step thermal analysis might lead to more accurate simulation results, the thermal boundary conditions have to be placed on non-design elements to ensure proper heat transfer.

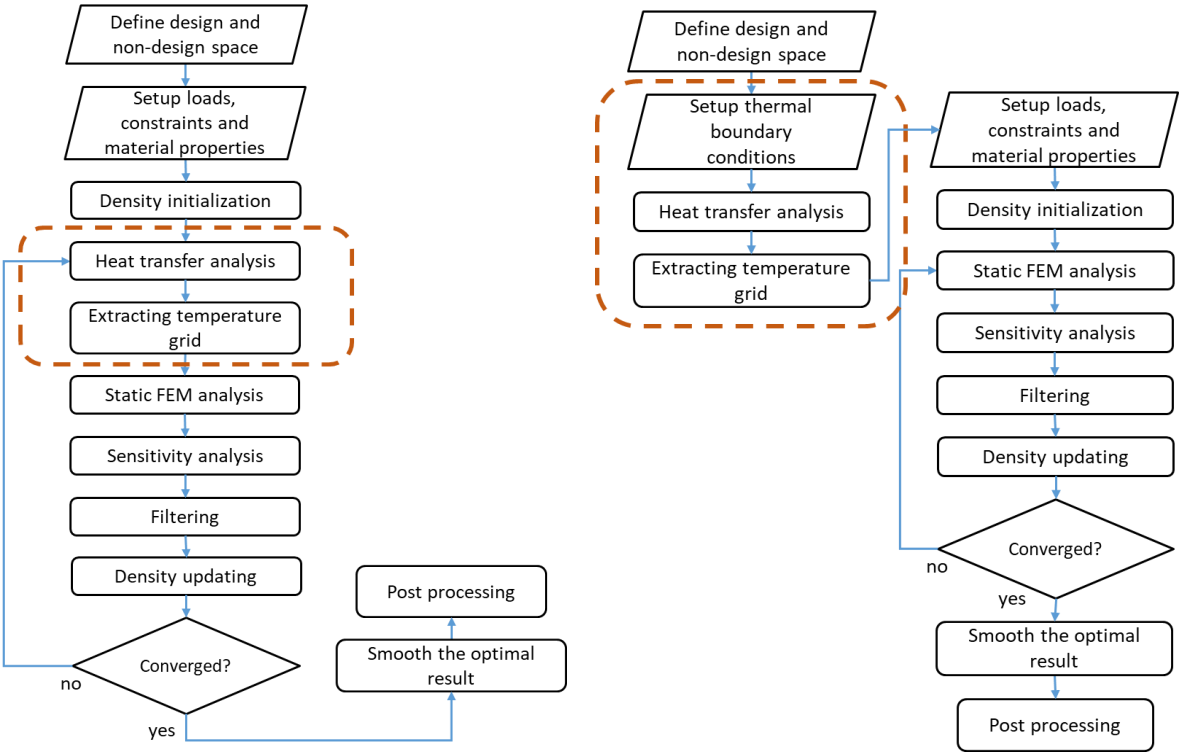

(a) (b)

Figure 3.8 The schematic diagrams for thermo-mechanical topology optimization

The second approach, presented in Figure 3.8 (b), is similar to the first approach. This approach starts with defining the design and non-design spaces. Then, the thermal boundary condition is set and a one-time heat transfer analysis is performed. The next step is to extract the temperature gradient into an output file. At this point, the grid temperature is manually imported to the HyperMesh along with other mechanical boundary conditions. After that, FEM analysis, sensitivity analysis, filtering and design variable update should be conducted in sequence. This process should be repeated until the occurrence of convergence. Then the final steps would be smoothing and post-processing of the part. The only difference with the previous method is that in the one-way coupled thermo-mechanical topology optimization, the thermal analysis is out of the loop after the first iteration and will not update as the geometry does. This process may not be as accurate as of the first one, but it is applicable if the thermal boundary conditions are placed on design elements in which their density varies on each iteration. Moreover, implementing this method is more time-efficient since it does not need to update the temperature gradient on each iteration.

3.4 Design for additive manufacturing workflow

In order to redesign a component, a design/redesign process has been developed as shown in Figure 3.9. In the beginning, design and non-design spaces should be defined. The next step is to set up boundary conditions considering all the applied loads and constraints. Then, design criteria should be introduced to account for all the factors that can contribute to the topology optimization results. The goal of this stage is to recognize the most influential factors, consider them as variables, and then perform multiple topology optimization on them. Afterward, it is essential to come up with a decision-making process, to be able to choose the best results. The next step is

topology optimization based on all the important variables. After collecting all the results from the previous stage/s, the post-processing and refinement should be done to achieve the final design.

All of the proposed steps in this methodology for redesigning an existing component, as a case study, will be discussed in the next chapter.

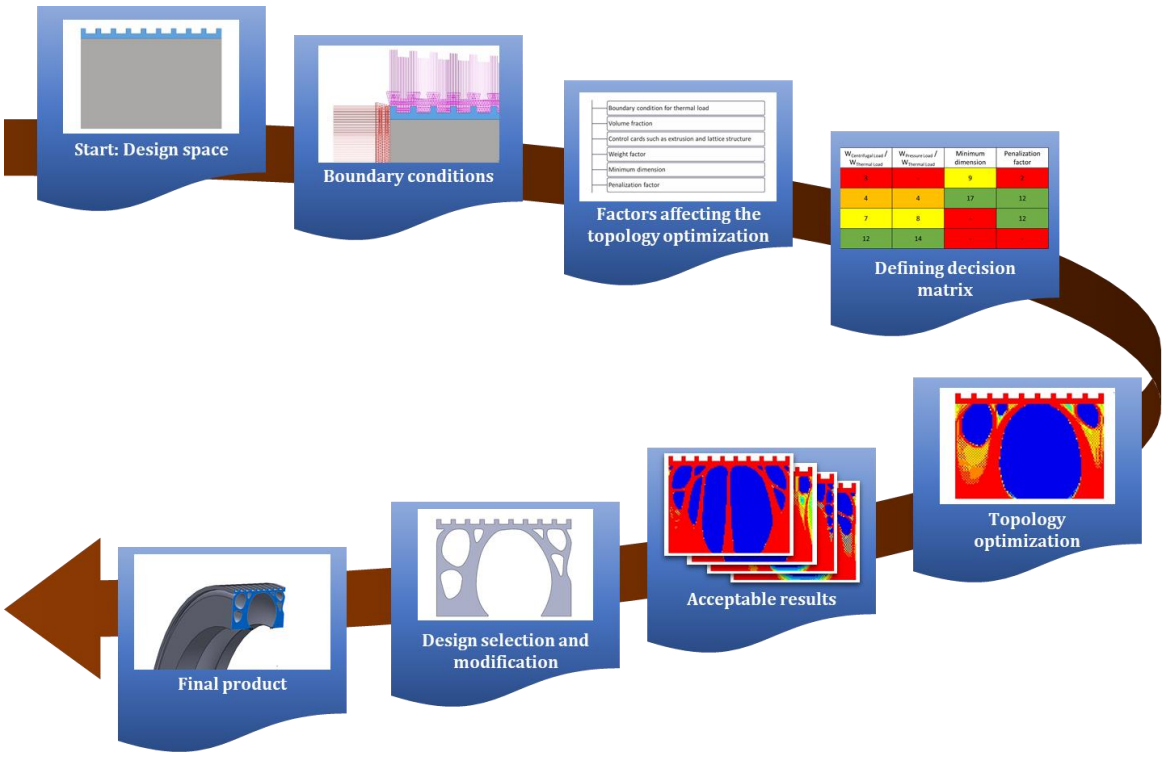

Figure 3.9 Schematic diagram of the workflow for generative design/redesign of a component by implementing the topology optimization algorithms imbedded in HyperMesh

3.5 Summary

In this chapter, at first, the density-based method and its relevant equations for topology optimization were investigated. Then, considering the thermal loads for thermo-mechanical topology optimization of the components was discussed. Next, HyperWorks and its topology optimization platform, HyperMesh, was discussed and chosen to pursue the study due to the outstanding controllability of the optimization process. Also, some of the HyperMesh features

were investigated. Thereafter, two methodologies for performing thermo-mechanical topology optimization were proposed. In the end, a workflow introduced to redesign a component using HyperMesh.

Chapter 4
Case Study: Gas Turbine Rotor Seal

4.1 Rotor seal

Based on the objective of this thesis, it is essential to investigate a case study subjected to multiple loadings including mechanical and thermo-mechanical loads. Based on this statement, a component from a gas turbine would be a good candidate for investigation. Components that are placed in the flow path, should be able to work in high temperatures. Some of the gas turbines are working in high-temperature cycles to increase the efficiency of the system. The flow of temperature in gas turbines can rise up to 1200 ^{o}C before entering the combustion chamber [78], [79]. Also, almost every piece in a gas turbine is exposed to high-pressure load conditions. Moreover, if the target component is part of the rotating section of the turbine, centrifugal force should be considered in FEM analysis. Designing a component capable of bearing the mentioned loads would be a challenging task to accomplish. Therefore, topology optimization is a great tool to employ for designing or redesigning a part with the aim of increasing efficiency.

Figure 4.1 shows a simplified cross-section of a gas turbine. Herein, the main parts are rotor and stator blades. Almost every other implemented component in the turbine is aimed to maintain the functionality of the rotor and stator as well as guaranteeing a smooth airflow between them. Among other important parts, different kinds of seals can be named. The main goal of these pieces is to prevent the hot and high-pressure airflow from entering the core section of the turbine [80]. Interstage seals, also known as rotor heat shields and rotor seals, are one of the mentioned components that are placed and fixed between two rotors and located at the tip of stators.

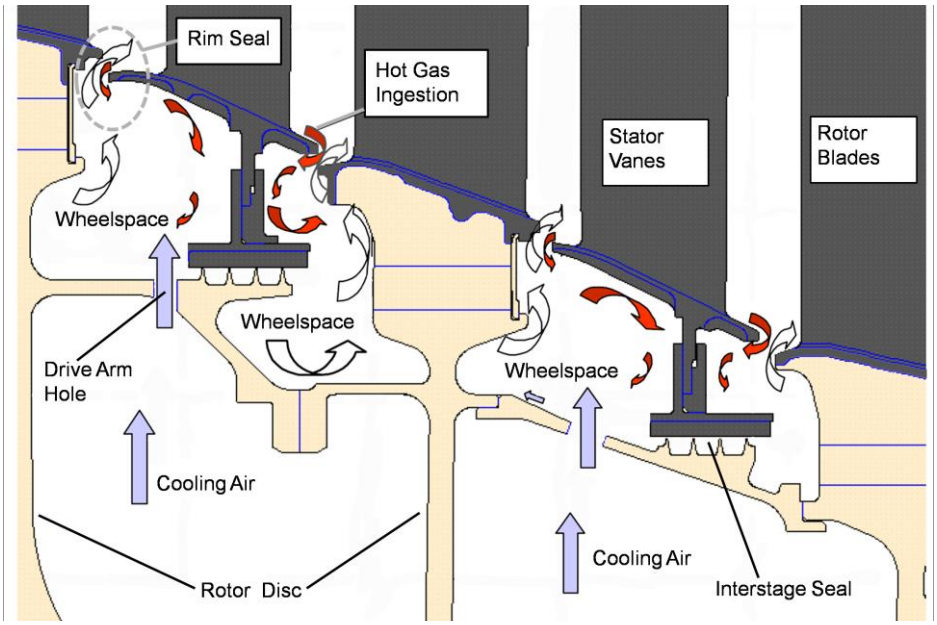

Figure 4.1 A cross-section view of a gas turbine [81]

Based on the mounting location of rotor seals and their turbine stage at which they are operating, they can have different geometries. Appropriate design of rotor seals is considered as one of the most challenging tasks to accomplish during the design of these turbines. Figure 4.2 is showing another typical gas turbine stage and the arrangement of the seals.

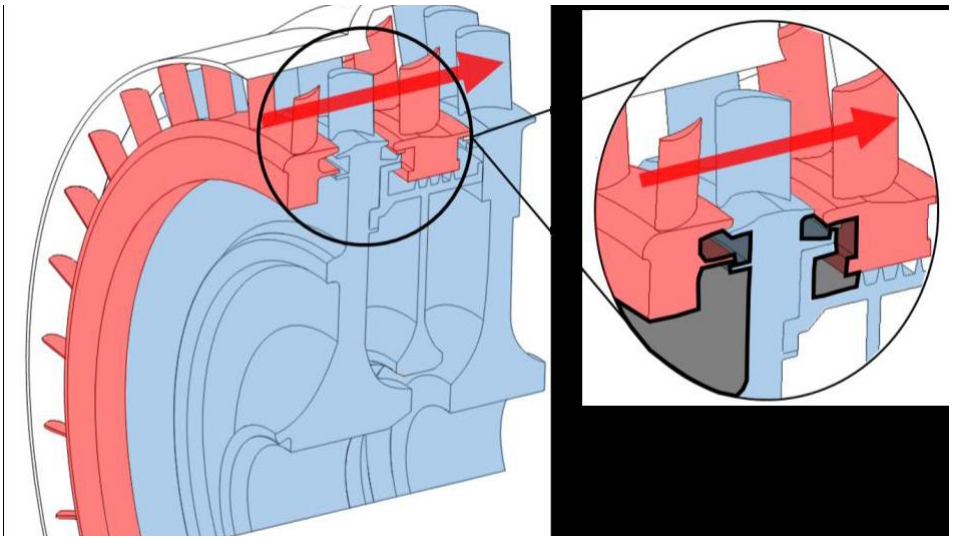

Figure 4.2 Rotating parts (in blue highlight) including rotor seal, and stationary parts (in red highlight) in a gas turbine stage [80]

In order to define a proper case study, a patent published in 1987 [82] is used to set up the basic design for topology optimization. In Figure 4.3, numbers 14 and 20 are showing the rotor blades, and numbers 12 and 18 are rotor discs that are responsible to hold blades and rotor seal in place. The stator blade tip is shown by number 36. Number 62 is showing the rotor seal which is our target component for topology optimization in this thesis. Based on the design of the rotor seal in this patent, there is enough space around the component to expand the boundaries of geometry for topology optimization. Also, the pressure and temperature distribution around the component make it a proper candidate for this study.

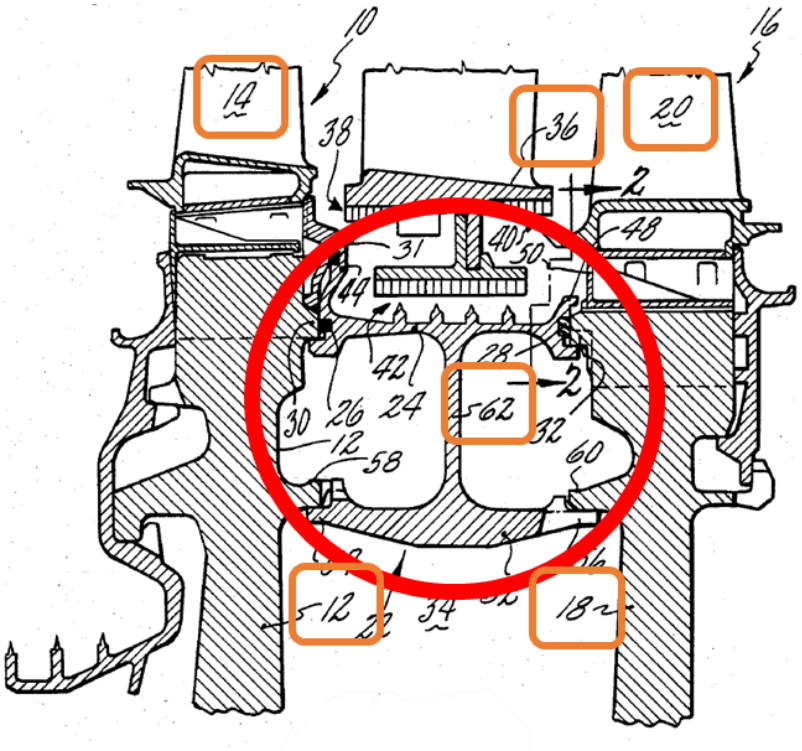

Figure 4.3 Rotating seal for gas turbine engine [82]

Figure 4.3 is used to create a 2D sketch of the rotor seal and then to produce a CAD file for further analysis. Some modification has been applied to simplify the geometry and to make it compatible to be used in topology optimization. These simplifications are as follows: (a) seal's teeth have been replaced by rectangular shapes, and (b) any screw or rivet hole was ignored to get a uniform profile. Figure 4.4 shows the CAD file produced based on the patent introduced by G.P. Peters [82].

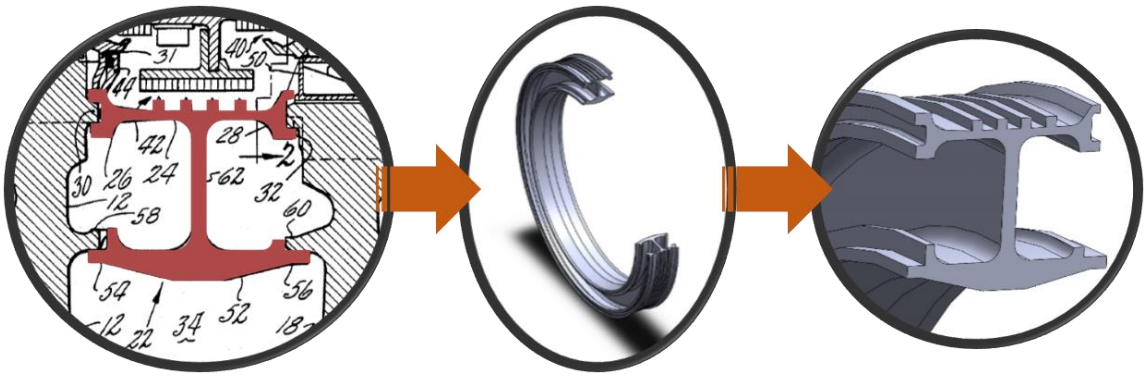

Figure 4.4 CAD file production of a rotor seal based on the patent introduced by G.P. Peters

Following, the proposed workflow in Chapter 3 (see Figure 3.9) is employed to redesign the rotor seal, and each step is presented and discussed in detail. But before continuing, based on the literature, Ti6Al4V is chosen for the material of the rotor seal [83]. Ti6Al4V has excellent corrosion resistivity and high strength with a low density which makes it an excellent candidate for rotor seals.[84] The properties of this material can be found in Table 4.1.

Table 4.1 Ti6Al4V material properties [85], [86]

Young's modulus [GPa]	Poisson's ratio	Density [g.cm^{-3}]	Thermal conductivity [W.(m K)$^{-1}$]	Thermal expansion coefficient [K^{-1}]	Reference temperature [^{o}C]
108	0.323	4.41	8.27	9.33×10^{-5}	25

4.2 Design space identification

After drawing a sketch from the original part, it is essential to expand the boundaries of the geometry. This step is necessary to make sure there is a reasonable amount of material to be removed by topology optimization. In the process of redefining the profile of the part, extra caution should be taken to preserve the critical design areas such as channels around the original component.

Also, other components around the target part should be considered in order to prevent any overlap between them.

Figure 4.5 presents the original (shaded in dark brown) and expanded (shaded in light brown) geometry boundaries for the rotor seal. The channels on the right and left (areas number 1 and 2) are designed for the flow of the cooler air. Hence, the boundaries in these areas are expanded in a way to preserve those channels. The boundary in the lower section geometry is extended downward to almost double the design space with the purpose of allowing the optimizer to remove unnecessary materials. Also, in the upper region (number 4), the top of the grippers are connected to the bottom of the nearest tooth.

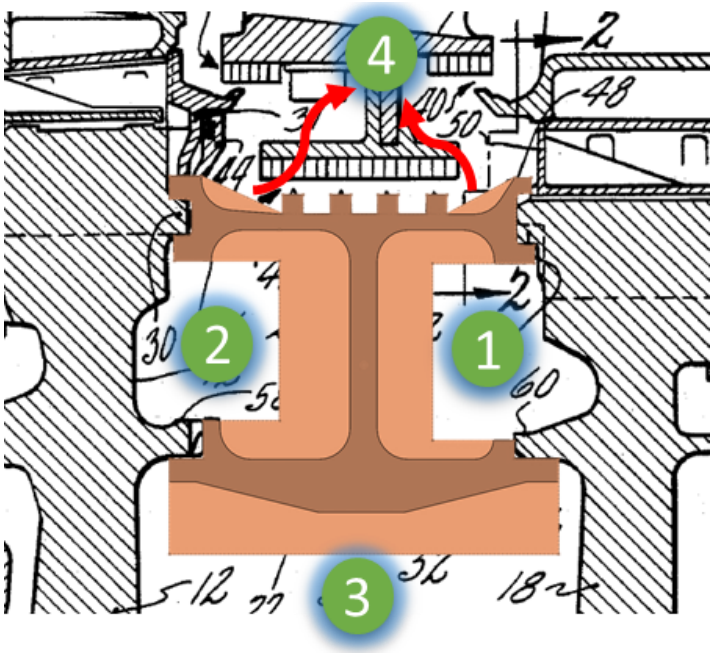

Figure 4.5 Expanding geometrical boundaries of the rotor seal

There are some parts in the design that their existence is essential for the part to remain functional. In the design of the rotor seal, all the teeth and gripper sections are necessary to be preserved (shown with blue color in Figure 4.6). These zones are taking part in FEM analysis, but

are not involving in topology optimization. The other area, represented in gray color, is considered as the design space for the current topology optimization problem. However the non-design areas could be considered in a way that the top grippers and the teeth would be connected to each other, but in order to keep the problem as much as open, it is tried to keep the preserved areas smaller

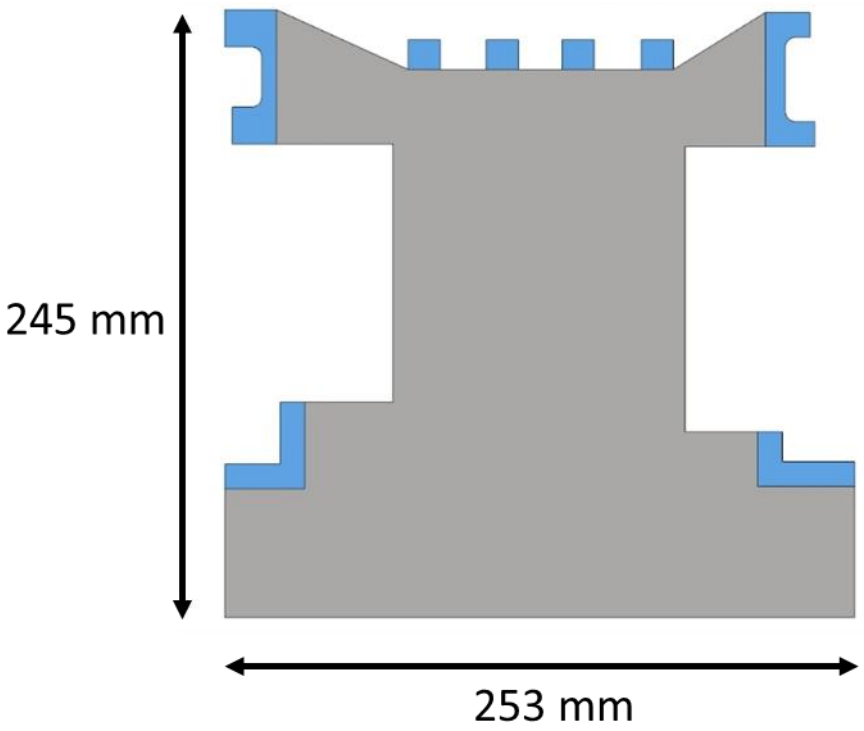

Figure 4.6 Rotor seal design (gray region) and non-design spaces (blue region)

4.3 Loads and boundary conditions

As discussed before, the rotor seal subjects to three load cases: pressure load, centrifugal load, and thermal load. Each load is discussed below.

4.3.1 Pressure load

Since there is no FEM analysis on this particular rotor seal in the literature, there is no record of accurate numbers for the pressure loads on this part. However, estimate values can set based on the literature [87].

The pressure loads applied to the rotor seal are divided into four segments as displayed in Figure 4.7. As mentioned in previous sections, the seal is placed at the tip of the stator, right below the hot air flow; therefore, it is assumed that the rotor seal subjects to higher pressure on the top. Since the air pressure increases over each stage of the compressor, the pressure applied to the seal is gradually increasing. Thus, P_1 assumed to be increasing linearly from 70 to 85 bars from the right section to the left.

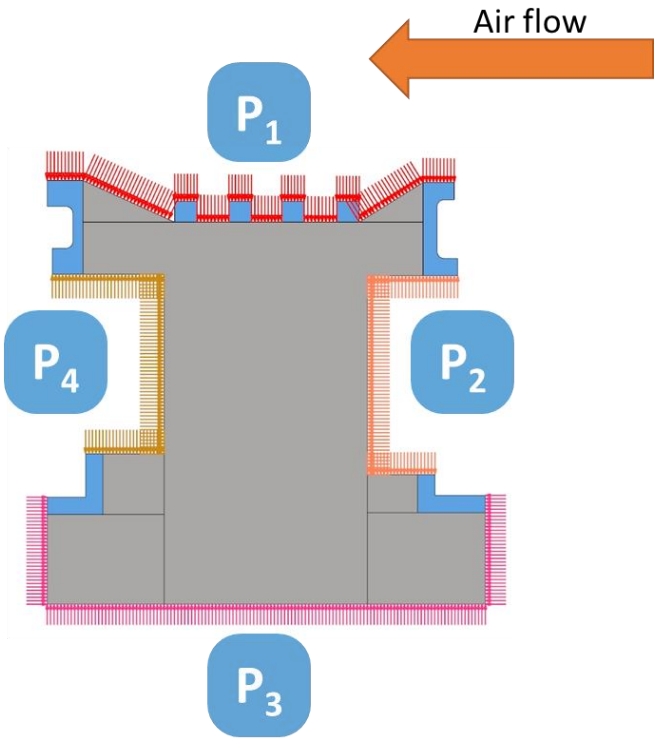

Figure 4.7 Applied pressure on rotor seal

Lower pressure air is maintained below the rotor seal. Since there is not much of a flow variation under this part, P_3 is considered uniform and set to 60 bars. The value of the pressure is the lowest amongst all.

P_2 and P_4 placed on each side of the seal. Pressure on each of these zones does not vary much over the area but they have different values. Their pressures set to a value between the load on the top and bottom of each side and are fixed to P_2=65 bars, and P_4=70 bars.

4.3.2 Centrifugal force

Based on the literature, turbines are working at different rotational speeds. Generally, they are working within the range of 3000 rpm to 3600 rpm [87], [88]. The value of 3600 rpm is chosen for this study and can be calculated for each element from the following equation:

$$F = mr\omega^2 \qquad 4.1$$

$$and: \quad \omega = 2\pi n$$

Above, ω is the rotational speed (rad/s), m is the weight of each element (tonne), r is the distance of the element from the center of rotation (mm), and n is the number of rotations per second.

4.3.3 Thermal load

Similar to the other forces, there is no record for thermal analysis and boundary conditions on this particular component in the literature. Thereby, a thermal condition that is reasonably close to the actual case is chosen to be applied to the rotor seal based on the literature. This condition will be further explained below.

The temperature in the latest stages of a high-efficiency turbine can rise up to 1200 ^{o}C on the blades [78], [79]. However, as Figure 4.3 shows, the rotor seal is placed with a distance from the hot airflow. Also, assuming the rotor seal is located on mid-stages of the turbine, it subjects to

lower temperatures. Figure 4.8 demonstrates the boundary condition applied for the rotor seal on this study. The hot air with the temperature of 480 ^{o}C flows on top of the seal and the cold air with the temperature of 340 ^{o}C flows beneath the part. Then, temperatures on the side of the rotor seal are chosen according to the already-defined temperatures as well as the physics of the problem.

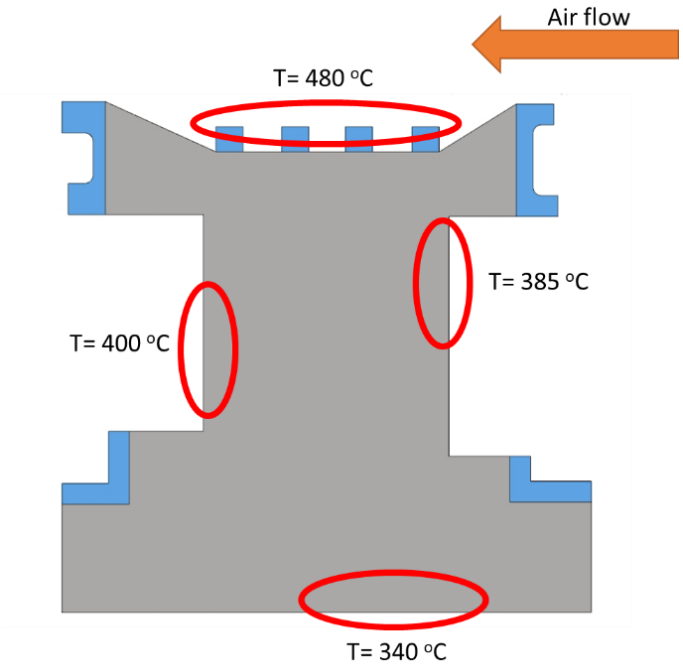

Figure 4.8 Thermal boundary condition for rotor seal

After applying the thermal boundary conditions, a finite element thermal analysis is performed to obtain the temperature distribution map as shown in Figure 4.9. This temperature map will be used in later stages of topology optimization.

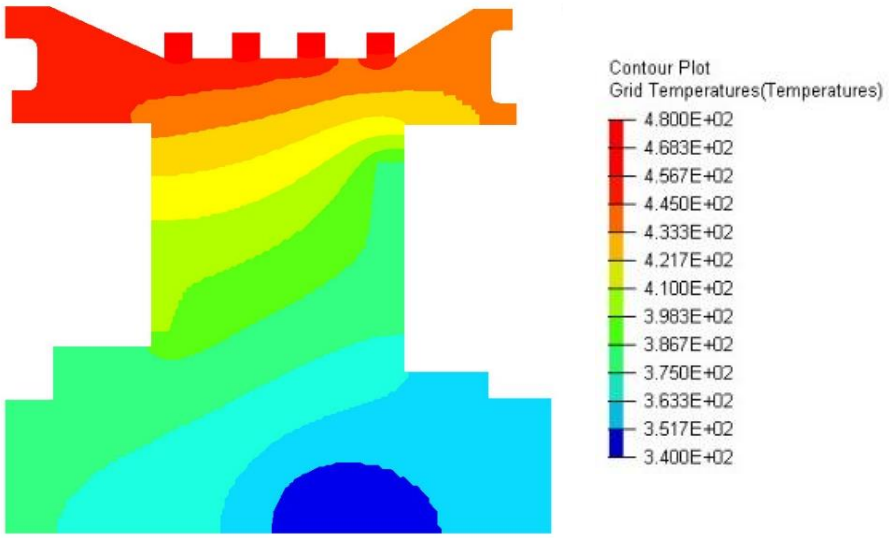

Figure 4.9 Temperature distribution of the rotor seal

4.3.4 Constraints

Based on the original design, the displacement of the part is constrained in gripping sections. Therefore, the circled areas in Figure 4.10 are fixed on X and Y directions.

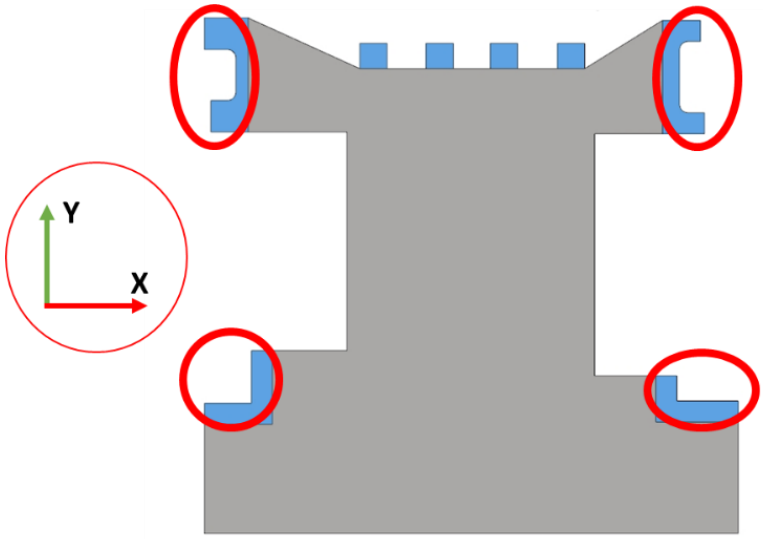

Figure 4.10 Constraints on the rotor seal

4.4 Design criteria

As it is discussed before, different factors can affect topology optimization results. Some of them are presented in Figure 4.11. In this section, the effect of each criterion on the topology optimization of the rotor seal is briefly discussed. Then, based on the prediction of their effect on the optimization process, a set of variables is presented to perform topology optimization.

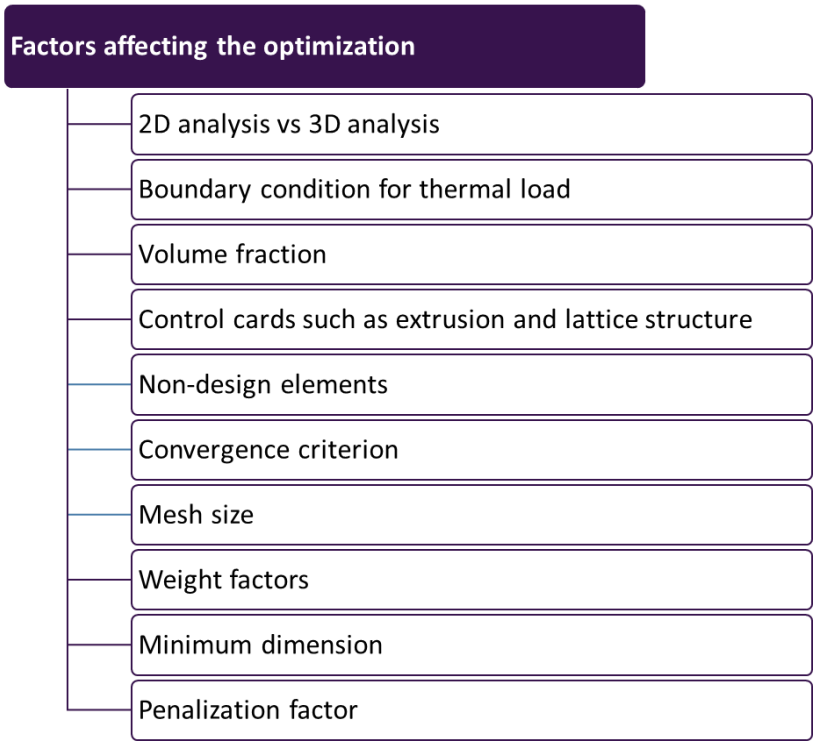

Figure 4.11 Factors and control cards affecting topology optimization

4.4.1 Factors to be set before topology optimization

4.4.1.1 2D Vs. 3D analysis

Sometimes, the 3D FEM analysis of components can be simplified into a 2D problem. This is a proper assumption specifically if a component has a high aspect ratio with a uniform loading along the part. In this case, the rotor seal, a uniform profile is revolved around the center of the engine and loading distribution is the same in every cross-section of the component. Thus, the

optimization can be performed on a cross-section of the rotor seal and then the component can be reproduced by revolving the 2D profile.

4.4.1.2 Fully-coupled vs one-way coupled thermal load

In Chapter 3, two methodologies presented to perform thermo-mechanical topology optimization in HyperMesh: fully-coupled and one-way coupled thermal load. In the former one, as mentioned before, thermal calculations will be performed at each iteration which makes the approach time-consuming. However, in the latter one, the thermal calculation will be performed once, and it will serve as a prerequisite to continue the simulation. In this study, since multiple optimizations are required to obtain the final geometry, it is better to perform topology optimization based on the one-way coupled method to reduce the computational time. In the one way coupled.

4.4.1.3 Volume fraction

The volume fraction for topology optimization of the rotor seal is calculated by dividing the surface area of the component presented in the patent to the surface area of the optimizing geometry. With this definition, the volume fraction is set to 35%.

4.4.1.4 Control cards

Since the topology optimization is decided to perform on a 2D space, control cards such as lattice structure, and features like extrusion and draw cannot be implemented. Also, since there is no symmetry or pattern in the design, repetition patterns and symmetry patterns are disabled.

4.4.1.5 Non-design elements

In some cases, the quantity of the non-design elements (constraints area and teeth on the seal) can greatly affect topology optimization, especially if the centrifugal load is dominant among other

exerted forces. That being said, by performing a set of optimization, it is realized that increasing or decreasing non-design elements quantities does not have a significant effect in this case study.

4.4.1.6 Convergence criterion

As it is mentioned in the previous chapter, choosing a high value for convergence criterion can terminate the topology optimization in the early stages. By performing multiple topology optimization on the rotor seal it is observed that a convergence criterion of 0.0005 results in sufficiently accurate outputs without compromising the computational time. It means that if the relative change in the objective function (compliance) between two iterations becomes less than 0.05%, the final design is achieved.

4.4.1.7 Mesh size

In this case study, a mesh size of 2 mm is chosen and 10368 2D elements with linear (first-order) shape functions were generated to form the part. Most of these elements are rectangular. However, the generation of triangular elements is inevitable due to the diagonal lines on irregular geometry boundaries.

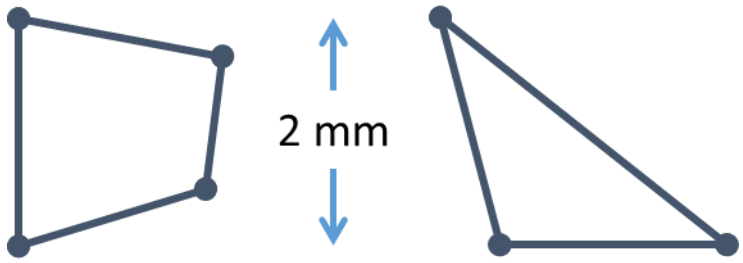

Figure 4.12 Sample of triangular and rectangular elements used for the used mesh

4.4.2 Variables to change in topology optimization

4.4.2.1 Minimum dimension

In topology optimization, changing the minimum dimension or minimum feature size can significantly affect the final result. In order to investigate the effect of this filter on the final geometry, four values are chosen for the minimum dimension. These values vary from a low to a high number and also include two mid-range values to change on each topology optimization. The highest value for this filter is set to 24 mm which is equal to the width of 12 elements. Mid-range values set to 12 mm and 6 mm. And for the lowest one, the minimum dimension filter is disabled.

4.4.2.2 Penalization factor

Different interpolation functions for the density-based method was introduced in Chapter 3. In HyperMesh the penalization factor for the SIMP method can be monitored and desired values can be set to this factor. Similar to the trend used for choosing values for minimum dimension, here a low value of P_1=1, two mid-range values of P_2=4, and P_3=8, and a high value of P_4=16 are chosen to be used in topology optimization.

4.4.2.3 Weight factors

In this study, 3 different loading conditions, which can be controlled using weight factors, affect the topology optimization of the rotor seal. Changing each of these conditions can change the final result. Thus, different optimization analysis can be performed based on different weight factors. Since the thermal load usually results in higher compliance, the load factor value for this load is set to the lowest value compared to others. The weight factors for pressure loads and centrifugal loads are defined relative to the thermal load weight factor.

In order to get proper values for weight factors, a set of topology optimizations were performed with different weighting values. A minimum dimension of 9 mm and a penalization factor of 6 are

chosen for these analyses. The objective of this set of topology optimization is to get equivalent weighted compliances for thermal, centrifugal, and pressure loads by changing the weight factors. Equivalent compliance means that all the loads are equally involved in the topology optimization. Table 4.2 shows weight factors for thermal, centrifugal, and pressure loads that result in equal participation in topology optimization.

Table 4.2 Weight factors for equal participation in topology optimization

	Weight factor	Weighted compliance [mJ]	$\frac{\text{Weighted compliance}}{\text{Total compliance}} \times 100$ [%]
Thermal load	1	1.52×10^{6}	34
Centrifugal load	2100	1.47×10^{6}	33
Pressure load	5400	1.54×10^{6}	34

Based on the mentioned weight factors, a table consist of a set of values can be established to alternate in the topology optimization. These values that are set to change in four levels from low to high numbers are presented in Table 4.3 along with other variables. In this table, levels 1, 2, 3, and 4 are respectively representing low to high values for each variable.

Table 4.3 Specified values to selected factors (variables) in the topology optimization

	$\frac{W_{\text{Centrifugal load}}}{W_{\text{Thermal load}}}$	$\frac{W_{\text{Pressure load}}}{W_{\text{Thermal load}}}$	Minimum dimension [mm]	Penalization factor (P)
Level 1	0.7×10^3	1.8×10^3	-	2
Level 2	1.4×10^3	3.6×10^3	6	4
Level 3	2.8×10^3	7.2×10^3	12	8
Level 4	5.6×10^3	14.4×10^3	24	16

- $W_{\text{Thermal load}}$ is set to 1 in all of the topology optimizations

4.5 Decision-making process

After performing the topology optimization by changing the variables, numerous results are generated. A decision process is necessary in order to select the best result. Figure 4.13 demonstrates a schematic flow of the proposed decision-making process.

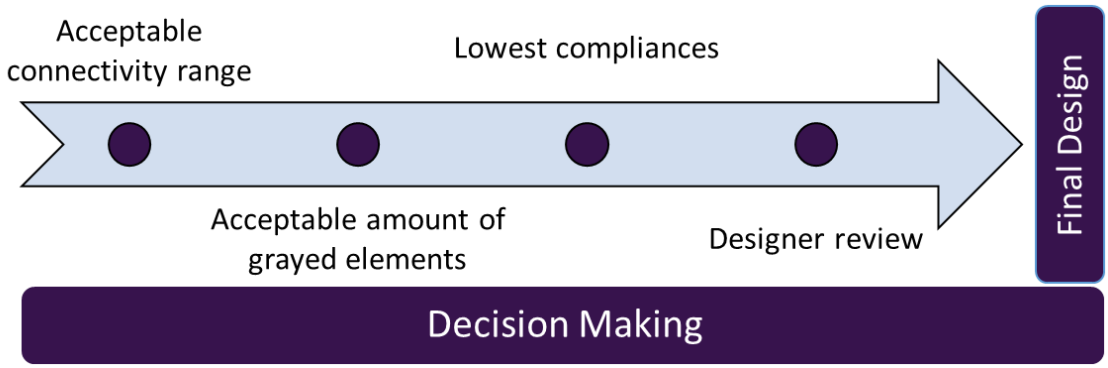

Figure 4.13 The flow of choosing the best result

4.5.1 Connectivity

An issue in implementing thermo-mechanical topology optimization in this study is that the final results may not form a single structure while maintaining all the non-design elements connected to each other. This phenomenon is happening because of the existence of thermal and centrifugal load in the process. Since it is important that all of the defined critical areas remain connected in the final design, hence, the first step is to eliminate designs that are not entirely connected. In order to achieve this goal, a Matlab code is generated to process the image of the output result from topology optimization and calculate the connectivity of the part (see Appendix A). If all the non-design spaces are connected to each other, the part is fully connected (connectivity is 100%) and if none of those sections are connected to each other, the output for connectivity is 0%. This code is reading all of the generated pictures from the topology optimization, performing an image processing on them, and automatically remove designs with low connectivity.

The inputs for the Matlab code are the picture of the material distribution on each optimization and all the points that need to be connected. Then, it checks the connectivity between each set of two points and if they are connected the result for connectivity is 1. The Matlab code continues

this process for all the imported points and then it generates a matrix as the output. Later, the connectivity of the design is calculated as the total number of connectivities between every two nodes divided by the total possible number of connection ways between nodes (two by two). The percentage of connectivity for n number of nodes is calculated as follow:

$$Percentage\ of\ Connectivity = \frac{\left(\sum_{i=1}^{n}\sum_{j=1}^{n} C_{i,j}\right)\text{-}n}{2\sum_{i=1}^{n}(i\text{-}1)} \times 100 \qquad 4.2$$

$$where: C_{i,j} = \begin{cases} 1 & if\ i\ and\ j\ are\ connected \\ 0 & if\ i\ and\ j\ are\ not\ connected \end{cases}$$

In this study, the connectivity is checked for the total number of 8 nodes while each of the selected nodes is placed on the specified non-design space, as mentioned before. To clarify the Matlab code function, an example is demonstrated in Figure 4.14. This picture shows one of the results generated by topology optimization with $\frac{W_{Centrifugal\ load}}{W_{Thermal\ load}} = 0.7 \times 10^3$, $\frac{W_{Pressure\ load}}{W_{Thermal\ load}} = 1.8 \times 10^3$, the minimum dimension of 12 mm, and the penalty factor of $P=8$.

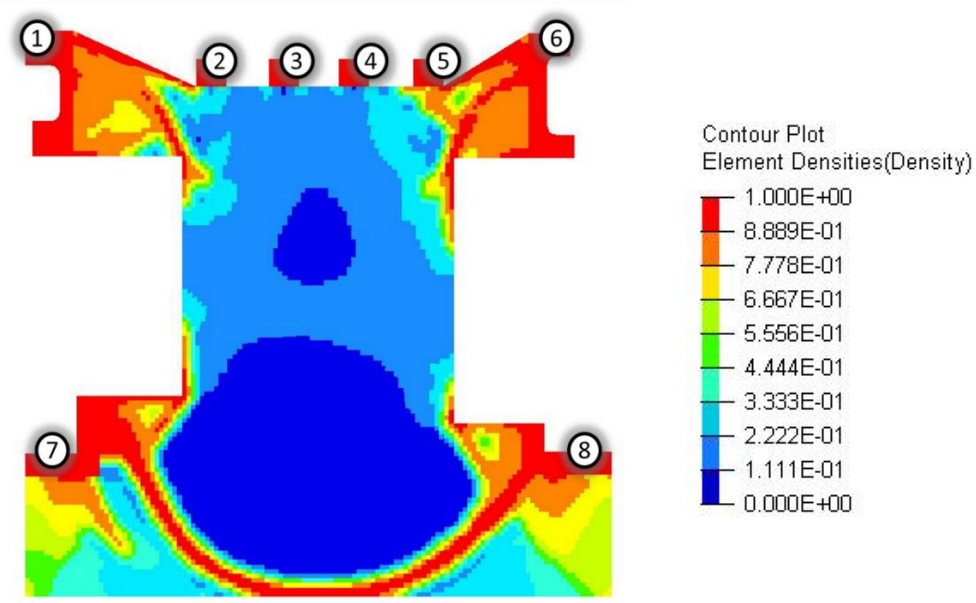

Figure 4.14 An example for checking the connectivity of the topology optimization result

As demonstrated in Figure 4.14, there are three pairs of connections (1-2, 5-6, and 7-8) formed in this specific simulation. To find these connections, the Matlab code is checking if any two pre-defined points on non-designed spaces (points 1 to 8) are connected by a fully-dense path (follow red areas in Figure 4.14). Otherwise, no connection is generated. Based on equation 4.2, a connection matrix is generated as shown in Figure 4.15. The connectivity is calculated as the ratio of the total number of formed connections to the total possible connections, i.e. $\frac{3}{28} \times 100 = 10.7\%$. This can also be calculated from the matrix in Figure 4.15 based on equation 4.2. This ratio is a remarkably small number and therefore, it is quite possible to result in a non-connecting structure. To avoid this, such optimization outputs will be removed automatically from the acceptable optimization results.

	Point 1	Point 2	Point 3	Point 4	Point 5	Point 6	Point 7	Point 8
Point 1	1	1	0	0	0	0	0	0
Point 2	1	1	0	0	0	0	0	0
Point 3	0	0	1	0	0	0	0	0
Point 4	0	0	0	1	0	0	0	0
Point 5	0	0	0	0	1	1	0	0
Point 6	0	0	0	0	1	1	0	0
Point 7	0	0	0	0	0	0	1	1
Point 8	0	0	0	0	0	0	1	1

Figure 4.15 Connectivity matrix for the example of Figure 4.15

In order to prevent any error in the image processing and the connection calculation, all designs with the connectivity of 75% or more, are allowed to proceed to the next step.

4.5.2 Partial-dense elements

In topology optimization, a preferred result is a discrete design made of full-dense and non-dense elements (voids). But, sometimes, especially when one of the loads is pressure or temperature, achieving a completely discrete design may not be possible. Most of the time, the final design contains some partial-dense elements (also known as grayed elements) as well. HyperMesh provides information about the density of the elements. This information contains the percentage of the total number of elements for a specific density. The density distribution for the previous example is presented in Table 4.4. In this scale, the densities are distributed between 0 and 1 wherein 0 is represents void, and 1 represents full-dens elements.

Table 4.4 An example of the density distribution of a design

Density	Percentage of elements [%]
0.0-0.1	25.2
0.1-0.2	25.8
0.2-0.3	11.4
0.3-0.4	5.6
0.4-0.5	2.5
0.5-0.6	3.3
0.6-0.7	4.2
0.7-0.8	6.2
0.8-0.9	10.4
0.9-1.0	5.4

The percentage of partial-dense elements is defined as the sum of all the elements with density within the range of 0.2 and 0.8. In the presented example, based on the defined criteria, 33% of all the elements are partial-dense elements.

It is considered that if more than 25% of the density distribution plot contains partially dense elements, the design will be eliminated. In other words, more than 75% of all the elements in a design should be full-dense (close to 1) or void (close to 0) to pass this step. Also, a Matlab code is generated to read the output file of all the topology optimization and decide which designs pass this stage (see Appendix B).

4.5.3 Compliance

In this step, all the results that passed the previous two steps are being sorted with respect to their compliances and printed on the output folder by the Matlab code (Appendix B). Compliances are divided by the total weighted compliances on the first iteration to represent a normalized value. In this way, the normalized compliance demonstrates the improvement of a design based on the first iteration. Also, it is easier to compare each design with others with normalized compliances. The designer can check these results and proceed to the next step.

4.5.4 Designer review

In this section, the designer is checking the few results that passed previous steps and decides the best design for the part.

4.6 Topology optimization

Considering the combination of all the factors/variables that are intended to change in this study, the total number of 256 (4×4×4×4) topology optimizations are performed. In addition, 3 more topology optimization analysis is done to observe the effect of each load on the geometry. In these

additional analyses, the penalization factor of P=6, and the minimum dimension of 9 are chosen to perform the optimization.

4.6.1 Topology optimization for thermal load

The result of topology optimization considering thermal load is presented in Figure 4.16. As expected in the literature [89], [90], the SIMP method may not provide the proper interpolation function for the topology optimization for the thermal load. As presented in this picture, the result may include many partial-dense elements and does not form a geometry.

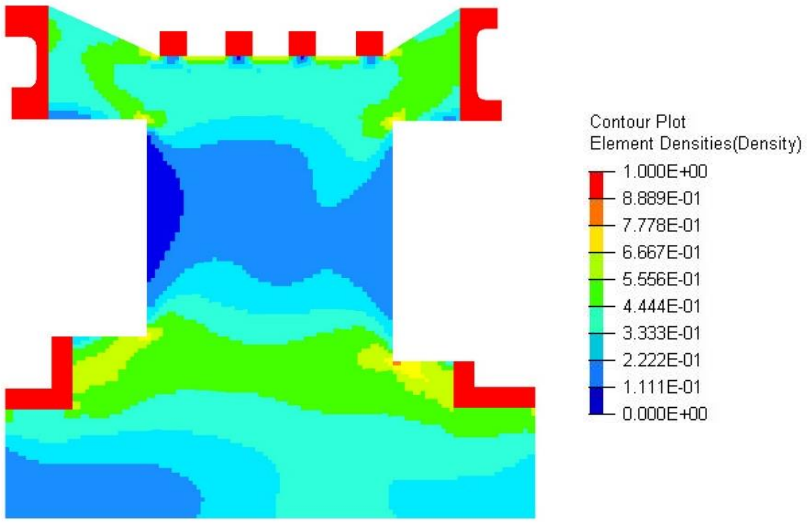

Figure 4.16 Topology optimization of the rotor seal for Thermal load

4.6.2 Topology optimization for pressure load

The layout of topology optimization for pressure load is shown in Figure 4.17. This picture demonstrates that several convex features were formed at the boundary of the part. These features are mainly formed to strengthen the structure against the loads applied on the edges of the rotor seal.

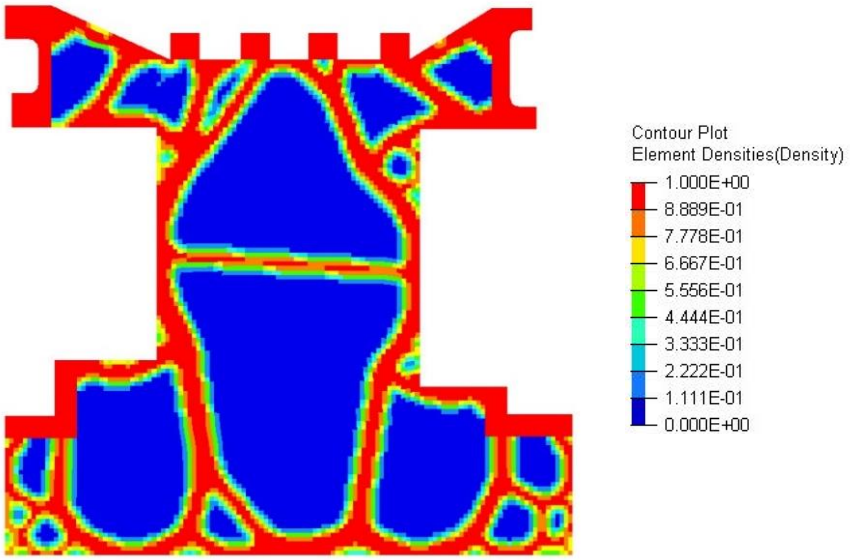

Figure 4.17 Topology optimization of the rotor seal for pressure load

4.6.3 Topology optimization for centrifugal load

When the centrifugal load is applied, the optimizer tries to add more material in areas that are restricted in the y-direction (centrifugal load is upward). Figure 4.18 shows that most of the material formed around the constrained sections on bottom and top and also, the optimization process tried to support the teeth of the rotor seal on top.

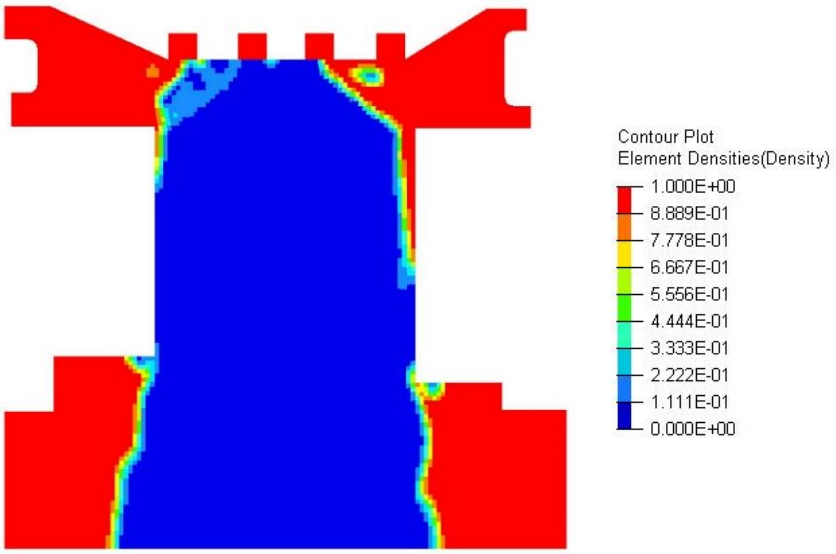

Figure 4.18 Topology optimization of the rotor seal for centrifugal load

4.6.4 Topology optimization considering all loads

By changing the variable parameters, 256 designs are generated. Some of these results are presented in Figure 4.19. The density distribution in Figure 4.19 (a) shows that this result contains lots of partial-dense elements. This happens because of the high effect of thermal load due to low weight factors for the pressure and centrifugal loads. Figure 4.19 (b) shows lots of material focused around the grippers. The higher value for centrifugal weight factor confirms the similarity between this picture and the one in Figure 4.18 is because of the centrifugal force is the dominant load in this analysis. However, the arc shape feature on the bottom section of the rotor seal shows the effect of the pressure load on the simulation. Also, the design in Figure 4.19 (c) reveals that the pressure is the dominant force on this analysis.

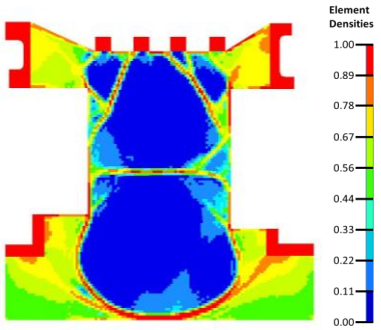

(a) $Min.Dim. = disabled \ \ , P = 4,$

$\frac{W_{Centrifugal\ load}}{W_{Thermal\ load}} = 700, \frac{W_{Pressure\ load}}{W_{Thermal\ load}} = 1800$

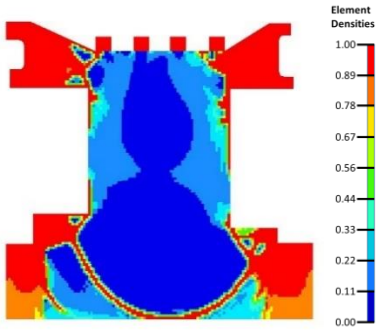

(b) $Min.Dim. = disabled \ \ , P = 16,$

$\frac{W_{Centrifugal\ load}}{W_{Thermal\ load}} = 5600, \frac{W_{Pressure\ load}}{W_{Thermal\ load}} = 3600$

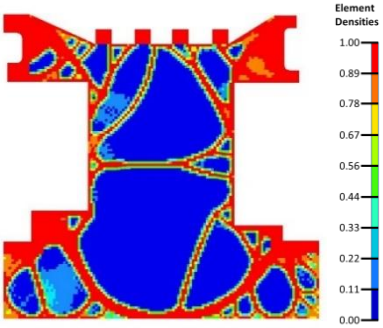

(c) $Min.Dim. = 6 \ \ , P = 8,$

$\frac{W_{Centrifugal\ load}}{W_{Thermal\ load}} = 1400, \frac{W_{Pressure\ load}}{W_{Thermal\ load}} = 14400$

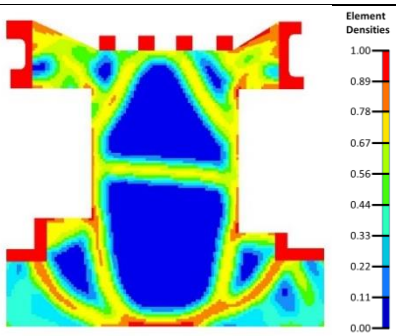

(d) $Min.Dim. = 24 \ \ , P = 2,$

$\frac{W_{Centrifugal\ load}}{W_{Thermal\ load}} = 700, \frac{W_{Pressure\ load}}{W_{Thermal\ load}} = 14400$

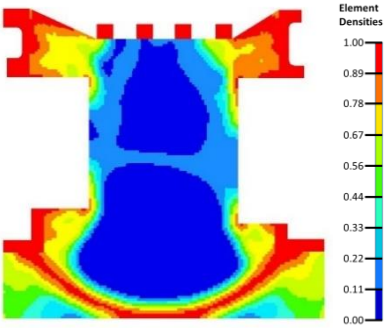

(e) $Min.Dim. = 24 \ \ , P = 2,$

$\frac{W_{Centrifugal\ load}}{W_{Thermal\ load}} = 2800, \frac{W_{Pressure\ load}}{W_{Thermal\ load}} = 1800$

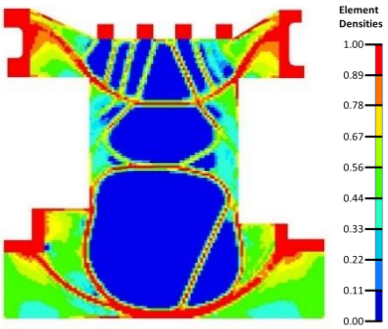

(f) $Min.Dim. = disabled \ \ , P = 2,$

$\frac{W_{Centrifugal\ load}}{W_{Thermal\ load}} = 2800, \frac{W_{Pressure\ load}}{W_{Thermal\ load}} = 14400$

Figure 4.19 Some of the results for the rotor seal topology optimization

Figure 4.19 (d-f) are showing some of the results, mainly with a high number of partial-dense elements. Usually, low numbers for penalty factors prevent the optimizer to fully develop a

structure and therefore, lots of partial-dens elements remain in the design. Figure 4.19 (d) shows that a structure was formed, but not completely developed. In Figure 4.19 (e), some full-dense elements produced, but critical areas of the structure are not well-connected. And, Figure 4.19 (f) presents a developed structure with thin features, but the amount of partial-dense elements makes it not suitable for a proper design.

After performing topology optimization for all 256 possible combinations of variables, the Matlab code in Appendix B is employed to extract the acceptable results for this study. The code filtered undesired designs and sorted them with respect to the lowest normalized compliance. In this process, 235 designs are eliminated, and the remaining 21 results are kept to proceed to the designer review step. These schemes are presented in Table 4.5.

Table 4.5 shows that all of the output results have 100% connectivity. The calculated partial-dense elements are less than 25% for all the presented designs with the lowest number of 15.6%. Also, the column on the right shows the calculated total normalized compliance of the designs.

Table 4.5 All the acceptable results for rotor seal topology optimization sorted with respect to lowest normalized compliances

No	$\frac{W_{Centrifugal\ load}}{W_{Thermal\ load}}$	$\frac{W_{Pressure\ load}}{W_{Thermal\ load}}$	Minimum dimension (mm)	Penalization factor (P)	Connectivity [%]	Partial-dense elements [%]	Normalized compliance
1	5600	3600	-	4	100	23.6	0.138183602
2	5600	7200	-	8	100	17.9	0.139209646
3	5600	7200	6	8	100	16.7	0.140014565
4	5600	3600	6	4	100	21	0.14180894
5	5600	7200	-	4	100	23.4	0.151618293
6	5600	7200	6	4	100	21.5	0.157432696
7	5600	14400	-	8	100	16.3	0.161156287
8	5600	14400	6	8	100	15.9	0.16205337
9	5600	14400	-	4	100	22.9	0.171940911
10	5600	14400	6	4	100	21.4	0.178573895
11	2800	7200	6	8	100	18.2	0.202343738
12	2800	7200	6	4	100	24	0.224476367
13	2800	14400	-	8	100	16.1	0.225998223
14	2800	14400	6	8	100	15.6	0.227252229
15	2800	14400	6	4	100	23.2	0.247889863
16	1400	7200	6	8	100	18.6	0.289626802
17	1400	14400	-	8	100	16.2	0.294660774
18	1400	14400	6	8	100	15.9	0.298566654
19	700	14400	-	8	100	17.5	0.373032469
20	700	14400	6	8	100	16.3	0.375869686
21	700	7200	6	8	100	24.1	0.41367383

4.7 Acceptable variable criteria

Based on the acceptable results from Table 4.5, a decision matrix can be provided demonstrating the proper criteria for variable factors affecting the topology optimization result. Presented numbers in this table are illustrating the total number of acceptable designs with values within the range of respective levels for each factor (levels can be reviewed in Table 4.3). In Table 4.6, green color represents the highest number of acceptable results at each level. Respectively, yellow and orange colors stand in second and third place statistically. Also, the cells with red color mean none of the acceptable results, represent these values.

Table 4.6 A decision matrix for acceptable variable criteria

	$\frac{W_{\text{Centrifugal load}}}{W_{\text{Thermal load}}}$	$\frac{W_{\text{Pressure load}}}{W_{\text{Thermal load}}}$	Minimum dimension	Penalization factor
Level 1	3	-	8	-
Level 2	3	2	13	8
Level 3	5	8	-	13
Level 4	10	11	-	-

This table reveals that to get the best result, it is better to choose higher values for centrifugal and pressure weight factors. However, it does not necessarily mean that choosing lower values leads to undesired results, as the two of the top four designs sorted by the Matlab code have a low weight factor for pressure (Level 2). Moreover, the table shows that none of the acceptable results represent a high level of minimum dimension. For most of these results, the minimum dimension

is set to 6 mm, and for others, this filter has been disabled. Also for the penalization factor, using a value between level 2 (P=4) and level 3 (P=8) is required to come up with an acceptable result.

4.8 Design selection and modification

The top four designs presented in Table 4.5 with the lowest normalized compliances are shown in Figure 4.20. As these pictures show, all four designs are following the same trend with an arc in the bottom of the design, big hollow areas in the middle, and small structures to support all the teeth.

The designs in Figure 4.20 (b, c) seem incomplete since some partial-dense elements are formed in the middle and left section, but did not convert to full-dense elements. Designs in Figure 4.20 (a, d) look similar to each other. Since the pressure load on the boundary of the initial design does not move, it resulted in the formation of lots of partial-dense elements in this section. However, based on the generated data, the design in Figure 4.20 (d) has relatively less partial dense elements while their normalized compliances are comparably similar. This design is compared to other acceptable results and is chosen as the final design to be used for the initial draft in designing the rotor seal.

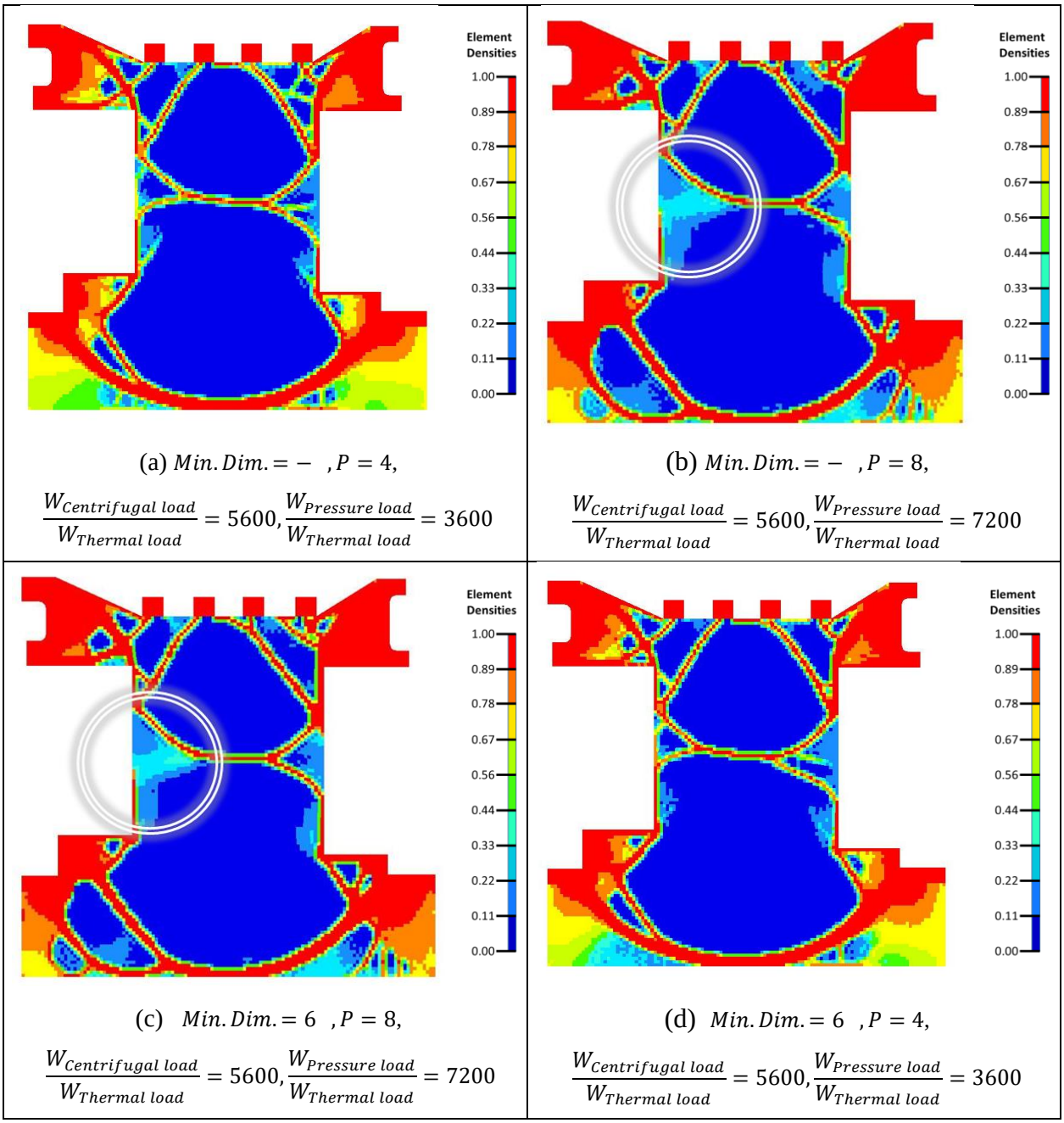

Figure 4.20 The top four designs with the lowest normalized compliance numbers

After selecting the final design, the boundaries are reconstructed using SolidWorks. A schematic of the defined areas is presented in Figure 4.21. The black color represents the preserved area for the final design. Since the partial dense elements at the bottom of the picture represent the existence of the pressure load on the bottom, they are not included in the design criteria. If the

pressure load could move according to the updated geometry after each iteration in topology optimization, all the elements in this area would turn to non-dens elements.

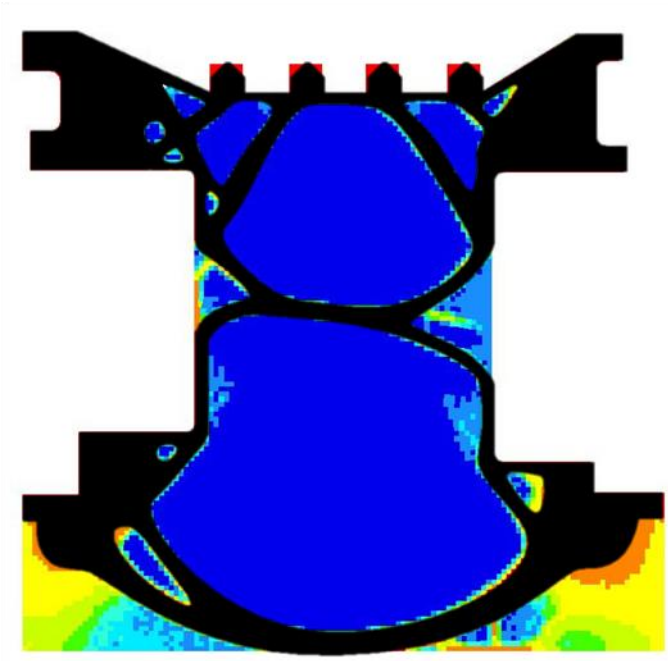

Figure 4.21 Reconstruction of the rotor seal based on the selected design

4.9 Final product

After constructing the final boundaries in SolidWorks, and producing the geometry, a CAD file of the rotor seal can be constructed by revolving the profile around the centerline. The final part for rotor seal designed based on coupled thermo-mechanical topology optimization is presented in Figure 4.22

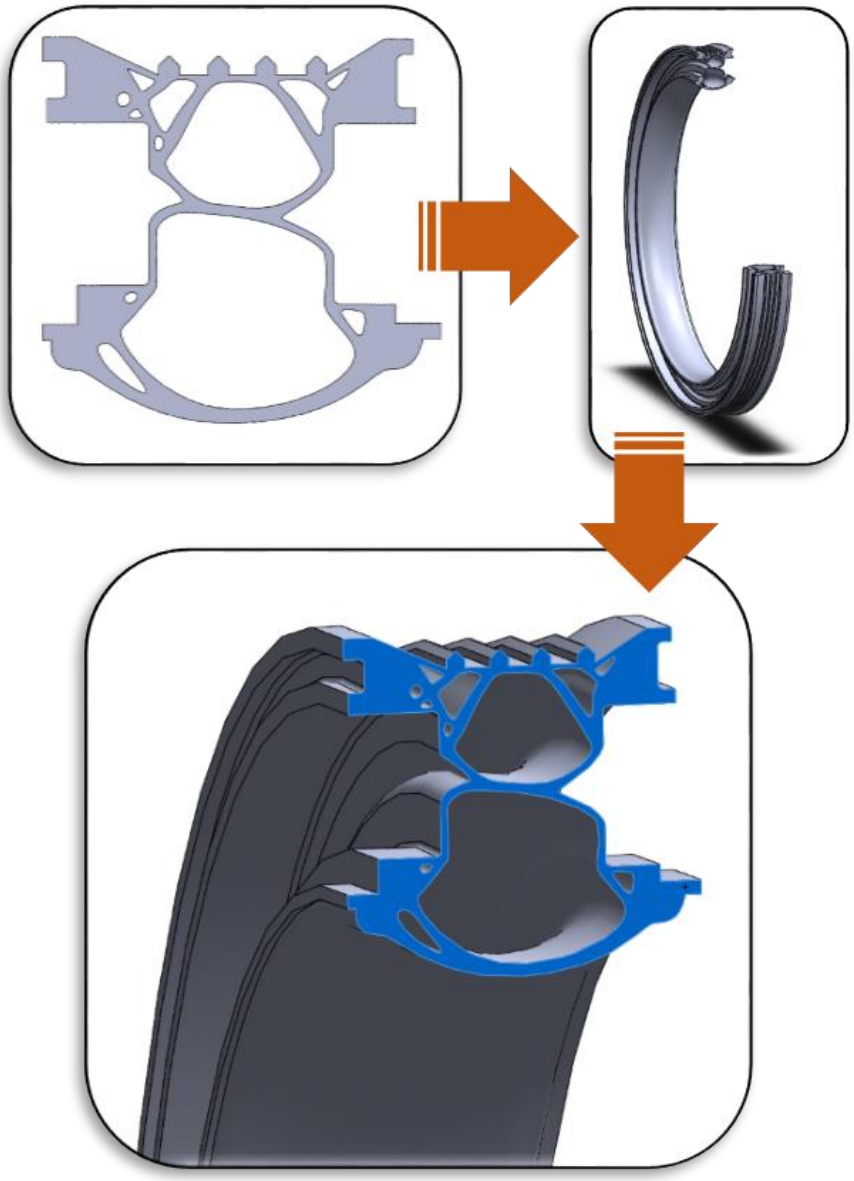

Figure 4.22 The final design for rotor seal

4.10 Summery

In this chapter, a rotor seal, which is a major gas turbine component, is chosen as a case study to perform thermo-mechanical topology optimization. The rotor seal subjects to pressure, centrifugal, and thermal loads. Then, the proposed workflow for redesigning a component in Chapter 3 is employed to redesigning the rotor seal. In this methodology, the effect of four

variables (centrifugal load weight factor, pressure load weight factor, penalization factor, and minimum dimension) is investigated. Next, 256 topology optimization simulation is performed by considering four values for each variable (4×4×4×4=256). Then, a Matlab code is generated to analyze all the 256 generated designs by topology optimization. The Matlab code selected 21 designs for the designer review. In the end, one result is selected and a CAD file for the rotor seal is generated based on the recommended design extracted from thermo-mechanical topology optimization.

Chapter 5
Experimental Validation

5.1 Introduction

Validating the computational study of the thermomechanical performance of the gas turbine components designed using topology optimization is associated with extensive challenges. A component with a simple geometry subjected to a single load case can be a good candidate to validate the result of mechanical topology optimization. However, designing an experiment to validate the result of a thermo-mechanical topology optimization can be more challenging.

Since performing experimental analysis on the designed rotor seal presented in Chapter 4 requires sophisticated equipment, it is difficult to validate its performance at the University of Waterloo. Thus in this chapter, a simple cantilever is chosen to perform thermo-mechanical topology optimization. Then an experimental setup is proposed and designed to validate the result of thermo-mechanical topology optimization performed on HyperMesh. In this experiment, the resultant geometry from thermo-mechanical topology optimization is compared to three other components: a part generated from the result of pure mechanical optimization, a traditional design for the part, and a design created by the author. From this point onward, the latter one is called manually designed part.

5.2 Design and geometry generation

In this section, a part is designed based on the process proposed in Figure 3.9. All steps for designing the part for thermo-mechanical topology optimization are given below and a short description of each step is presented.

5.2.1 Design space and boundary conditions

In this design, the topology optimization is performed on a simple cantilever in 3D space. The design and non-design spaces are presented in Figure 5.1.

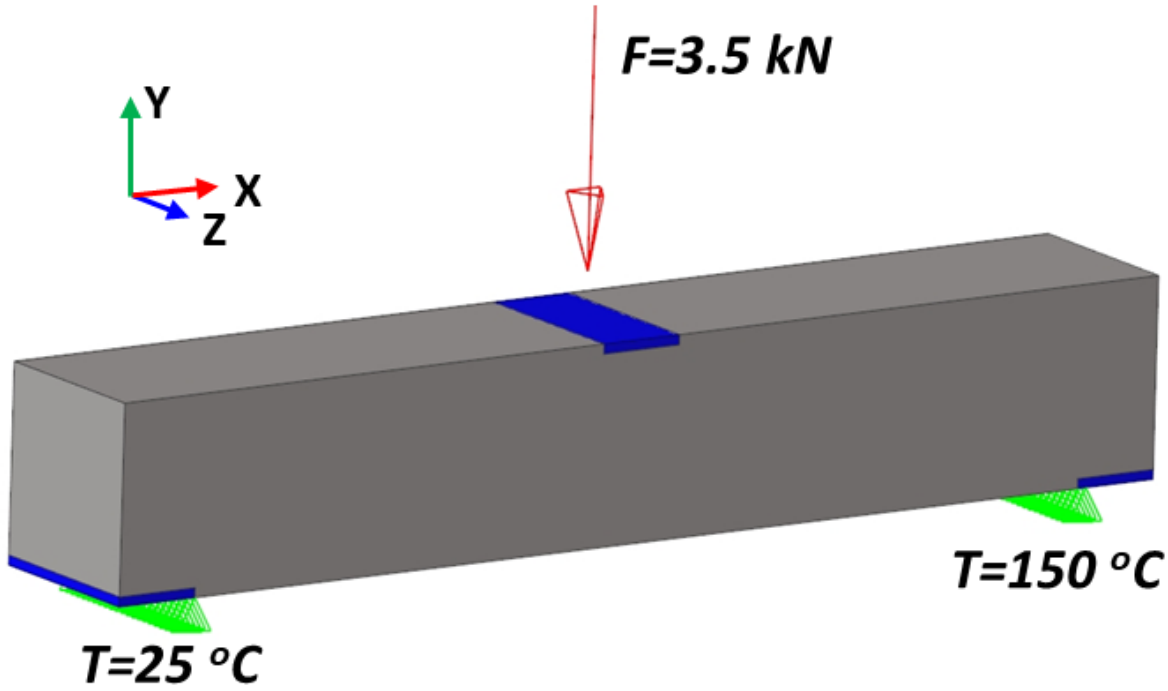

Figure 5.1 Design and non-design spaces for thermo-mechanical topology optimization

The blue areas in Figure 5.1 present non-design spaces and should be preserved to apply loads and constraints on these sections. The dimensions of the part are set to 13×13×80 mm^3. The red arrow on the top represents the load applied to the cantilever (F=3.5 kN) and the green color shows where the constraints are applied to prevent movement in the Y direction. Also, a low temperature of 25ºC and a high temperature of 150ºC are applied to the surfaces under the blue areas on the left and right sections, respectively.

5.2.2 Factors and decision process

The effect of the factors mentioned in the previous chapters is considered in the thermo-mechanical topology optimization of the cantilever. The parameters to be set before topology optimization are explained below.

- **2D vs 3D analysis:** Since no uniform profile is required in this study, it is chosen to perform 3D topology optimization to obtain more accurate results.
- **Thermal boundary condition:** To perform thermo-mechanical topology optimization on this part, a fully-coupled method for thermo-mechanical optimization is selected. Thus the topology optimization is subjected to a thermal analysis on each iteration.
- **Volume fraction:** In this analysis, the volume fraction of 25% is considered to obtain the final geometry with a quarter of the initial volume of the cantilever.
- **Control cards:** The control cards such as extrusion, draw, symmetry, patterns, and lattice structure are disabled to perform this optimization.
- **Convergence criterion:** The optimization is converged when the changes between the two iterations become less than 0.05 %.
- **Mesh size:** In this set of optimization, the mesh size is set to 0.65 mm. The total number of 49200 uniform elements is produced. These cubic elements are set to be first order.
- **Minimum dimension:** Based on the decision matrix produced in Table 4.6 for thermo-mechanical topology optimization performed on the rotor seal, the minimum dimension filter is disabled in this optimization.
- **Penalization factor:** This factor is also chosen based on the matrix produced in Table 4.6 and it is set to P=6.

Weight factors: the only variable in the process of thermo-mechanical topology optimization of the cantilever is the weight factor. Multiple weight factors are implemented to obtain the desired

design as the final geometry. After a couple of optimizations, a weight factor of $\frac{W_{Pressure\ load}}{W_{Thermal\ load}} = 1.5$ is chosen.

Decision process: The process of choosing the best result is to plot the density distribution for each topology optimization, and then remove those which does not form proper geometry. Then, the topology optimization with the lowest compliance is selected as a final result.

5.2.3 Topology optimization and acceptable result

5.2.3.1 Thermo-mechanical topology optimization for the cantilever

After performing the required optimizations acceptable design is presented in Figure 5.2. Figure 5.2 (a) shows the density distribution in the cantilever. Figure 5.2 (b-d) represents the isometric view, top view, and front view of the design while densities less than 0.56 are filtered to be excluded from the density plots. As it is presented in the figure, more materials are formed around the low-temperature area in the optimized design, while in the right section with high temperatures, less material is preserved. In addition, an extra truss shape is formed in the right half of the design to support the applied force on the top.

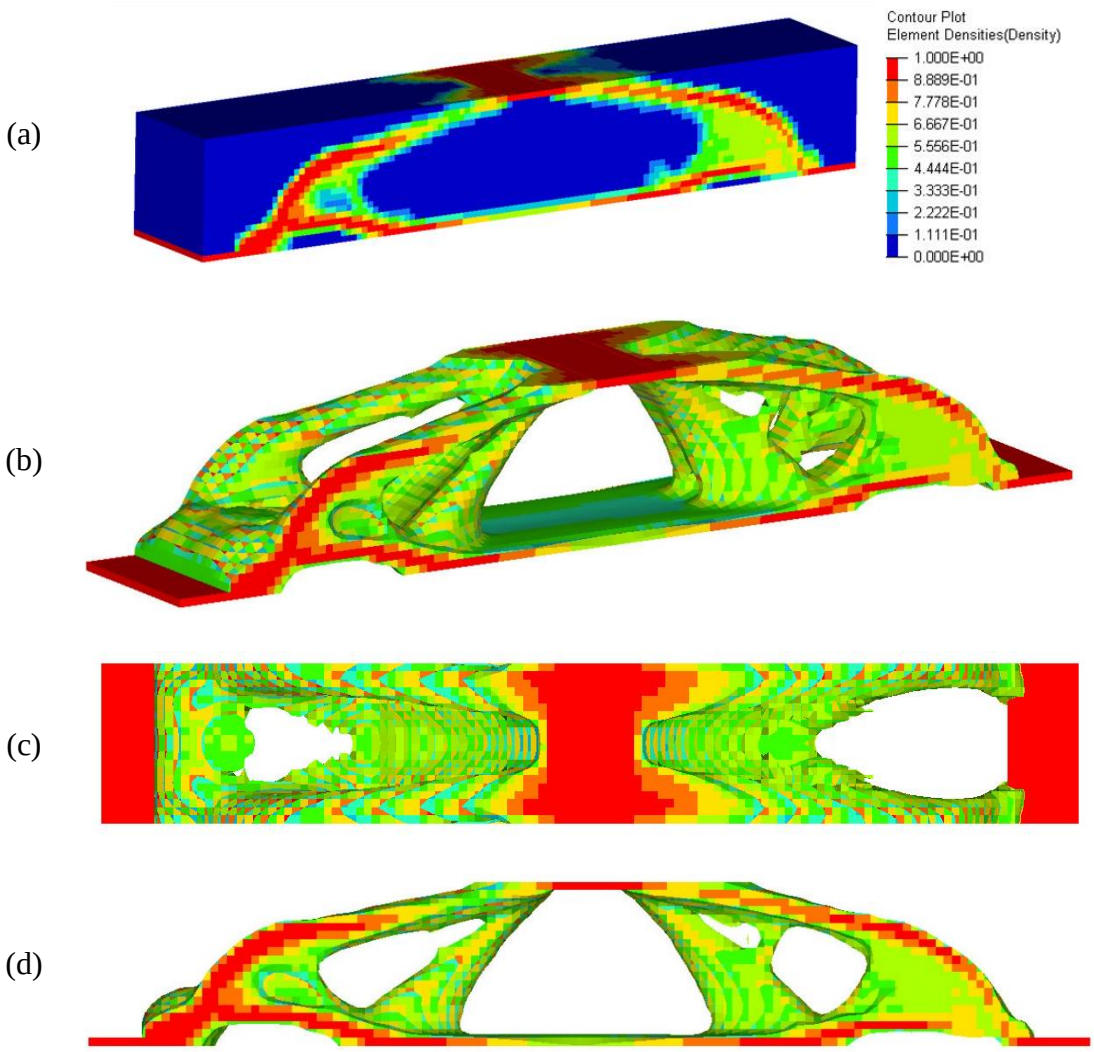

Figure 5.2 Density distribution resulted from coupled thermo-mechanical topology optimization of the cantilever. a) and b) isometric view, c) top view, d) side view

5.2.3.2 Mechanical topology optimization for the cantilever

As mentioned before, one of the designs to compare with the result of thermo-mechanical topology optimization is the geometry generated based on mechanical topology optimization. In order to perform mechanical topology optimization for the force of F=3.5kN, the same setup is used for optimization. Since there is no need for weight factor, performing only one optimization is enough to produce the geometry.

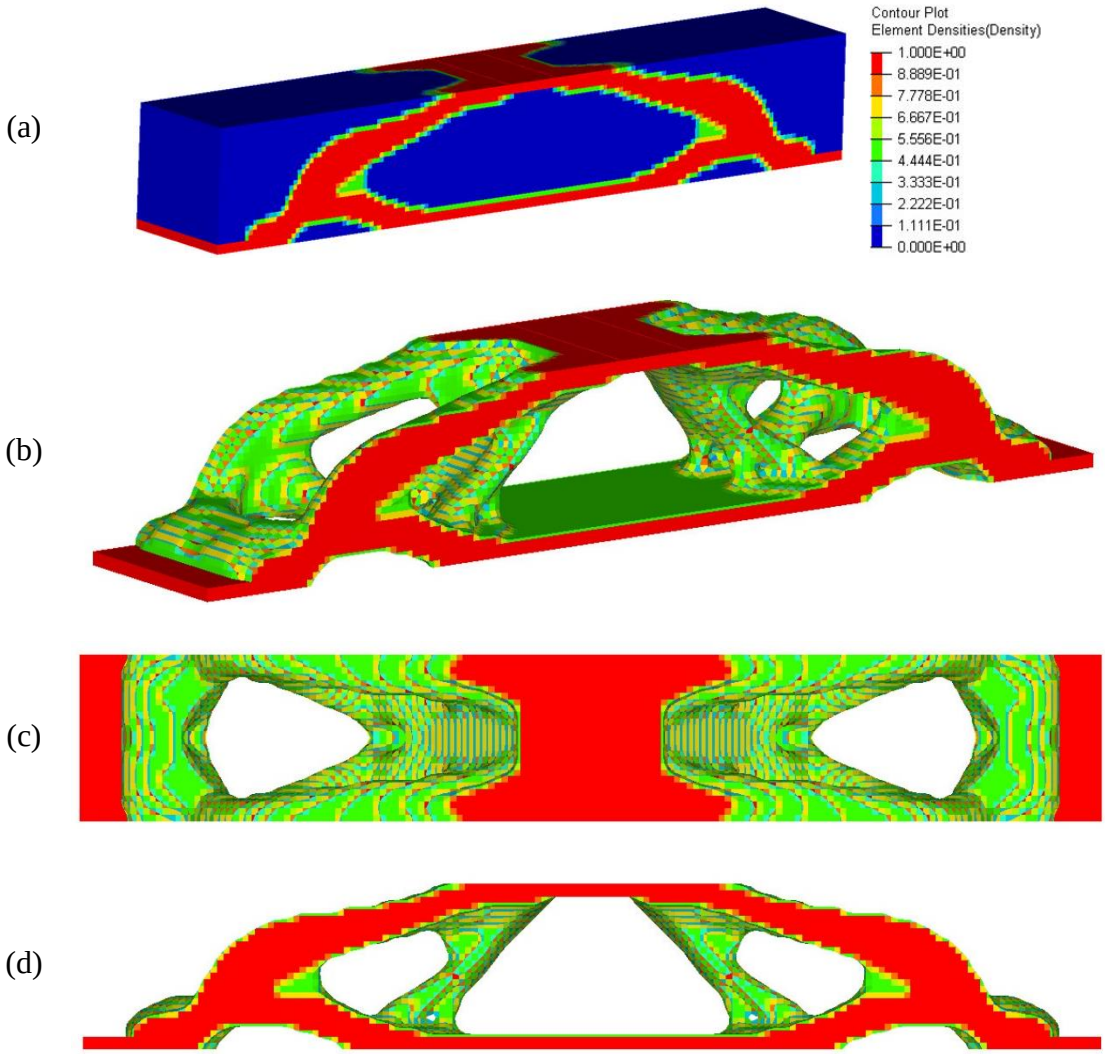

Figure 5.3 Density distribution resulted from mechanical load topology optimization. a) and b) isometric view, c) top view, d) side view

Figure 5.3 shows the density distribution for mechanical topology optimization subjected to F=3.5kN force. This figure shows the density distribution is more discrete compared to the coupled thermo-mechanical optimization. In other words, less portion of the design is containing the partial-dense elements because of suppressing the thermal load. Also, the generated density distribution is completely symmetric, however, the symmetry feature has not been employed. The symmetric design means the applied force is uniformly distributed.

5.3 Manufacturing

Performing mechanical and coupled thermo-mechanical topology optimizations and extracting relevant results, the next step is to produce STL files that are required for 3D printing. The following steps are presenting the generation of the STL files.

5.3.1 Geometry construction

5.3.1.1 Geometry extraction from HyperMesh

One of the capabilities of HyperMesh is to produce an STL file from the FEM file. In order to achieve this, the result of topology optimization is imported to HyperMesh using the OSSMOOTH command. This command filters the elements with densities less than a given threshold and preserves the remaining elements. In this study, the value of the threshold is set to 0.56 to obtain a result with 25% of the volume of the original design (cantilever). Then, 2D elements can be created from the imported 3D elements using another command called “Shrink Wrap”. This command is capable to create a smooth surface. Following these steps using the mentioned commands, a smooth geometry can be produced. The final geometries can be exported as STL files to be used as an input to the 3D printer.

Figure 5.4 displays generated geometries using HyperMesh for coupled thermo-mechanical and mechanical topology optimization. These figures illustrate that the surfaces of the geometries are smoothed enough to be additively manufactured.

(a)

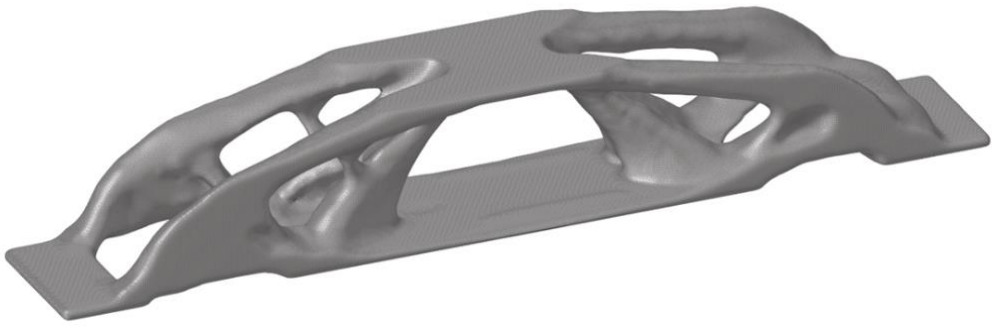

(b)

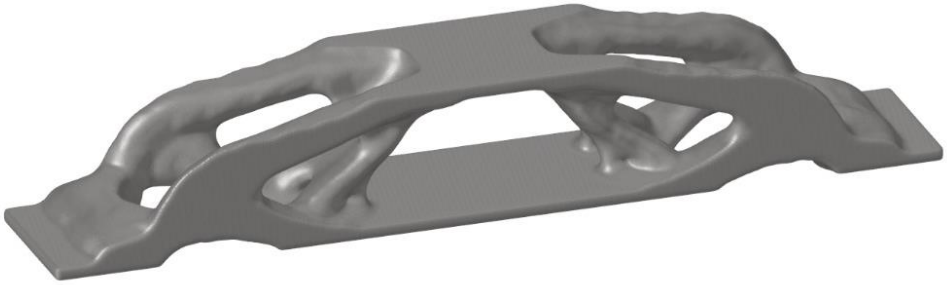

Figure 5.4 Geometries generated using HyperMesh for a) coupled thermo-mechanical, and b) mechanical topology optimization

5.3.1.2 Geometry extraction from SolidWorks

Earlier in this chapter, the results of mechanical and coupled thermo-mechanical optimizations were compared to other designs in this experiment. One of these designs is a simple hollow bar that is cut to form a trapezoid shape. The other one is manually designed to withstand the applied force on top of the part. This part is designed based on the designer's knowledge and understanding of the force distribution.

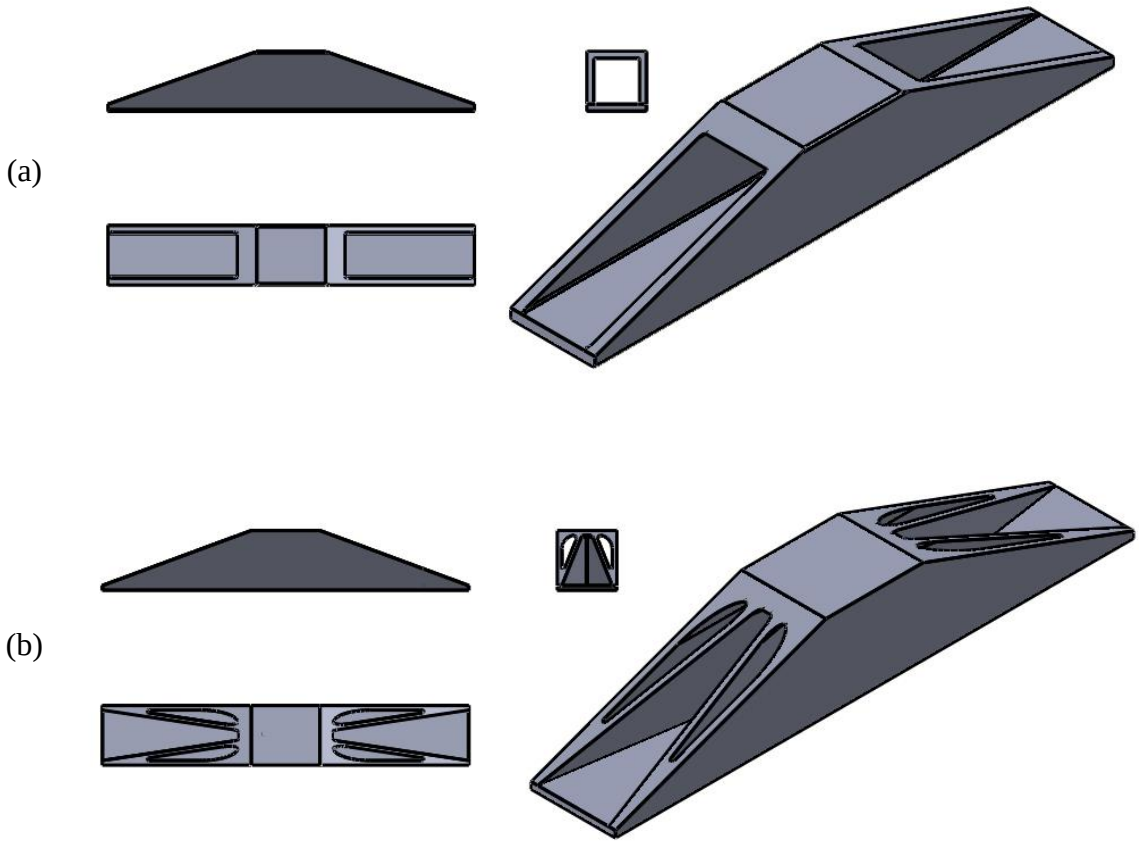

Figure 5.5 Isometric and 3D views of a) hollow bar, and b) designed part

The isometric and 3D views of the hollow bar and the designed part are presented in Figure 5.5. These components are designed with the same dimensions (13×13×80 mm^3) and the same volume (3400 mm^3) to represent the same size and volume as the optimized parts thus a proper comparison can be established. The hollow bar is generated with equal wall thicknesses of t=1.5 mm. On the other hand, the designed part consists of a hollow bar combined with a cross-shape structure within the design. The wall thickness of the outer structure is set to t=1 mm, and the wall thickness of the cross-shape structure is set to t=0.9 mm. It should be noted that this part is designed especially for AM and therefore it is difficult to manufacture it in traditional ways.

5.3.2 3D printing

In order to print the designed components, the STL files are imported into Renishaw QuantAM software to build the support structure for each design. After the generation of required support, three repetitions of each component are provided to print. Ready-to-print files are presented in Figure 5.6. In the process of creation of support structure, the least support is used for the designed part in Figure 5.6 (d). When the files are ready, the output file is sent to Renishaw AM 400 for printing. The material used to print these structures is Ti6Al4V alloy.

The total number of 12 components (3 of each design) were successfully printed to pursue to the experimental test. An example of the 3D printed parts compared to the STL file is shown in Figure 5.7 and the printed parts after removing the support structure are presented in Figure 5.8 (from left to right: parts optimized based on mechanical load, coupled thermo-mechanical load, manually designed, and hollow bar).

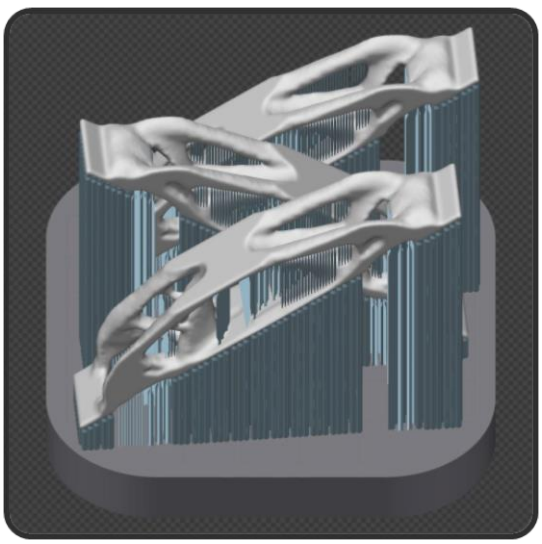

(a)

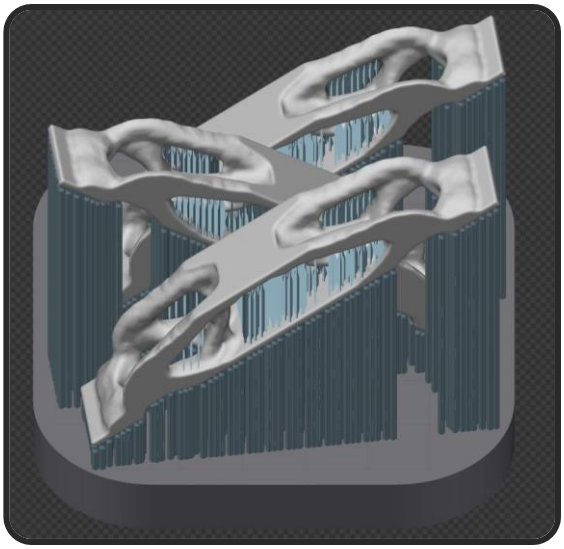

(b)

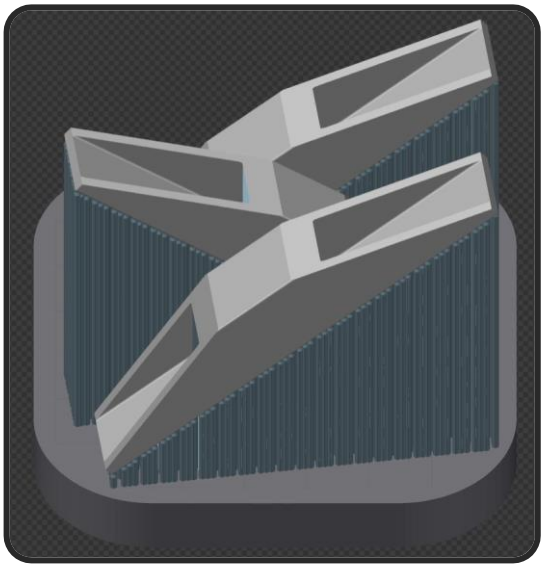

(c)

(d)

Figure 5.6 Applied support structures to the components and build plates for a) coupled thermo-mechanical optimized, b) mechanical optimized, c) hollow bar, and d) designed part

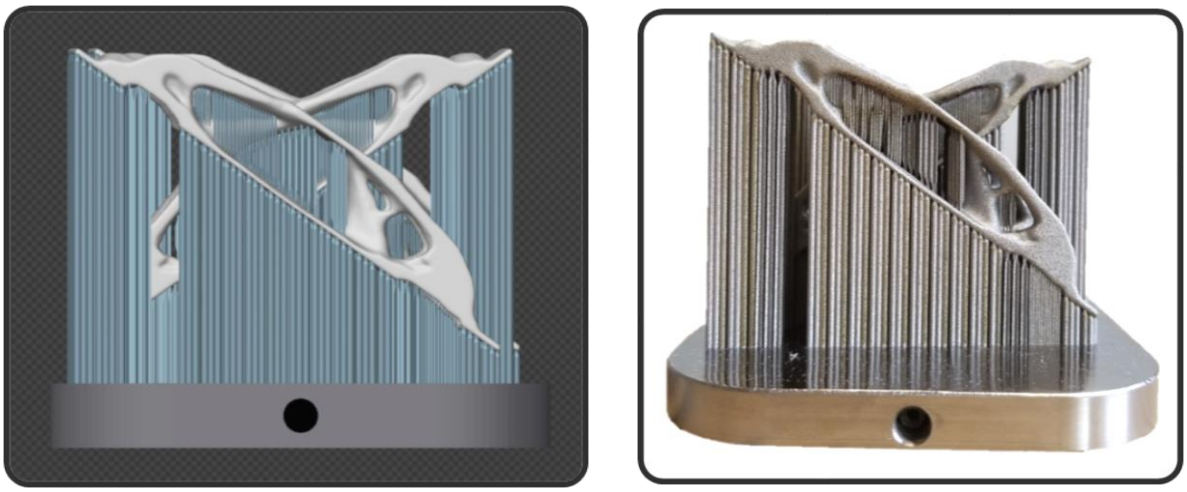

(a) (b)

Figure 5.7 a) created file to print and b) printed structure based on the file

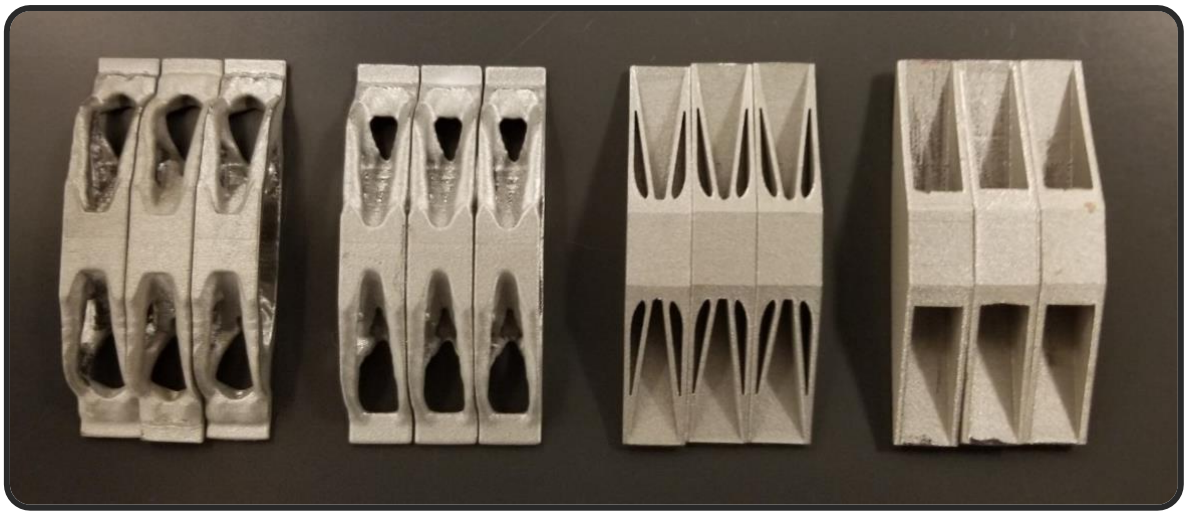

Figure 5.8 Printed parts after removing the support structure

A high-precision optical scanner, contact-free AICON SmartScan, is used to re-create an STL file from the printed components. This is done after removing the support structures. The re-created STL file is compared with the original STL file to estimate the geometrical accuracy of the printed parts. Figure 5.9 shows the deviation of the printed samples from the imported STL files.

The distortion happens because of the residual stresses induced during the printing. The maximum deviation belongs to the hollow bar with 0.8 mm distortion on the edge of the sample. Other samples have lower distortion because they have inner features that make these parts stiffer and more resistant to deflection caused by the residual stress. Amongst all, the mechanically optimized samples have the least deflection (almost half of the hollow bar).

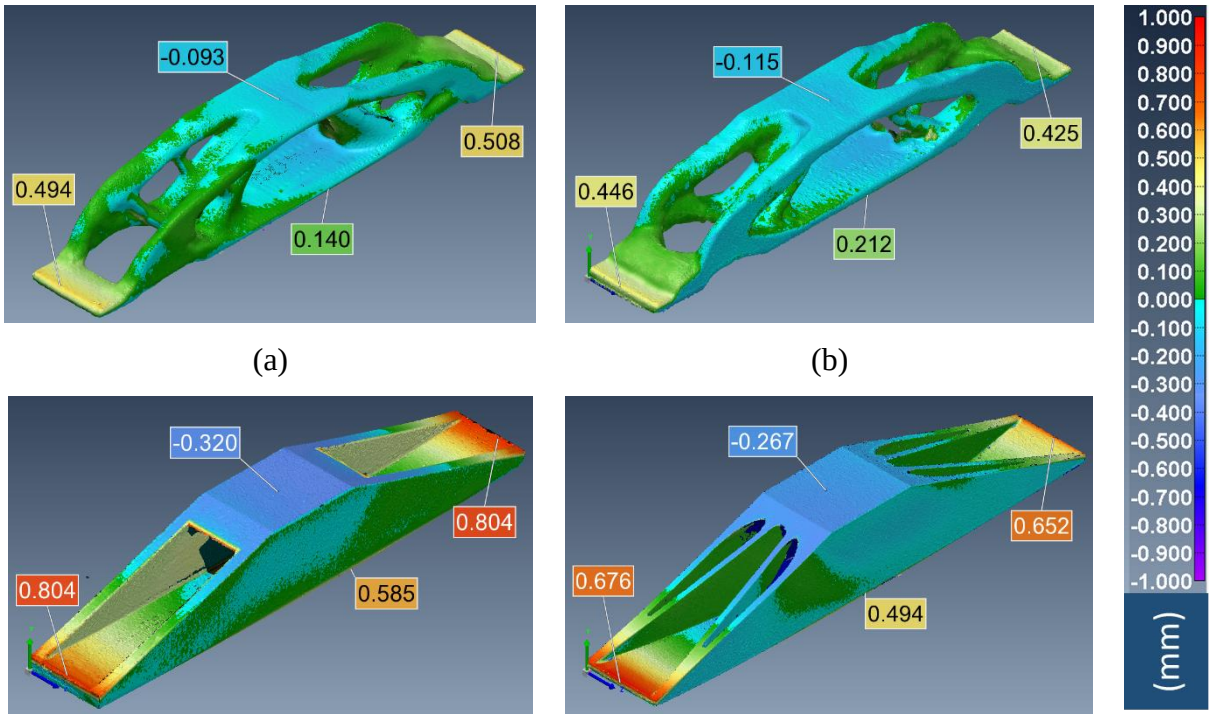

Figure 5.9 The CCM result of the printed samples for the distortion of a) coupled thermo-mechanical optimized, b) mechanical optimized, c) hollow bar, d) designed part

5.4 Experiment setup

Thermo-mechanical tests are not ordinary experiments to be performed. In order to have a thermal and mechanical load in the same experiment, a special setup is needed to be designed. Figure 5.10 shows the proposed experimental setup for applying thermal and mechanical loads at the same time. First of all, a press die set is provided to form the structural base of this setup. In

the press shown in this picture, number 1 presents the press die set ram and number 6 shows the bed or base of the die set that is sliding through guideposts (number 9).

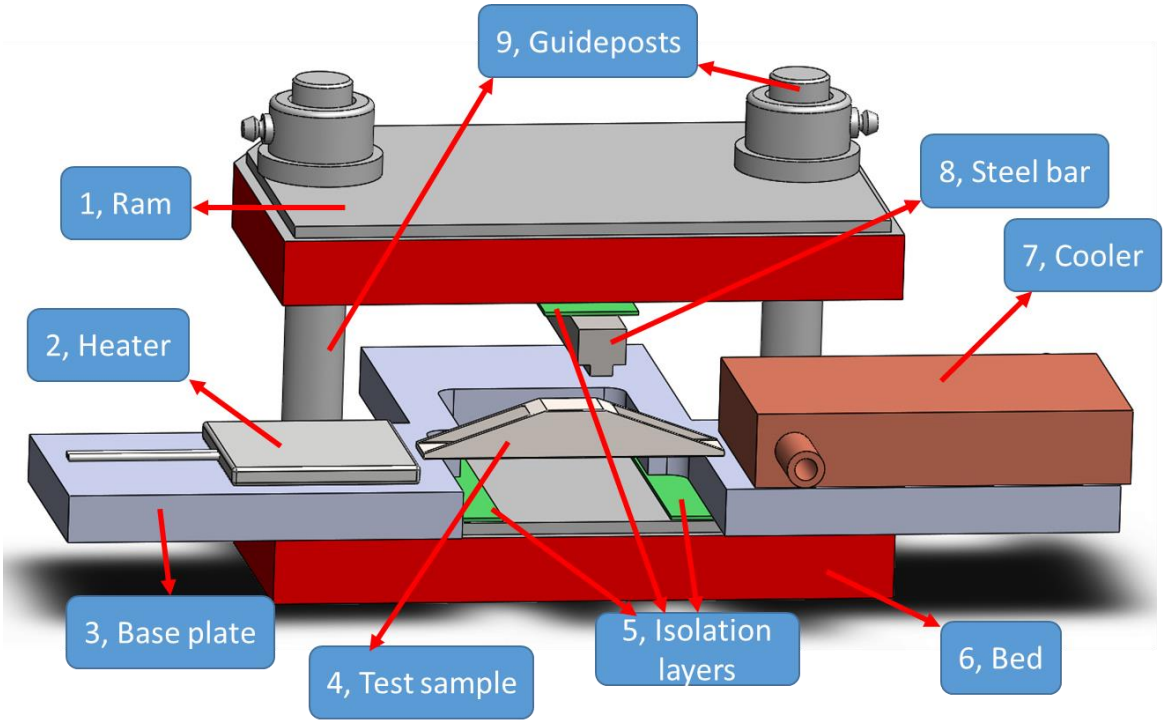

Figure 5.10 Experimental setup for thermo-mechanical loads

In Figure 5.10, number 2 presents the heater employed to apply the thermal load. Also, cold water is used to run through the copper part shown by number 7 to cool down the other side of the specimen. The cooler and the heater are placed on a metal sheet designed for this purpose (number 3). The other task of this steel-made sheet is to act as constraints for the printed part shown by number 4. On the top section, number 8 is presenting a steel bar that is used to apply force on top of the printed parts. Furthermore, pieces shown by number 5 are small silicon plates used for isolating the setup in order to lower heat loss through the contact surfaces. Figure 5.11 shows the heater on the right, cooler on the left side of the picture. Implanted thermocouples, shown by red circles, are connected to a controller to monitor and control temperatures on the contact points

during the test. The test specimens are accurately placed on top of these areas to obtain a better measurement of temperatures.

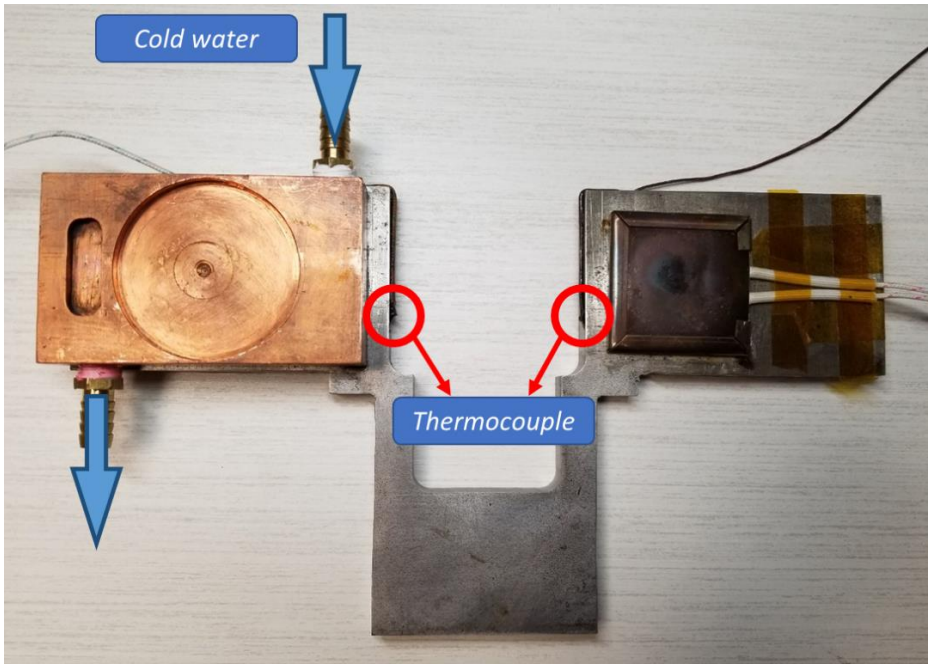

Figure 5.11 The cooler and heater placed on the metal sheet

After assembling the experimental setup, it is placed between the upper and lower crossheads of the tensile machine to apply the mechanical load. Performing a few numbers of tests, it was difficult to reach the desired temperature due to heat dissipation through crossheads. Thus, additional isolation was required. In order to provide more isolation, two layers of paper sheets are placed between the crossheads and the press die set. Paper sheets are almost incompressible while they provide enough isolation. A picture of the final setup is shown in Figure 5.12.

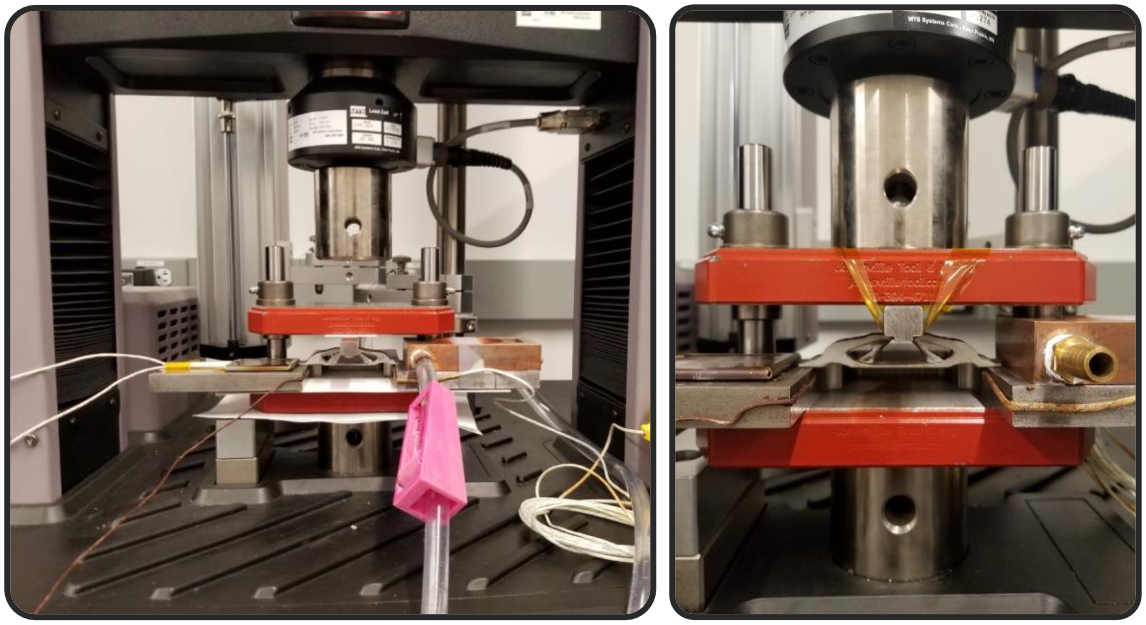

Figure 5.12 Experimental setup for thermo-mechanical loading

5.5 Results

In order to perform the experiments, each one of the parts was placed on the plate, exactly on top of the thermocouples. The process of the experiment can be explained as below:

The heater is turned on until the reading temperature from the thermocouple shows 150 ^{o}C. Then, the cold water runs through the cooler on the right section. The next step is to wait for some time until the heat transfer becomes steady-state with the temperatures of 35 ^{o}C on the right and 150 ^{o}C on the left side of the specimen. Then, the upper crosshead starts moving downward with the pace of 0.15 mm.s^{-1} until the applied force becomes 3.5 kN. The crosshead subjects to a 5-second pause and then it starts going upward to its original level. The same process was applied to all the 12 specimens and the required raw data was extracted.

Figure 5.13 and Figure 5.14 show the plots of force vs displacement for the samples optimized based on mechanical and thermo-mechanical deformations, respectively. The force vs

displacement for the manually designed part and hollow bar are presented in Figure 5.15 and Figure 5.16, respectively. The resulted graphs are demonstrating that none of these components are subjected to plastic deformation due to the formation of a straight line from 0 to 3.5 kN in the loading process. In the unloading process, a drop is observed in all diagrams. The reason for this phenomenon can be explained as below.

In the force vs displacement plots, a slope is observed at the beginning of the unloading stage. To explain this phenomenon, it should be noted that other than the printed samples, other components are under loading in the experiment setup as well. Mainly, the steel plate, the bar on top, the silicon plates and the papers used for isolation are under the pressure. Amongst the parts in the experimental setup and the samples, the ones with the highest stiffness (highest elastic modulus) are reacting to the unloading process before others. This phenomenon can be the reason behind the forming of the slope in the graph. Then after a short time, other components are involved in the process and the gradient of unloading grows into the same value as loading criteria.

Also, in the generated force-displacement graphs, the area between the loading and unloading lines can be related to hysteresis energy. Hysteresis is the dissipated energy in one cycle of loading and unloading. The graph in Figure 5.17 is showing the average of force vs displacement for all the samples for each design. As this graph shows, the displacement of the mechanically optimized and thermo-mechanically optimized component are close to each other and lower than the displacement of the hollow bar and manually designed part. A detailed comparison between the simulated and experimental displacement is presented in the following pages.

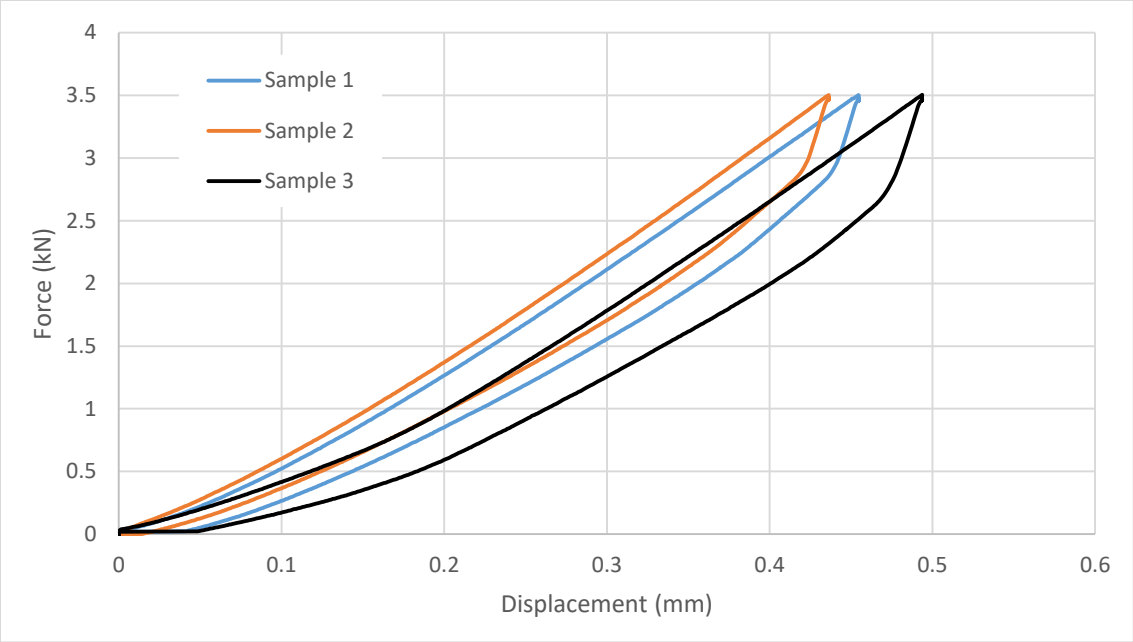

Figure 5.13 Force vs displacement graph for 3 samples regarding mechanical topology optimization

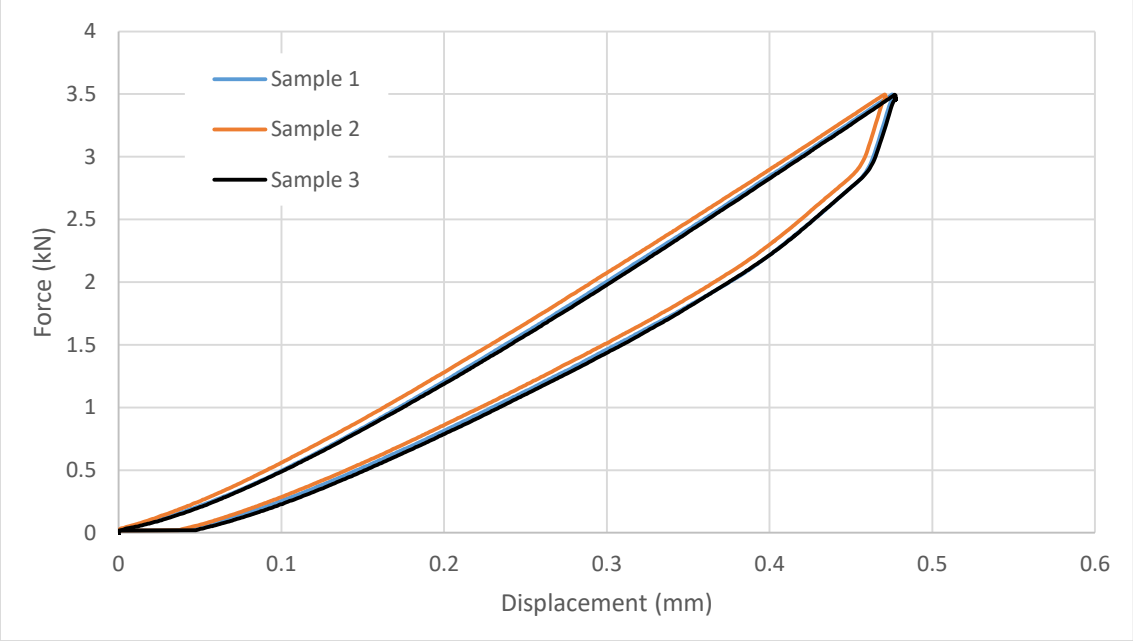

Figure 5.14 Force vs displacement graph for 3 samples regarding coupled thermo-mechanical topology optimization

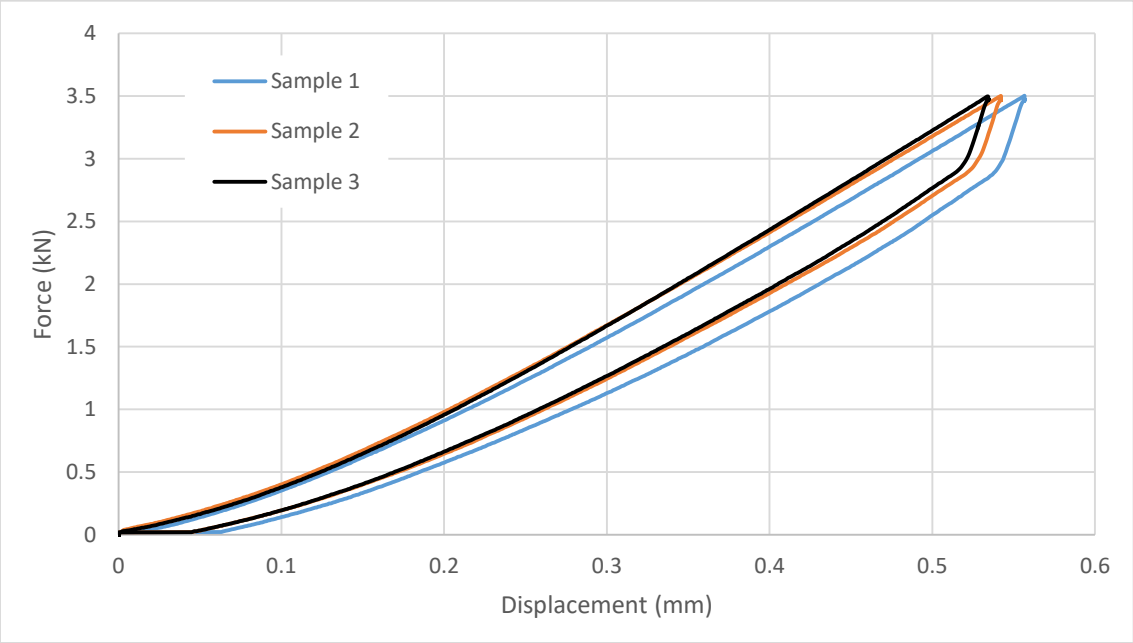

Figure 5.15 Force vs Displacement graph for 3 samples of manually designed part

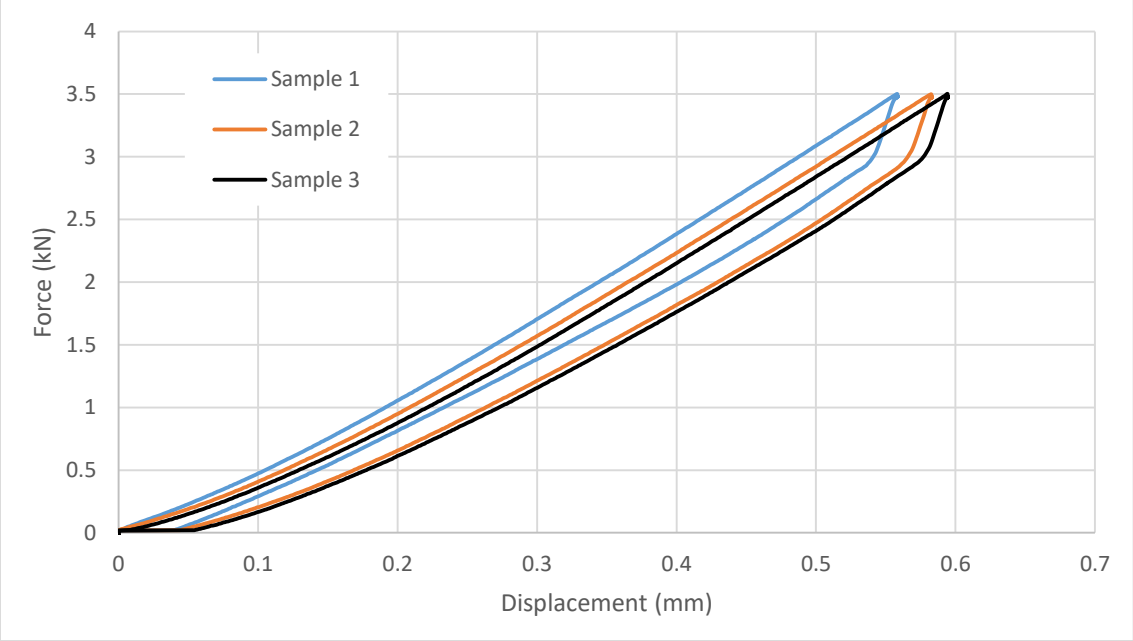

Figure 5.16 Force vs Displacement graph for 3 samples of hollow bar

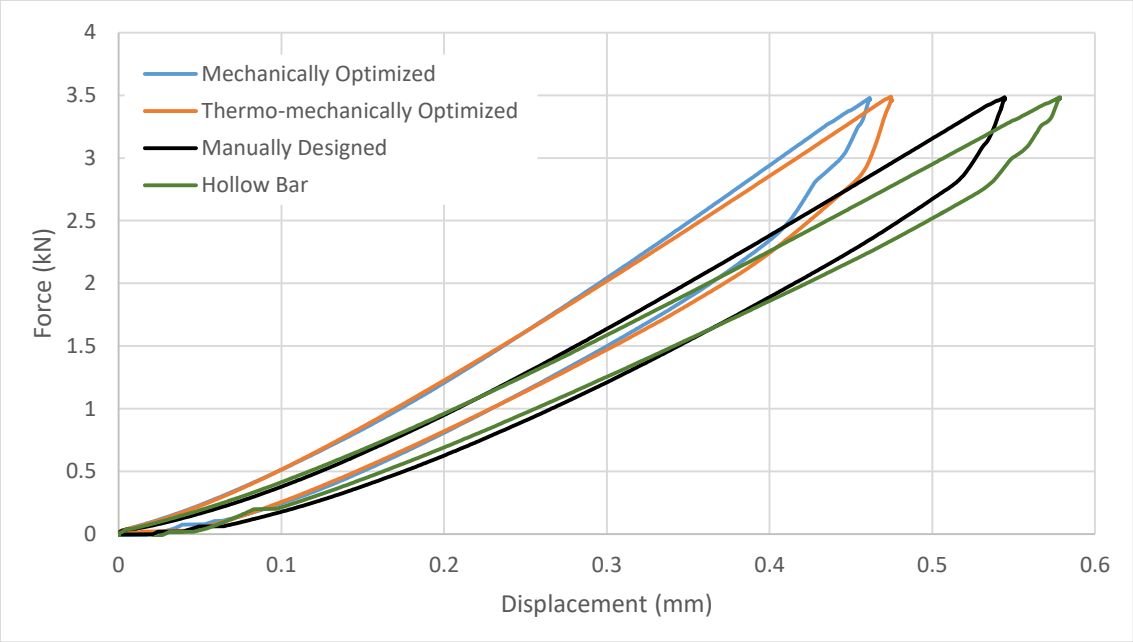

Figure 5.17 Average Force vs Displacement graph for different designs

Specimens displacement plots based on the applied load are shown in Figure 5.18. As these plots demonstrate, the displacement in the vertical direction is symmetric for all the parts except the one that is designed based on thermo-mechanical optimization which is expected due to the non-symmetrical geometry of the part.

A comparison of the temperature and displacement between the FE analysis and experimental analyses of each sample is given in Table 5.1. In this table, the low and high temperatures on each side of samples are presented and then the relative displacement is measured. In all the results, the calculated errors are from 25% to 35%. These errors are caused by different sources. First of all, the printed parts from STL files are subjected to deformation and warpage that was described before. The mismatch of the manufactured parts with the simulated ones can increase the inaccuracy. Also, by isolating the experiment system using the silicon plates and papers, the

measured displacement is exposed to a significant amount of error. Similarly, the simulation analysis does not include the press die set, the steel plate on the bottom, and the bar on the top of the tested samples. In order to get more accurate results, these parts should be taken into account in the simulation. Furthermore, the measured displacement is less than 0.6 mm. The low level of displacement may raise the error of measuring by the tensile machine. Last but not least, it should be mentioned that the tensile machine is subjected to a measurement error itself. All of these can cause a variation between the measured and simulated displacements.

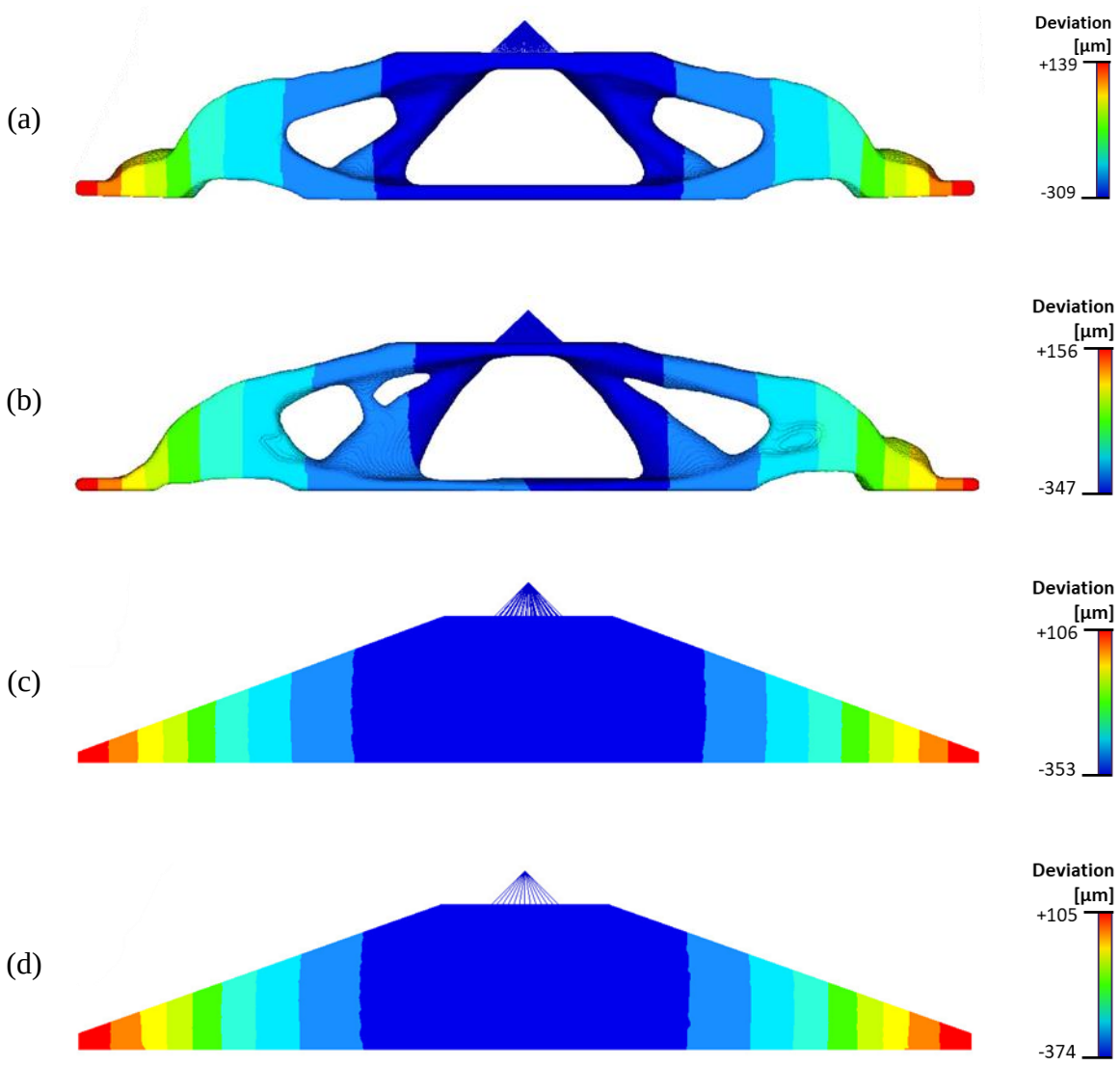

Figure 5.18 Displacement plots based on the mechanical load in the vertical direction for a) topology optimized based on mechanical load, b)topology optimized part based on thermo-mechanical load, c) manually designed part, and d) hollow bar

Table 5.1 shows that the samples designed based on mechanical topology optimization are stiffest components since they are subjected to the lowest displacements. The second stiff sample is the component designed based on fully-coupled thermo-mechanical topology optimization.

Manually designed and the hollow bar are in the third and fourth place. These results confirm that the assumptions and simulations are correct and reliable.

Table 5.1 Comparison between the simulation and experimental results

Design	Sample	Temperature [°C]		Displacement [μm]			Error [%]
		Lower Temp.	Higher Temp.	Experiment	Average	Simulation	
Topology optimized based on mechanical load	1	24	146	454	461	309	32.9
	2	24	164	436			
	3	27	140	493			
Topology optimized based on thermo-mechanical load	1	25	149	476	475	347	26.9
	2	25	150	471			
	3	27	143	478			
Manually designed	1	25	150	556	544	353	35.2
	2	26	150	542			
	3	25	149	535			
Hollow bar	1	26	146	558	578	374	35.3
	2	25	148	582			
	3	26	151	594			

In the experimental process, in addition to recording temperature through the type K thermocouples, the temperature gradients are also captured with a thermal camera (FLIR ONE

Pro). The temperature gradient of the experimental setup on the tensile machine is presented in Figure 5.19. In this picture, the heater is shown in the left area with the red color and the blue color on the right section of the setup is presenting the cooler with connecting tubes and controlling valve.

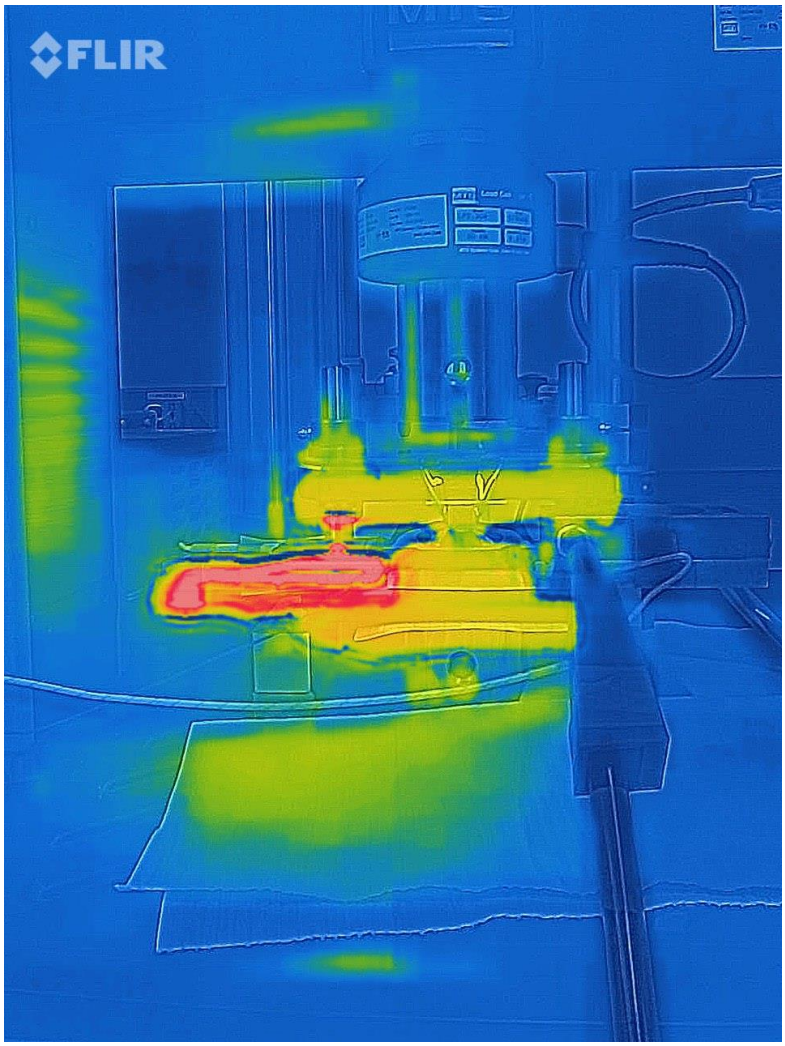

Figure 5.19temperature map of the experimental setup

The temperature contour map from the FEM analysis and the experiment are shown in Figure 5.20. This figure confirms the general heat flow is simulated properly, however, the temperatures on the left and right section (where thermocouples are located) are slightly different

due to the inaccuracy of the thermal camera. Furthermore, the temperatures at the top middle section of specimens show that the design based on thermo-mechanical topology optimization is subjected to a lower temperature in that area. Thus, the thermo-mechanically topology optimized part is not only withstanding the applied force but also, subjected to lower temperatures within the design.

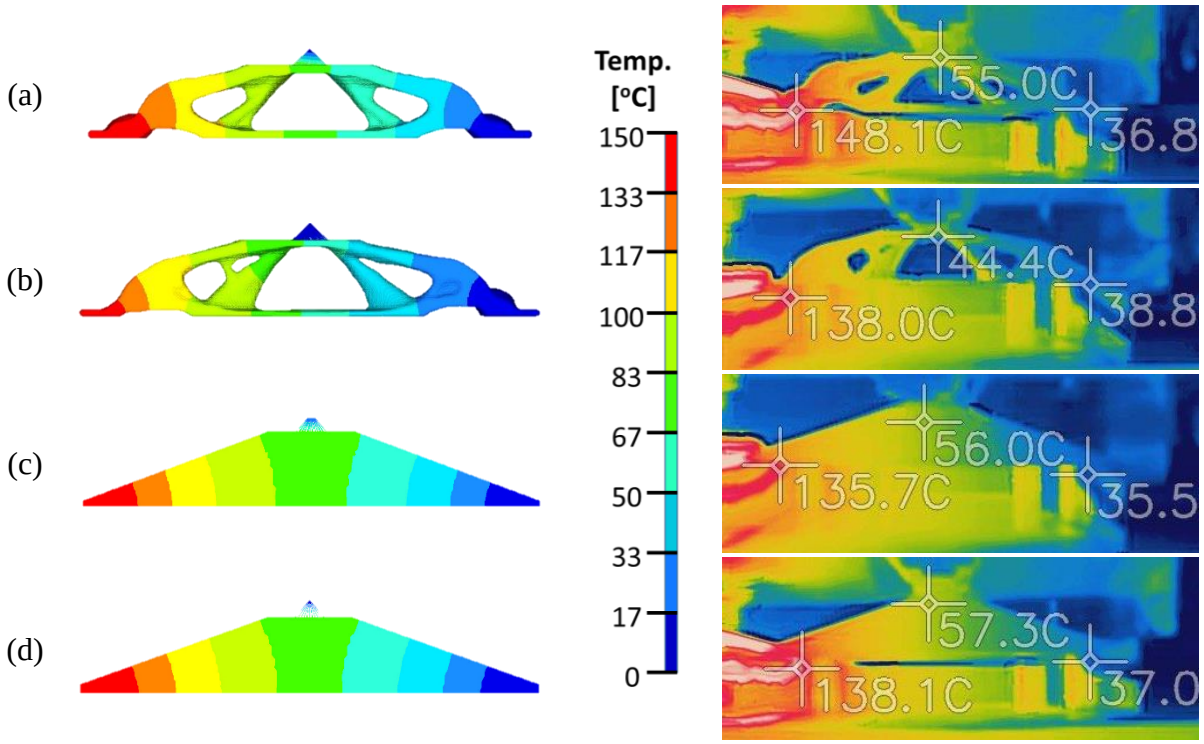

Figure 5.20 Temperature gradients in experimental and simulation for a) topology optimized based on mechanical load, b)topology optimized part based on thermo-mechanical load, c) manually designed part, and d) hollow bar

In the simulation, the thermal compliances for each component are presented in Table 5.2. This table shows that the thermal compliance of the thermo-mechanically optimized component is almost 64% of the mechanically optimized and 74% of the hollow bar and manually designed part.

Table 5.2 Compliance of printed parts under thermal load

	Thermal compliance [mJ]
Topology optimized based on mechanical load	7.57×10^4
Topology optimized based on thermo-mechanical load	4.86×10^4
Manually designed	6.43×10^4
Hollow bar	6.68×10^4

It should be mentioned that in the heat transfer analysis only heat transformation based on conduction is considered. But, in the experiment, convection heat transfer and radiation are also effecting the final temperature distributions. The effect of radiation is demonstrated by the white circle in Figure 5.21. The brighter side of the truss in the circled area is representing a higher temperature caused by radiation from the heater located on the left side of the picture (with the measured temperature of around 300 ^{o}C).

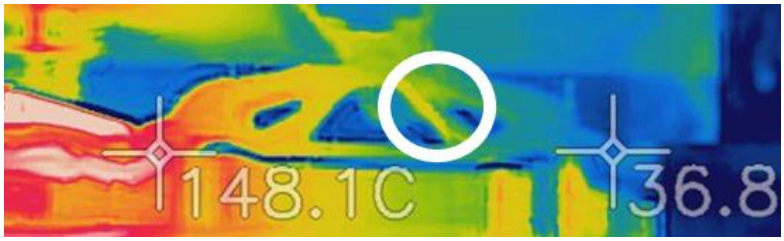

Figure 5.21 Temperature contour map for the sample regarding mechanical topology optimization

5.6 Summary

In this chapter, the proposed optimization process is employed to perform a topology optimization on a cantilever subjected to mechanical and thermal loads and the results are validated by experimental studies. In addition, the optimized parts are also compared with the parts optimized for the case that just mechanical loads exist. An STL file of all of these components is provided and imported to QuantAM software to generate the support structure. Then 3 samples of each design are 3D printed with the Renishaw AM 400 with the powder of Ti6Al4V. The printed parts are compared to the imported STL files to check the geometrical accuracy of the prints. Then, an experimental setup is designed and built to apply thermo-mechanical loads. Finally, the results of FEM simulations are compared to the experiments and validated the design of fully-coupled thermo-mechanical topology optimization.

Chapter 6

Summary, Conclusion, and Future Work

In this thesis, a workflow for thermo-mechanical topology optimization based on HyperWorks, one of the most powerful software tools available for topology optimization, was presented. In this workflow, optimization can be performed based on fully-coupled as well as one-way-coupled thermo-mechanical loads. Then a workflow for DfAM based on thermo-mechanical topology optimization is proposed. In this methodology, multiple topology optimization methods based on different initialization is required before obtaining the desired final product.

The proposed workflow was implemented to redesign a gas turbine rotor seal that is subjected to high temperature and pressure loads as well as centrifugal load. In this study, the effects of the weight factors, the minimum dimension filter, and the penalization factor on the optimization of rotor seal geometry were investigated. A total number of 256 thermo-mechanical topology optimization was performed in a 2D space. Then, the output of each optimization was analyzed by the generated Matlab code to filter unacceptable and undesired results. In the output, 21 designs were selected for the final review by the designer. A decision matrix was driven to present the proper initial conditions for the thermo-mechanical topology optimization of the gas turbine rotor seal. It is found that the generation of meaningful results from thermo-mechanical topology optimization is more likely with the higher weight factors for pressure and centrifugal loads. Also, it is better to use penalization factors between 4 and 8 to get the desired result.

In the last chapter, the same process was simulated on a component with a smaller scale of complexity to validate the results of the thermo-mechanical topology optimization. First, a set of

thermal and mechanical loads were defined on a simple cantilever to perform a coupled thermo-mechanical optimization in 3D space. The topologically optimized part was printed along 3 other components including a mechanically optimized geometry, a hollow bar, and a manually designed component with the same dimensions and volume. In order to compare the thermal distribution and mechanical performances of these parts, an experimental setup was designed and assembled. Finally, the results of the FEM simulation were compared to experimental values. The temperature distributions and performance of the printed samples under the loading conditions show that the thermo-mechanically optimized components are performing as expected.

The main contribution in this theses can be summarized as follow:

1. Using the proposed methodology for DfAM, 256 simulations were performed based on different combination of penalization factor, minimum dimension filtering, and weight factors for pressure, centrifugal, and thermal loads. Among these simulations, 21 results were acceptable to use.

2. The proposed methodology for fully-coupled thermo-mechanical topology optimization is validated by the result obtained from the designed experimental setup which applies thermal and mechanical loads simultaneously.

3. In the designed experiment, the topology optimization for thermo-mechanical load reduced the thermal compliance by 26% with respect to the hollow bar and manually designed part. Also, compared to the part that is optimized based on mechanical topology optimization, there was a 36% reduction in thermal compliance.

While in this thesis the effect of a few filters and variables is investigated, for future work, more filters can be taken into account.

- The overhang angle is a filter that is specially designed to be used in the design for additive manufacturing. Producing support free topologies for printing is possible using this filter. Thus, it can be a worthy candidate to investigate and considered as a variable in thermo-mechanical topology optimization.

- Interpolation function is another important issue that can affect the final design. The HyperWorks software is performing topology optimization based on the SIMP method and recently the company (Altair) presented the level-set method in their software for topology optimization. The RAMP method can also be used in some specific applications. The effect of these interpolation functions can be explored and examined for thermo-mechanical topology optimization.

- Topology optimization of the lattice structures is also very challenging especially when the component is subjected to the thermo-mechanical loading conditions. This feature is currently not available for fully-coupled thermo-mechanical topology optimization. Thus, in order to use this feature, one-way-coupled optimization should be implemented.

- Manufacturability of the designed parts is a major concern in topology optimization. This subject can be considered in the decision process of choosing the design to make sure the final product can be manufactured properly.

Also, in the experimental validation, more accurate experimental equipment can be used to obtain more realistic results with less deviation. Furthermore, using a more rigid setup with stiffer isolation layers can improve reduce the deviation between simulation and experimental results.

References

[1] M. K. Thompson *et al.*, "Design for Additive Manufacturing: Trends, opportunities, considerations, and constraints," *CIRP Ann. - Manuf. Technol.*, vol. 65, no. 2, pp. 737–760, 2016, doi: 10.1016/j.cirp.2016.05.004.

[2] D. Herzog, V. Seyda, E. Wycisk, and C. Emmelmann, "Additive manufacturing of metals," *Acta Mater.*, vol. 117, pp. 371–392, 2016, doi: 10.1016/j.actamat.2016.07.019.

[3] K. V. Wong and A. Hernandez, "A Review of Additive Manufacturing," *ISRN Mech. Eng.*, vol. 2012, pp. 1–10, 2012, doi: 10.5402/2012/208760.

[4] W. E. Frazier, "Metal additive manufacturing: A review," *J. Mater. Eng. Perform.*, vol. 23, no. 6, pp. 1917–1928, 2014, doi: 10.1007/s11665-014-0958-z.

[5] A. Chaudhuri, J. Jayaram, I. Flores Ituarte, P. Veng Søberg, and S. H. Khajavi, "Design for additive manufacturing: Motivations, competencies and performance impact," *26 th EurOMA Conf. Oper. adding value to Soc.*, no. August, pp. 1–8, 2019.

[6] Z. Doubrovski, J. C. Verlinden, and J. M. P. Geraedts, "Optimal design for additive manufacturing: Opportunities and challenges," *Proc. ASME Des. Eng. Tech. Conf.*, vol. 9, no. May 2014, pp. 635–646, 2011, doi: 10.1115/DETC2011-48131.

[7] O. Sigmund and K. Maute, "Topology optimization approaches: A comparative review," *Struct. Multidiscip. Optim.*, vol. 48, no. 6, pp. 1031–1055, 2013, doi: 10.1007/s00158-013-0978-6.

[8] Q. Wang *et al.*, *Investigation of condensation reaction during phenol liquefaction of waste woody materials*, vol. 9, no. 5. 2014.

[9] ASTM INTERNATIONAL, "ASTM F2792-12a," *Rapid Manuf. Assoc.*, pp. 1–3, 2013, doi: 10.1520/F2792-12A.2.

[10] Wohlers Associate, "Wohlers Report 2015 – History of Additive Manufacturing," p. 34, 2015.

[11] Q. Peng, Z. Tang, O. Liu, and Z. Peng, "Rapid prototyping-assisted maxillofacial reconstruction," *Ann. Med.*, vol. 47, no. 3, pp. 186–208, 2015, doi: 10.3109/07853890.2015.1007520.

[12] B. Mohajeri, J. Poesche, I. Kauranen, and T. Nyberg, "Shift to social manufacturing: Applications of additive manufacturing for consumer products," *Proc. - 2016 IEEE Int. Conf. Serv. Oper. Logist. Informatics, SOLI 2016*, pp. 1–6, 2016, doi: 10.1109/SOLI.2016.7551652.

[13] "3D hubs," *New Des.*, no. 107, p. 40, 2014.

[14] D. Ding, Z. Pan, D. Cuiuri, and H. Li, "Wire-feed additive manufacturing of metal components: technologies, developments and future interests," *Int. J. Adv. Manuf. Technol.*, vol. 81, no. 1–4, pp. 465–481, 2015, doi: 10.1007/s00170-015-7077-3.

[15] H. Fayazfar *et al.*, "A critical review of powder-based additive manufacturing of ferrous alloys: Process parameters, microstructure and mechanical properties," *Mater. Des.*, vol. 144, pp. 98–128, 2018, doi: 10.1016/j.matdes.2018.02.018.

[16] Y. Zhai, D. A. Lados, and J. L. Lagoy, "Additive Manufacturing: Making imagination the major Limitation," *Jom*, vol. 66, no. 5, pp. 808–816, 2014, doi: 10.1007/s11837-014-0886-

2.
[17] B. Graf, S. Ammer, A. Gumenyuk, and M. Rethmeier, “Design of experiments for laser metal deposition in maintenance, repair and overhaul applications,” *Procedia CIRP*, vol. 11, pp. 245–248, 2013, doi: 10.1016/j.procir.2013.07.031.
[18] J. Delgado, J. Ciurana, and C. A. Rodríguez, “Influence of process parameters on part quality and mechanical properties for DMLS and SLM with iron-based materials,” *Int. J. Adv. Manuf. Technol.*, vol. 60, no. 5–8, pp. 601–610, 2012, doi: 10.1007/s00170-011-3643-5.
[19] T. Duda and L. V. Raghavan, “3D Metal Printing Technology,” *IFAC-PapersOnLine*, vol. 49, no. 29, pp. 103–110, 2016, doi: 10.1016/j.ifacol.2016.11.111.
[20] S. F. S. Shirazi *et al.*, “A review on powder-based additive manufacturing for tissue engineering: Selective laser sintering and inkjet 3D printing,” *Sci. Technol. Adv. Mater.*, vol. 16, no. 3, 2015, doi: 10.1088/1468-6996/16/3/033502.
[21] E. Louvis, P. Fox, and C. J. Sutcliffe, “Selective laser melting of aluminium components,” *J. Mater. Process. Technol.*, vol. 211, no. 2, pp. 275–284, 2011, doi: 10.1016/j.jmatprotec.2010.09.019.
[22] L. C. Zhang, H. Attar, M. Calin, and J. Eckert, “Review on manufacture by selective laser melting and properties of titanium based materials for biomedical applications,” *Mater. Technol.*, vol. 31, no. 2, pp. 66–76, 2016, doi: 10.1179/1753555715Y.0000000076.
[23] “STAM - Science and Technology in Advanced Manufacturing - Mechanical & Manufacturing Engineering - Trinity College Dublin.” [Online]. Available: https://www.tcd.ie/mecheng/research/stam/research/projects/current/impact.php. [Accessed: 15-Jan-2020].
[24] “EOS Additive Manufacturing Systems and Materials.” [Online]. Available: https://www.eos.info/systems_solutions/. [Accessed: 22-Oct-2019].
[25] “A Comprehensive List of all the Metal 3D Printer Manufacturers - 3Dnatives.” [Online]. Available: https://www.3dnatives.com/en/metal-3d-printer-manufacturers/. [Accessed: 22-Oct-2019].
[26] “EOS: 3D Printers Company.” [Online]. Available: https://www.sculpteo.com/en/glossary/eos/. [Accessed: 22-Oct-2019].
[27] “Equipment - MSAM.” [Online]. Available: https://msam-uwaterloo.ca/equipment/. [Accessed: 22-Oct-2019].
[28] Y. Zhang, A. Bernard, R. K. Gupta, and R. Harik, “Evaluating the design for additive manufacturing: A process planning perspective,” in *Procedia CIRP*, 2014, vol. 21, pp. 144–150, doi: 10.1016/j.procir.2014.03.179.
[29] R. Hague, I. Campbell, and P. Dickens, “Implications on design of additive manufacturing,” *Science (80-.).*, vol. 217, no. 1, pp. 25–30, 2003.
[30] R. H. King, “Lupins,” *Non-Traditional Feed. Use Swine Prod.*, no. Lm, pp. 237–246, 2017, doi: 10.1201/9780203711248.
[31] A. W. Gebisa and H. G. Lemu, “Design for manufacturing to design for Additive Manufacturing: Analysis of implications for design optimality and product sustainability,” *Procedia Manuf.*, vol. 13, pp. 724–731, 2017, doi: 10.1016/j.promfg.2017.09.120.
[32] M. Orquéra, S. Campocasso, and D. Millet, “Design for Additive Manufacturing Method for a Mechanical System Downsizing,” *Procedia CIRP*, vol. 60, pp. 223–228, 2017, doi: 10.1016/j.procir.2017.02.011.
[33] K. Salonitis and S. Al Zarban, “Redesign optimization for manufacturing using additive

layer techniques," *Procedia CIRP*, vol. 36, pp. 193–198, 2015, doi: 10.1016/j.procir.2015.01.058.
[34] U. Khaleeq uz Zaman, A. Siadat, M. Rivette, A. A. Baqai, and L. Qiao, "Integrated product-process design to suggest appropriate manufacturing technology: a review," *Int. J. Adv. Manuf. Technol.*, vol. 91, no. 1–4, pp. 1409–1430, 2017, doi: 10.1007/s00170-016-9765-z.
[35] E. Asadollahi-Yazdi, J. Gardan, and P. Lafon, "Integrated Design for Additive Manufacturing Based on Skin-Skeleton Approach," *Procedia CIRP*, vol. 60, no. 2212, pp. 217–222, 2017, doi: 10.1016/j.procir.2017.02.007.
[36] Di. S. Nguyen and F. Vignat, "Topology optimization as an innovative design method for additive manufacturing," *IEEE Int. Conf. Ind. Eng. Eng. Manag.*, vol. 2017-Decem, pp. 304–308, 2018, doi: 10.1109/IEEM.2017.8289901.
[37] S. Hällgren, L. Pejryd, and J. Ekengren, "(Re)Design for Additive Manufacturing," *Procedia CIRP*, vol. 50, pp. 246–251, 2016, doi: 10.1016/j.procir.2016.04.150.
[38] B. Zhang, A. Goel, O. Ghalsasi, and S. Anand, "CAD-based design and pre-processing tools for additive manufacturing," *J. Manuf. Syst.*, vol. 52, no. February, pp. 227–241, 2019, doi: 10.1016/j.jmsy.2019.03.005.
[39] G. Kharmanda, N. Olhoff, A. Mohamed, and M. Lemaire, "Reliability-based topology optimization," *Struct. Multidiscip. Optim.*, vol. 26, no. 5, pp. 295–307, 2004, doi: 10.1007/s00158-003-0322-7.
[40] A. Kaveh and S. Talatahari, "Size optimization of space trusses using Big Bang-Big Crunch algorithm," *Comput. Struct.*, vol. 87, no. 17–18, pp. 1129–1140, 2009, doi: 10.1016/j.compstruc.2009.04.011.
[41] A. Theory, A. Dr, Q. Qing, and Q. Liang, "Performance-Based Optimization of Structures Performance-Based Optimization of Structures."
[42] G. Bekdaş, S. M. Nigdeli, and X. S. Yang, "Sizing optimization of truss structures using flower pollination algorithm," *Appl. Soft Comput. J.*, vol. 37, pp. 322–331, 2015, doi: 10.1016/j.asoc.2015.08.037.
[43] S. Kirkpatrick, C. D. Gelatt, and M. P. Vecchi, "Optimization by simulated annealing," *Science (80-.).*, vol. 220, no. 4598, pp. 671–680, 1983, doi: 10.1126/science.220.4598.671.
[44] X. S. Yang and S. Deb, "Cuckoo search: Recent advances and applications," *Neural Comput. Appl.*, vol. 24, no. 1, pp. 169–174, 2014, doi: 10.1007/s00521-013-1367-1.
[45] J. H.-A. Arbor and U. 1975, "Adaptation in Natural and Artificial Systems", University of Michigan Press."
[46] M. Dorigo and G. Di Caro, "Ant colony optimization: A new metaheuristic, evolutionary computation," *CEC 99. Proc. 1999 Congr.*, vol. 2, 1999.
[47] Σ. Τ. Εφαρμογων, "Πτυχιακη Εργασια Particle Swarm Optimization," pp. 1942–1948, 2013.
[48] C. V. Ramakrishnan and A. Francavilla, "Structural Shape Optimization using Penalty Functions," *J. Struct. Mech.*, vol. 3, no. 4, pp. 403–422, 1974, doi: 10.1080/03601217408907275.
[49] M. Papadrakakis, Y. Tsompanakis, and N. D. Lagaros, "Structural shape optimization using evolution strategies," *Eng. Optim.*, vol. 31, no. 4, pp. 515–540, 1999, doi: 10.1080/03052159908941385.
[50] R. T. Haftka and R. V. Grandhi, "Structural shape optimization-A survey," *Comput. Methods Appl. Mech. Eng.*, vol. 57, no. 1, pp. 91–106, 1986, doi: 10.1016/0045-7825(86)90072-1.

[51] H. A. Eschenauer and N. Olhoff, “Topology optimization of continuum structures: A review,” *Appl. Mech. Rev.*, vol. 54, no. 4, pp. 331–390, 2001, doi: 10.1115/1.1388075.
[52] G. I. N. Rozvany, “A critical review of established methods of structural topology optimization,” *Struct. Multidiscip. Optim.*, vol. 37, no. 3, pp. 217–237, 2009, doi: 10.1007/s00158-007-0217-0.
[53] K. D. Tsavdaridis, J. J. Kingman, and V. V. Toropov, “Application of structural topology optimisation to perforated steel beams,” *Comput. Struct.*, vol. 158, pp. 108–123, 2015, doi: 10.1016/j.compstruc.2015.05.004.
[54] G. I. N. Rozvany, M. Zhou, and T. Birker, “Generalized shape optimization without homogenization,” *Struct. Optim.*, vol. 4, no. 3–4, pp. 250–252, Sep. 1992, doi: 10.1007/bf01742754.
[55] M. P. Bendsøe, “Optimal shape design as a material distribution problem,” *Struct. Optim.*, vol. 1, no. 4, pp. 193–202, Dec. 1989, doi: 10.1007/BF01650949.
[56] M. Y. Wang, X. Wang, and D. Guo, “A level set method for structural topology optimization,” *Comput. Methods Appl. Mech. Eng.*, vol. 192, no. 1–2, pp. 227–246, Jan. 2003, doi: 10.1016/S0045-7825(02)00559-5.
[57] X. Huang and Y. M. Xie, “A further review of ESO type methods for topology optimization,” *Struct. Multidiscip. Optim.*, vol. 41, no. 5, pp. 671–683, 2010, doi: 10.1007/s00158-010-0487-9.
[58] X. Huang and Y. M. Xie, “Evolutionary topology optimization of continuum structures with an additional displacement constraint,” *Struct. Multidiscip. Optim.*, vol. 40, no. 1–6, pp. 409–416, 2010, doi: 10.1007/s00158-009-0382-4.
[59] O. Sigmund, “A 99 line topology optimization code written in matlab,” *Struct. Multidiscip. Optim.*, vol. 21, no. 2, pp. 120–127, 2001, doi: 10.1007/s001580050176.
[60] N. P. Van Dijk, K. Maute, M. Langelaar, and F. Van Keulen, “Level-set methods for structural topology optimization: A review,” *Struct. Multidiscip. Optim.*, vol. 48, no. 3, pp. 437–472, 2013, doi: 10.1007/s00158-013-0912-y.
[61] M. Yulin and W. Xiaoming, “A level set method for structural topology optimization and its applications,” *Adv. Eng. Softw.*, vol. 35, no. 7, pp. 415–441, 2004, doi: 10.1016/j.advengsoft.2004.06.004.
[62] S. Osher and J. A. Sethian, “Fronts propagating with curvature-dependent speed: Algorithms based on Hamilton-Jacobi formulations,” *J. Comput. Phys.*, vol. 79, no. 1, pp. 12–49, 1988, doi: 10.1016/0021-9991(88)90002-2.
[63] T. Yamada, K. Izui, S. Nishiwaki, and A. Takezawa, “A topology optimization method based on the level set method incorporating a fictitious interface energy,” *Comput. Methods Appl. Mech. Eng.*, vol. 199, no. 45–48, pp. 2876–2891, 2010, doi: 10.1016/j.cma.2010.05.013.
[64] J. D. Deaton and R. V. Grandhi, “A survey of structural and multidisciplinary continuum topology optimization: Post 2000,” *Struct. Multidiscip. Optim.*, vol. 49, no. 1, pp. 1–38, 2014, doi: 10.1007/s00158-013-0956-z.
[65] S. N. Reddy, I. Ferguson, M. Frecker, T. W. Simpson, and C. J. Dickman, “Topology optimization software for additive manufacturing: A review of current capabilities and a real-world example,” in *Proceedings of the ASME Design Engineering Technical Conference*, 2016, vol. 2A-2016, doi: 10.1115/DETC2016-59718.
[66] F. Jensen, “Topology Optimization of Turbine Manifold in the Rocket Engine Demonstrator Prometheus,” 2018.

[67] “Siemens: The digital twin of the expanded value chain - News and background.” [Online]. Available: https://www.plmportal.org/en/siemens-the-digital-twin-of-the-expanded-value-chain/articles/siemens-the-digital-twin-of-the-expanded-value-chain.html. [Accessed: 02-Jan-2020].
[68] “Altair Unveils Software Licensing Model for solidThinking > ENGINEERING.com.” [Online]. Available: https://www.engineering.com/DesignSoftware/DesignSoftwareArticles/ArticleID/17590/Altair-Unveils-Software-Licensing-Model-for-solidThinking.aspx. [Accessed: 03-Jan-2020].
[69] “3D-Printing & Additive Manufacturing - Performance-Driven Design & Optimization Software.” [Online]. Available: https://altairhyperworks.com/solution/Additive-Manufacturing. [Accessed: 03-Jan-2020].
[70] M. P. Bendsøe and O. Sigmund, *Typology Optimization ebook*. 2004.
[71] G. Vantyghem, W. De Corte, V. Boel, and M. Steeman, “Structural and Thermal Performances of Topological Optimized Masonry Blocks,” 2017.
[72] A. Sutradhar, J. Park, D. Carrau, T. H. Nguyen, M. J. Miller, and G. H. Paulino, “Designing patient-specific 3D printed craniofacial implants using a novel topology optimization method,” *Med. Biol. Eng. Comput.*, vol. 54, no. 7, pp. 1123–1135, 2016, doi: 10.1007/s11517-015-1418-0.
[73] J. Koga, J. Koga, and S. Homma, “Checkerboard Problem to Topology Optimization of Continuum Structures,” *CoRR*, vol. abs/1309.5, 2013.
[74] S. L. Vatanabe, T. N. Lippi, C. R. d. Lima, G. H. Paulino, and E. C. N. Silva, “Topology optimization with manufacturing constraints: A unified projection-based approach,” *Adv. Eng. Softw.*, vol. 100, pp. 97–112, 2016, doi: 10.1016/j.advengsoft.2016.07.002.
[75] J. Liu *et al.*, “Current and future trends in topology optimization for additive manufacturing,” *Struct. Multidiscip. Optim.*, vol. 57, no. 6, pp. 2457–2483, 2018, doi: 10.1007/s00158-018-1994-3.
[76] C. G. Lopes, R. B. dos Santos, and A. A. Novotny, “Topological derivative-based topology optimization of structures subject to multiple load-cases,” *Lat. Am. J. Solids Struct.*, vol. 12, no. 5, pp. 834–860, 2015, doi: 10.1590/1679-78251252.
[77] D. Li, X. Zhang, Y. Guan, and J. Zhan, “Topology optimization of thermo-mechanical continuum structure,” *IEEE/ASME Int. Conf. Adv. Intell. Mechatronics, AIM*, pp. 403–408, 2010, doi: 10.1109/AIM.2010.5695845.
[78] T. Verstraete and R. Van den Braembussche, “a Novel Method for the Computation of Conjugate Heat Transfer With Coupled Solvers,” no. January, pp. 1–17, 2011, doi: 10.1615/ichmt.2009.heattransfgasturbsyst.570.
[79] M. Rezazadeh Reyhani, M. Alizadeh, A. Fathi, and H. Khaledi, “Turbine blade temperature calculation and life estimation - a sensitivity analysis,” *Propuls. Power Res.*, vol. 2, no. 2, pp. 148–161, 2013, doi: 10.1016/j.jppr.2013.04.004.
[80] M. Patinios, J. Scobie, C. Sangan, and G. Lock, “Performance of Rim-Seals in Upstream and Downstream Cavities over a Range of Flow Coefficients,” *Int. J. Turbomachinery, Propuls. Power*, vol. 2, no. 4, p. 21, 2017, doi: 10.3390/ijtpp2040021.
[81] S. Schrewe, “Experimental investigation of the interaction between purge and main annulus flow upstream of a guide vane in a low pressure turbine,” 2015.
[82] Peters and G.P., “Rotating seal for gas turbine engine.” 24-Feb-1987.
[83] S. Dhivya and A. Karthikeyan, “Design and analysis of gas turbine blade with cooling,”

EAI Endorsed Trans. Energy Web, vol. 18, no. 20, pp. 1097–1104, 2018, doi: 10.4108/eai.12-9-2018.155742.

[84] R. R. Boyer, "An overview on the use of titanium in the aerospace industry," *Mater. Sci. Eng. A*, vol. 213, no. 1–2, pp. 103–114, 1996, doi: 10.1016/0921-5093(96)10233-1.

[85] T. Mukherjee, W. Zhang, and T. DebRoy, "An improved prediction of residual stresses and distortion in additive manufacturing," *Comput. Mater. Sci.*, vol. 126, pp. 360–372, 2017, doi: 10.1016/j.commatsci.2016.10.003.

[86] J. Song *et al.*, "Role of scanning strategy on residual stress distribution in Ti-6Al-4V alloy prepared by selective laser melting," *Optik (Stuttg).*, vol. 170, no. May, pp. 342–352, 2018, doi: 10.1016/j.ijleo.2018.05.128.

[87] F. Cangioli, S. Chatterton, P. Pennacchi, L. Nettis, and L. Ciuchicchi, "Thermo-elasto bulk-flow model for labyrinth seals in steam turbines," *Tribol. Int.*, vol. 119, no. July 2017, pp. 359–371, 2018, doi: 10.1016/j.triboint.2017.11.016.

[88] Y. W. Tian and J. G. Yang, "Research on vibration induced by the coupled heat and force due to rotor-to-stator rub," *JVC/Journal Vib. Control*, vol. 17, no. 4, pp. 549–566, 2011, doi: 10.1177/1077546309356241.

[89] T. Gao and W. Zhang, "Topology optimization involving thermo-elastic stress loads," *Struct. Multidiscip. Optim.*, vol. 42, no. 5, pp. 725–738, 2010, doi: 10.1007/s00158-010-0527-5.

[90] J. D. Deaton and R. V. Grandhi, "Stress-based Topology Optimization of Thermal Structures," *10 th World Congr. Struct. Multidiscip. Optim.*, pp. 1–10, 2013, doi: 10.2514/6.2013-1466.

Appendix A

The code for checking the connectivity of design is presented below:

```
function connectivity_array = connectivity(points, matrix)
   global mark
   global picture
   global queue
   picture = matrix;
   [row, column] = size(matrix(:,:,1));
   number_of_points = size(points, 1);
   connectivity_array = false(number_of_points, number_of_points);

   for p_index = 1:number_of_points
      p = points(p_index, :);
      mark = false(row, column);
      queue = [p];
      mark(p(1), p(2)) = true;
      dfs();
      for other_point_index = 1:number_of_points
         u = points(other_point_index, :);
         connectivity_array(p_index, other_point_index) = mark(u(1), u(2));
      end
   end
end

function dfs()
   global mark
   global picture
   global queue
   [row, column] = size(picture(:,:,1));
   while size(queue, 1) > 0
      p = queue(1, :);
      neighbors = get_adjacents(p, row, column);
      for i = 1:size(neighbors, 1)
         u = neighbors(i, :);
         if is_connected(p, u, picture) == false
            continue;
         end
         if mark(u(1), u(2)) == false
            mark(u(1), u(2)) = true;
            queue = [queue; u];
         end
```

```
        end
        if size(queue, 1) == 1
            break;
        end
        queue = queue(2:size(queue, 1), :);
    end
end

function x = is_connected(p1, p2, matrix)
    red_limit=uint8(200);
    blue_limit=uint8(20);
    if matrix(p1(1),p1(2),1) < red_limit
        fprintf("---> there is an error in point (%d , %d), please check it again\n", p1(1,1), p1(1,2));
    elseif matrix(p2(1),p2(2),1) >= red_limit && matrix(p2(1),p2(2),3) < blue_limit
        x = true;
    else
        x = false;
    end
end



function result = get_adjacents(p, row, column)
    neighbors = zeros(8, 2);
    neighbor_index = 1;
    for i = -1:1
        for j = -1:1
            if i == 0 && j == 0
                continue;
            end
            if p(1) + i > row || p(2) + j > column || p(1) + i < 1 || p(2) + j < 1
                continue;
            end
            neighbors(neighbor_index, 1) = p(1) + i;
            neighbors(neighbor_index, 2) = p(2) + j;
            neighbor_index = neighbor_index + 1;
        end
    end
    result = neighbors(1:neighbor_index - 1, :);
end
```

Appendix B

The Matlab code generated for the decision-making process to sort the final results is presented below:

```
clc
clear


%  Entering Data
Main_Folder = input ( 'Enter the main folder directory.        Main_Folder = ' , 's' );
Main_Folder = strcat(Main_Folder,'\')

W_C = input ( '\nEnter total number of W_centrifugal.                    W_C = ' );
W_P = input ( 'Enter total number of W_pressure.                  W_pressure = ' );
Min_Dim = input ( 'Enter total number of Min_dimention.              Min_dimention = ' );
P = input ( 'Enter total number of Penalty_factor.            Penalty_factor = ' );

Out_File = input ( 'Enter output file name.                          Output_file = ' , 's' ) ;      % Written output file
points= input ( 'Enter a matrix of poits to check the connectivity    Point_matrix = ');
% for checking the connectivity

% Defining percentages for partial-dense elements
percent(1,:) = '0.0-0.1';
percent(2,:) = '0.1-0.2';
percent(3,:) = '0.2-0.3';
percent(4,:) = '0.3-0.4';
percent(5,:) = '0.4-0.5';
percent(6,:) = '0.5-0.6';
percent(7,:) = '0.6-0.7';
percent(8,:) = '0.7-0.8';
percent(9,:) = '0.8-0.9';
percent(10,:) = '0.9-1.0';

des = 1;                    %   design number or number of experiment
number_of_scanned_files = 0;    % number of scanned files

%% Extracting all the results and useful information

for var_1 = 11 : 10+W_C
```

```
   for var_2 = 21 : 20+W_P
      for var_3 = 31 : 30+Min_Dim
         for var_4 = 41 : 40+P

%%  Opening and reading the folder and file
            filename = strcat(num2str(var_1),'-',num2str(var_2),'-',num2str(var_3),'-',num2str(var_4));
            filedirectory = strcat(num2str(var_1),'-',num2str(var_2),'-',num2str(var_3),'-',num2str(var_4),'\');
            foldername = strcat(Main_Folder,filedirectory,Out_File);

            fileID = fopen(foldername,'r');
            file = fscanf(fileID,'%c');

            iteration = 0;

            for j = 1:size(file,2) - 12

               from_file = file(1,j:j+12);

%% Reading CPU and simulation time
               elapsed(1,:) = 'ELAPSED TIME ';
               cpu(1,:) = 'CPU TIME     ';

               if from_file == elapsed
                  ELAPSED_TIME(1,:,des) = [str2num(file(1,j+56:j+57)),str2num(file(1,j+59:j+60))];
                  CPU_TIME(1,:,des) = [str2num(file(1,j+120:j+121)),str2num(file(1,j+123:j+124))];
               end

%%  Calculating partial dense elements
               dummy(1,:) = 'Density     %';

               if (from_file == dummy)
                  iteration = iteration + 1;

                  for i=j+10:j+280

                     if (file(1,i:i+6) == percent(1,:))
                        density(iteration,1) = str2num(file(1,i+8:i+14));
                     elseif (file(1,i:i+6) == percent(2,:))
                        density(iteration,2) = str2num(file(1,i+8:i+14));
                     elseif (file(1,i:i+6) == percent(3,:))
                        density(iteration,3) = str2num(file(1,i+8:i+14));
                     elseif (file(1,i:i+6) == percent(4,:))
                        density(iteration,4) = str2num(file(1,i+8:i+14));
                     elseif (file(1,i:i+6) == percent(5,:))
                        density(iteration,5) = str2num(file(1,i+8:i+14));
                     elseif (file(1,i:i+6) == percent(6,:))
                        density(iteration,6) = str2num(file(1,i+8:i+14));
                     elseif (file(1,i:i+6) == percent(7,:))
                        density(iteration,7) = str2num(file(1,i+8:i+14));
                     elseif (file(1,i:i+6) == percent(8,:))
                        density(iteration,8) = str2num(file(1,i+8:i+14));
                     elseif (file(1,i:i+6) == percent(9,:))
                        density(iteration,9) = str2num(file(1,i+8:i+14));
                     elseif (file(1,i:i+6) == percent(10,:))
```

```
                density(iteration,10) = str2num(file(1,i+8:i+14));
            elseif (file(1,i:i+11) == 'Weight*Comp.')

%% Calculating Compliances
                Comp(iteration,1)=str2num(file(1,i+34:i+47));          %Comp. for load 1 (Pressure)
                Comp(iteration,2)=str2num(file(1,i+107:i+120));        %Comp. for load 2 (Centrifugal)
                Comp(iteration,3)=str2num(file(1,i+180:i+193));        %Comp. for load 3 (Thermal)
                Comp(iteration,4)=str2num(file(1,i+253:i+266));        %Comp. for load 4 (Combined)

                W_Comp(iteration,1)=str2num(file(1,i+72:i+85));        %weighted Comp. for load 1 (Pressure)
                W_Comp(iteration,2)=str2num(file(1,i+145:i+158));      %weighted Comp. for load 2
(Centrifugal)
                W_Comp(iteration,3)=str2num(file(1,i+218:i+231));      %weighted Comp. for load  3
(Thermal)
                W_Comp(iteration,4)=str2num(file(1,i+291:i+304));      %weighted Comp. for load 4
(Combined)
                W_Comp(iteration,5)=str2num(file(1,i+437:i+450));      %Sum of all weighted compliances




              end

           end
        end

%% Reading volume_fraction

           read_VF = '1 VOLFR Vol-F' ;
           if from_file == read_VF
              VF(1,des) = str2num(file(1,j+45:j+56));
           end



      end

           if VF(1,des) < 0.338
              fprintf ( 'Volume fraction is less than 0.34 on folder %s\n' , filedirectory)
           end

      density(:,11)=sum(density(:,1:10),2);       % sum of densities
      density(1:iteration,12)=[0:iteration-1];    % number of iterations
      par_den(:,:) = density(iteration,3:8);      % amount of partial dense elements is defined as elements with
density of 0.2 to 0.8

      Density_matrix(1:iteration,:,des) = density(1:iteration,:);
      Compliance_matrix (:,:,des) = Comp(iteration,:);
      Weighted_Compliance_matrix(:,:,des) = W_Comp(iteration,:);
      Partial_dens_matrix(:,:,des) = par_den;
```

```
            Total_compliance(des,:) = [var_1, var_2, var_3, var_4, 0,
Weighted_Compliance_matrix(1,5,des)/W_Comp(1,5)];
            Partial_dense_elemets(des,:) = [var_1, var_2, var_3, var_4, 0,sum(Partial_dens_matrix(:,:,des))];



%%  reading images

            imfile = strcat( num2str(var_1),'-',num2str(var_2),'-',num2str(var_3),'-',num2str(var_4),'.jpg');
            Image_dir=strcat(Main_Folder,filedirectory,imfile);
            I = imread(Image_dir);

            connect(:,:,des)=connectivity(points,I);

            connect_percent(des,:) = [var_1, var_2, var_3, var_4, 0, ((sum(sum(connect(:,:,des)))-
size(points,1))/2)/(size(points,1)*(size(points,1)-1)/2)*100];

%% Printing all the pictures to a folder
            New_Folder = strcat(Main_Folder,'All Pictures');
            if ~exist(New_Folder, 'dir')
               mkdir(New_Folder);
            end

            im_paste_dir=strcat(New_Folder,'\',imfile);%,'.jpg');
            imwrite(I,im_paste_dir)


%%  creating decision matrix

            desicion_matrix_1(des,:) = [var_1, var_2, var_3, var_4, 0, 0, 0, connect_percent(des,6),
sum(Partial_dens_matrix(:,:,des)), Comp(iteration,4)];
            desicion_matrix_2(des,:) = [var_1, var_2, var_3, var_4, 0, 0, 0, connect_percent(des,6),
Partial_dense_elemets(des,6), Total_compliance(des,6)];

            number_of_scanned_files = number_of_scanned_files+1;
            fprintf ( 'Number of scanned folders = %d\n' , number_of_scanned_files)
            des=des+1;
         end
      end
   end
end

xlswrite('decision matrix.xlsx',desicion_matrix_2)

%%  Finding acceptable results: removing unconnected parts
C=sortrows(desicion_matrix_2,8,'descend');

kk=1;
for ii=1:size(C,1)
   if (C(ii,8)<75)
      continue
   end
   D(kk,:)=C(ii,:);
```

```
    kk=kk+1;
end

%%  Finding acceptable results: removing parts with undesired amount of partial dense elements
C=sortrows(D,9);
D=[];
kk=1;
for ii=1:size(C,1)
    if (C(ii,9)>25)
        continue
    end
    D(kk,:)=C(ii,:);
    kk=kk+1;
end

%%  Finding acceptable results: sorting the acceptable results based on normalized compliances
C=sortrows(D,10);


%%  Printing pictures of the final results
New_Folder = strcat(Main_Folder,'Selected Result Pictures');
if ~exist(New_Folder, 'dir')
    mkdir(New_Folder);
end

for ii=1:size(C,1)

    imfile = strcat(num2str(C(ii,1)),'-',num2str(C(ii,2)),'-',num2str(C(ii,3)),'-',num2str(C(ii,4)),'.jpg');
    filedirectory = strcat(num2str(C(ii,1)),'-',num2str(C(ii,2)),'-',num2str(C(ii,3)),'-',num2str(C(ii,4)),'\');
    Image_dir=strcat(Main_Folder,filedirectory,imfile);
    I = imread(Image_dir);
    im_paste_dir=strcat(New_Folder,'\',num2str(ii),'---',imfile);
    imwrite(I,im_paste_dir)

end

%%  Printing the acceptable results on an excel sheet

Acceptable_result=sortrows(D,10);
xlswrite(strcat(Main_Folder,'Acceptable_Result.xlsx'),Acceptable_result)
fprintf ( '\n\n       %d folders were scanned \n    >>  End of the Process  << \n' , number_of_scanned_files)
```